University of Southern Queensland

Faculty of Health, Engineering and Sciences

Analysis of EEG Signals Using Complex Brain Networks

A Dissertation submitted by

Guohun Zhu, Bachelor of Engineering

For the award of

Doctor of Philosophy

2014

Abstract

The human brain is so complex that two mega projects, the Human Brain Project and the BRAIN Initiative project, are under way in the hope of answering important questions for peoples' health and wellbeing. Complex networks become powerful tools for studying brain function due to the fact that network topologies on real-world systems share small world properties. Examples of these networks are the Internet, biological networks, social networks, climate networks and complex brain networks. Complex brain networks in real time biomedical signal processing applications are limited because some graph algorithms (such as graph isomorphism), cannot be solved in polynomial time. In addition, they are hard to use in single-channel EEG applications, such as clinic applications in sleep scoring and depth of anaesthesia monitoring.

The first contribution of this research is to present two novel algorithms and two graph models. A fast weighted horizontal visibility algorithm (FWHVA) overcoming the speed limitations for constructing a graph from a time series is presented. Experimental results show that the FWHVA can be 3.8 times faster than the Fast Fourier Transfer (FFT) algorithm when input signals exceed 4000 data points. A linear time graph isomorphism algorithm (HVGI) can determine the isomorphism of two horizontal visibility graphs (HVGs) in a linear time domain. This is an efficient way to measure the synchronized index between two time series. Difference visibility graphs (DVGs) inherit the advantages of horizontal visibility graphs. They are noise-robust, and they overcome a pitfall of visibility graphs (VG): that the degree distribution (DD) doesn't satisfy a pure power-law. Jump visibility graphs (JVGs) enhance brain graphs allowing the processing of non-stationary biomedical signals. This research shows that the DD of JVGs always satisfies a power-lower if the input signals are purely non-stationary.

The second highlight of this work is the study of three clinical biomedical signals: alcoholic, epileptic and sleep EEGs. Based on a synchronization likelihood and maximal weighted matching method, this work finds that the processing repeated stimuli and unrepeated stimuli in the controlled drinkers is larger than that in the alcoholics. Seizure detections based on epileptic EEGs have also been investigated with three graph features: graph entropy of VGs, mean strength of HVGs, and mean degrees of JVGs. All of these features can achieve 100% accuracy in seizure identification and differentiation from healthy EEG signals. Sleep EEGs are evaluated based on VG and DVG methods. It is shown that the complex brain networks exhibit more small world structure during deep sleep. Based on

DVG methods, the accuracy peaks at 88.9% in a 5-state sleep stage classification from 14,943 segments from single-channel EEGs.

This study also introduces two weighted complex network approaches to analyse the nonlinear EEG signals. A weighted horizontal visibility graph (WHVG) is proposed to enhance noise-robustness properties. Tested with two Chaos signals and an epileptic EEG database, the research shows that the mean strength of the WHVG is more stable and noise-robust than those features from FFT and entropy. Maximal weighted matching algorithms have been applied to evaluate the difference in complex brain networks of alcoholics and controlled drinkers.

The last contribution of this dissertation is to develop an unsupervised classifier for biomedical signal pattern recognition. A Multi-Scale Means (MSK-Means) algorithm is proposed for solving the subject-dependent biomedical signals classification issue. Using JVG features from the epileptic EEG database, the MSK-Means algorithm is 4.7% higher in identifying seizures than those by the K-means algorithm and achieves 92.3% accuracy for localizing the epileptogenic zone.

The findings suggest that the outcome of this thesis can improve the performance of complex brain networks for biomedical signal processing and nonlinear time series analysis.

Certification of Dissertation

I certify that the ideas, designs and experimental work, results, analyses and conclusions set out in this dissertation are entirely my own effort, except where otherwise indicated and acknowledged.
I further certify that the work is original and has not been previously submitted for assessment in any other course or institution, except where specifically stated.

Guohun Zhu, Bachelor of Engineering

0061017412

Signature of Candidate Date

ENDORSEMENT

Assoc Prof Yan Li ,Principalsupervisor Date

Assoc Prof Peng (Paul) Wen ,Co-supervisor Date

Acknowledgments

First, I would like to express my deepest gratitude to A/Prof. Yan Li, my principal supervisor for her endless commitments to directing the research and invaluable guidance. Without her continuous support, this thesis would not have been completed.

I would also like to thank A/Prof. Peng (Paul) Wen, my associate supervisor, for his support during my PhD research. I am also thankful to Bob Kemp for helping me with sleep EEG data discussions.

We thank Prof. Henri Begleiter at the Neurodynamics Laboratory at the State University of New York Health Centre at Brooklyn, USA whose group recorded the raw VEP data and Mr. Paul Conlon, of Sasco Hill Research, USA for sharing the alcoholic EEG data.

I would like to thank USQ for the PhD Scholarship that supported my study during the three years. A special thank to all my friends and colleagues at USQ.

Last but no least, I would like to dedicate this work to my parents, my brothers and sister. I am greatly indebted to them for their unconditional support, love and encouragement.

Guohun Zhu, Bachelor of Engineering

University of Southern Queensland
2014

Contents

List of Figures

List of Tables

Acronyms & Abbreviations

BIS	Bispectral Index
DD	Degree Distribution
DS	Degree Sequence
DVG	Differential Visibility Graph
DWT	Discrete Wavelet Transform
ECoG	Electrocorticography
EEG	Electroencephalographic
EMG	Electroencephalographic
EOG	Electroencephalographic
EZ	Epileptogenic Zone
FFT	Fast Fourier Transform
GE	Graph Entropy
FWHVA	Fast Weighted Horizontal Visibility Graph
HVG	Horizontal Visibility Graph
JVG	Jump Visibility Graph
fMRI	Functional Magnetic Resonance Imaging
PE	Permutation Entropy
SCN	Special Complex Network
SE	Sample Entropy
PSD	Power Spectral Density
SVM	Support Vector Machine
TCN	Temporal Complex Network
VG	Visibility Graph
XOR	Exclusive Or

Notation

A	Adjacency matrix
C	Mean local coefficient cluster of a graph
D	Mean degree of a graph
DS	Degree sequence
E	Edges set of a graph
G	A graph
L	Mean shortest path of a graph
Se	Sample entropy
X_m	m Dimension sequence.
V	Nodes set of a graph
$c(v_i)$	Coefficient cluster of a node v_i of a graph
$d(v_i)$	Degree of a node v_i of a graph
n	Length time series or number of graph nodes
$p(k)$	Degree distribution of a graph
$s(v_i)$	Strength of a node v_i of a graph
$t(n)$	Signal sample at time n

Associated Publications

The following publications were produced during the period of candidature:

[1] *G. Zhu*, Y. Li, P. p. Wen, and S. Wang, "Analysis of Alcoholic EEG signals based on Graph Entropy," Brain Informatics: Brain Data Computing and Health Studies. accepted, 2014.

The work in the paper is presented in Chapter 6.

[2] *G. Zhu*, Y. Li, P. p. Wen, and S. Wang, "Classifying epileptic EEG signals with delay permutation Entropy and multi-scale K-means," in Signal and Image Analysis for Biomedical and Life Sciences, T. B. Sun, T. D. Pham, P. Vallotton, and D. Wang, Eds., ed: Springer, Accepted, 2014.

The work in the paper is presented in Chapter 10.

[3] *G. Zhu*, Y. Li, and P. Wen, "Epileptic seizure detection in EEGs signals using a fast weighted horizontal visibility algorithm," Computer Methods and Programs in Biomedicine, vol. 115, pp. 64-75, 2014.

The work in the paper is presented in Chapter 5.

[4] *G. Zhu*, Y. Li, and P. Wen, "Analysis and Classification of Sleep Stages Based on Difference Visibility Graphs from a Single Channel EEG Signal," Biomedical and Health Informatics, IEEE Journal of, vol. PP, pp. 1-1, 2014. (formerly known as IEEE Transactions on Information Technology in Biomedicine)

The work in the paper is presented in Chapter 9.

[5] S. Wang, *G. Zhu*, Y. Li, P. Wen, and B. Song, "Analysis of Epileptic EEG Signals with Simple Random Sampling J48 Algorithm," International Journal of Bioscience, Biochemistry and Bioinformatics vol. 4, pp. 78-81, 2014.

The work in the paper is presented in Chapter 4.

[6] *G. Zhu*, Y. Li, P. P. Wen, S. Wang, and M. Xi, "Epileptogenic focus detection in intracranial EEG based on delay permutation entropy," AIP Conference

Proceedings, vol. 1559, pp. 31-36, 2013.

The work in the paper is presented in Chapter 10.

[7] *G. Zhu*, Y. Li, P. Wen, S. Wang, and N. Zhong, "Unsupervised Classification of Epileptic EEG Signals with Multi Scale K-Means Algorithm," in Brain and Health Informatics. vol. 8211, K. Imamura, S. Usui, T. Shirao, T. Kasamatsu, L. Schwabe, and N. Zhong, Eds., ed: Springer International Publishing, 2013, pp. 158-167.

The work in the paper is presented in Chapter 10..

[8] G. Wang, H. Wang, X. Tao, J. Zhang, and *G. Zhu*, "Finding a Weighted Positive Influence Dominating Set in E-learning Social Networks," International Journal of Computers & Technology, vol. 10, pp. 2136–2145, 2013.

The work in the paper is presented in Chapter 2.

[9] J. Liu, *G. Zhu*, and M. Xi, "A k-means algorithm based on the radius," Journal of Guilin University of Electronic Technology, vol. 33, pp. 134-138, 2013.

The work in the paper is presented in Chapter 10..

[10] *G. Zhu*, Y. Li, and P. P. Wen, "Analysing epileptic EEGs with a visibility graph algorithm," in 2012 5th International Conference on Biomedical Engineering and Informatics (BMEI2012) Chongqing, 2012, pp. 432-436.

The work in the paper is presented in Chapter 4.

[11] *G. Zhu*, Y. Li, and P. P. Wen, "An Efficient Visibility Graph Similarity Algorithm and Its Application on Sleep Stages Classification," in Brain Informatics. vol. 7670, F. Zanzotto, S. Tsumoto, N. Taatgen, and Y. Yao, Eds., ed: Springer Berlin Heidelberg, 2012, pp. 185-195.

The work in the paper is presented in Chapter 7.

[12] X. Jiang, *G. Zhu*, and J. Qin, "A recognition method on modulation signal based on wavelet network," Journal of Guilin University of Electronic Technology, vol. 32, pp. 122-124, 2012.

The work in the paper is presented in Chapter 7.

[13] *G. Zhu*, Y. Li, and P. P. Wen, "Evaluating Functional Connectivity in Alcoholics Based on Maximal Weight Matching," Journal of Advanced Computational Intelligence and Intelligent Informatics, vol. 15, pp. 1221-1227, 2011.

The work in the paper is presented in Chapter 6.

[14] Y. Wu, *G. Zhu*, H. Chen, and J. Qin, "WIN Algorithm for Discrete Online TSP," Journal of Advanced Computational Intelligence and Intelligent Informatics, vol. 15, pp. 1199-1202, 2011.

The work in the paper is presented in Chapter 2.

Chapter 1

Introduction

1.1 Background for human brain study

Two ambitious collaborative brain projects attracted a large amount of funding and media attention in 2013. The Human Brain Project (Insel et al. 2013) was chosen for 10-year funding of a one billion Euro project in Europe. It aims to simulate the human brain with supercomputers to better understand how the brain works and to diagnose brain disorders. It was announced on 28 January 2013. After about three months later, US President Barack Obama (Insel et al. 2013) officially announced another 10-year, 3 billion dollar BRAIN Initiative project. The plan is to further foster interdisciplinary collaborations to accelerate the development of new technologies, and thus to fuel much needed medical advances. As a result, researchers (Venter et al. 2001) compare these two mega projects to the Human Genome Project (HGP). Similar to the HGP, two brain projects aim to develop computing technologies not only for healthy people, but also for patients.

All of these projects need to process multimodal data. The HGP considers data from low level genes, to high level genomes, or from single RNAs to protein-protein interactions. The neuroscience researchers need to consider the signals from neuron cells to the scalp of the brain, such as electroencephalography (EEG) and functional magnetic resonance imaging (fMRI). In addition, all these projects have generated some public databases. For example, Genbank (Benson et al. 2008) and EMBL-Bank (Kanz et al. 2005) are two large databases for biological researchers. BLAST (Altschul et al. 1990) is a well known tool used to find the local similarity between any two input DNA sequences. In contrast, there is no standard method for measuring the similarity of two different EEG signals.

There are several neuroscience databases offering physiological data for brain studies, such as PhysioBank (Goldberger et al. 2000) and SenseLab (Morse 2007). This makes measuring the similarity between biomedical signals from different neuroscience databases challenging because traditional signals process methods

are hard to compare due to different frequency samplings and sizes of data.

Fortunately, complex networks (CN) are efficient tools to conduct the challenges study of brain function in small genes and long EEG waves. Because CNs have been widely applied in the study of biological systems, neural networks, social networks, the Internet and the World Wide Web (Boccaletti et al. 2006), it has been found that the topologies on these networks share some similar properties, such as small world properties (Watts & Strogatz 1998) and scale-free features (Barabási & Albert 1999). The characteristic of different complex systems sharing the same network structure leads biomedical engineers, physicists, mathematicians and computer scientists to participate in neuroscience research. For example, a robust network would be in power-law degree distribution (Albert et al. 2000). Then researchers would see that the complex brain networks from healthy subjects should be more like a small-world structure during sleep. Conversely, the dysfunctional brain networks, such as with seizure or alcoholism, should exhibit a random topology. In other words, researchers can find some meaningful results by means of CNs although there are no universally accepted complex brain network models.

Although CNs, as investigated by many researchers, bring numerous benefits to human brain studies, the techniques also present many challenges for scientists (He et al. 2013). Existing CNs used the correlation of nerve activity to measure the functional connectivity in different regions of the nervous system. For example, CNs based on fMRI signals use the average signals calculated in the brain regions (such as changes in blood oxygen signal) as a node, and the correlation between two regions as the edge of a network. These models would fail to analyse some network associated with clinical applications, such as single-channel EEG signals from anaesthesia or sleep, or EOG data recordings.

Another limitation for CNs in brain modelling is speed. Existing CNs are also not suitable for processing over a long period of clinical biomedical signals. For example, a clinical EEG for seizure detection might be recorded from one day to one week. And the duration of sleep EEG recordings is at least one night and recording size is normally above 50Meg as shown in PhysioBank (Goldberger et al. 2000). The existing brain function network computing model only records 30 seconds of sleep brain activity creating difficulties for real time applications. In addition, these network models cannot reflect the topological trends of brain function for more than 10 minutes because, with a personal computer, existing algorithms can fail to construct 6000 brain networks (each 30 seconds) within 10 minutes.

The final drawback of existing CNs is that the CNs are dependent on brain recording facilities, such as fMRI and positron emission tomography (PET). In fact, the existence public EEG signals, such as PhysioBank (Goldberger et al. 2000), mainly consist of EEG or EOG signals recordings.The existence CNs methods, however, cannot create more meaningful results from these signals than those using traditional time or frequency methods.

Although human brain projects have been influenced by the complex network technologies, the models of CNs associated with long-term recorded EEG signals are still a big challenge for researchers. There are few reports on the analysis of single-channel EEGs with CNs. This thesis tries to solve this challenge by comparing the topologies with the computer networks, society networks, and biological networks. In practice, these algorithms provide a robust and economical way to verify the network structures of both healthy and disordered brain function.

1.2 Research problems and hypothesis

The ultimate goals of this dissertation are to explore several novel complex networks based on clinical EEG signals to understand brain function of connectivity and to find more efficient algorithms for the identification of brain disorders. The performances are compared with traditional time-frequency domain methods. Three types of EEG signals: alcoholic, epileptic, and sleep EEGs, are analysed using complex brain network methods. Multi-channel EEG signals are studied by spatial complex networks, and single-channel EEG signals are analysed by temporal complex networks. Simulated chaotic signals and clinical EEG signals, such as alcoholism detection, epileptic focus, seizure detection, sleep scoring, are evaluated by different methods. The objectives are as follows:

1. How to efficiently identify seizures using complex networks from EEG signals
2. How to adopt CNs to select an optimal channel from multimodal-channel clinical EEG signals, such as the EEG signals of alcoholics or sleep subjects
3. How to use CNs efficiently to recognize awake and sleep EEG signals only by using a single-channel EEG
4. How to apply CNs to locate the epileptogenic zone from EEG signals
5. Find an efficient unsupervised classifier for biomedical signal classification.

The hypothesis in this study is that the parameters of a complex brain network are different when CNs are evaluated from various EEG signals, such as sleep and awake subjects, and healthy subjects and epileptic patients.

1.3 Justification for the research

A literature review of the research is provided in Chapter 2. The review shows that, there are existing research works supporting our hypothesis. For example,

Ferri et.al (2007) have shown that the functional connectivity of different EEG bands moves towards a small-world network structure during sleep. General anaesthetic EEG signals are associated with a significant reduction of the number of complex brain network connections (Lee et al. 2011).

To efficiently identify seizures from epileptic EEG signals, a previous work (Zhu et al. 2012*a*) has shown that seizures can be identified with 100% accuracy, but that identification speed is not perfect. On the other hand, entropies (Bai et al. 2007, Nicolaou & Georgiou 2012) are employed for identifying seizures with a fast speed but lower accuracy than those reported in Zhu et al. (2012*a*). There are two strategies that can improve the computing time and accuracy requirement. One is to improve the constructing graph speed, which has appeared in the author's previous work (Zhu, Li & Wen 2014*b*). the other is to strengthen the classifier, as shown in another of the author's works (Zhu, Li, Wen, Wang & Zhong 2013).

Clinical biomedical signals contain multi-modal signals. For example, alcoholic EEG signals include multi-channel EEG signals and two channel EOG signals (Zhu et al. 2011), while sleep recording devices, polysomnography (PSG), always includes two or three EEG signals and one or two channel EEG signals (Berthomier et al. 2007, Zhu et al. 2012*b*). For single-channel EEG signals, network topologies are studied within a graph in this study. On the other hand, for multi-channel EEG signals, the complex brain networks are evaluated by a graph isomorphism method. This method can be applied in EEG signals from different databases.

It is essential to find a solution with complex networks that the existing methods cannot solve. Traditional graph algorithms and complex network techniques will be combined to improve the performance for extracted features from clinical EEG signals on different conditions, such as deep sleep and anaesthetic induced immobility. For example, the delay permutation entropy (Zhu, Li, Wen, Wang & Xi 2013) associated with the epileptogenic zone shows a significant difference from that of the non-epileptogenic zone. However, there are no reports to show the topological difference between CNs from sleep EEG signals and those from epileptic EEG signals.

1.4 Contributions on each chapter

The work presented in this dissertation focuses on how to characterize the complex brain networks from healthy and disordered EEGs. The brain functions in healthy subjects are investigated from wake, light sleep and deep sleep states. The brain networks in disease are evaluated through epileptic, alcoholism and anaesthetized patients. In this thesis, multi-channel EEG recordings and single-channel EEG signals are addressed by spatial complex networks and temporal complex networks, respectively. To investigate the performances of these two brain networks for clinical EEGs, we focus on studying the efficient and low computational complexity properties, such as degrees, degree distributions, and strengths. To

investigate EEG signals' classification performance based on the extracted graph features, an unsupervised classification is presented. In order to solve the research problem in Section 1.2, the following contributions are proposed:

1. Investigate the epileptic EEG signals with visibility graphs
2. Introduce a fast horizontal visibility graph constructing algorithm to solve the speed limitations of VGs
3. Investigate the network topologies from sleep EEGs and EOG based on VG
4. Develop a difference visibility graph constructing algorithm to identify sleep stages with a single-channel EEG signal
5. Evaluate functional connectivity in alcoholics based on maximal weight matching
6. Present two multi-channel EEGs analysis methods for alcoholic EEGs and sleep EEGs
7. Implement unsupervised Multi-scale K-means methods to identify the epileptogenic zone.

These seven novel algorithms are implemented in R, Java, or C++. Each of them is simulated with chaotic signals and evaluated with biomedical signals. A brief discussion of these seven contributions is addressed below.

1.4.1 Identifying seizures with visibility graphs from epileptic EEGs

Firstly, visibility graphs (VGs) are applied to classify the seizure from epileptic EEG analysis. Five types of EEG signals, healthy with eyes open, healthy with eyes closed, inter-ictal from the epileptogenic zone, inter-ictal from the non-epileptogenic zone and seizure, are mapped into five types of complex networks based on VGs. Then mean degrees and degree distributions on these VGs are extracted. It is shown that the mean degree of a VG from an epileptic subject is larger than that from a healthy subject. The number of nodes having five-degree on a VG from a healthy subject is significantly different from the number of nodes having the same degree on the VG from an epileptic subject. The mean degree and the number of nodes with five and eight degrees are used to discriminate the healthy EEGs, seizure EEGs and inter-ictal EEGs. Experimental results demonstrate that the VG features with a support vector machine classifier has a high classification accuracy for identifying these five types of EEGs. The seizure EEG can be identified from the normal healthy EEG with 100% accuracy. However, the VG constructing speed is slow when the size of an EEG epoch is large.

1.4.2 Implementing a linear time horizontal visibility graph algorithm

To overcome the slow speed problem of the visibility graph algorithm, a fast horizontal weighted visibility graph algorithm (FWHVA) is presented. The FWHVA is also applied to identify epileptic EEG signals. The performance of the FWHVA is evaluated by comparing it with the Fast Fourier Transform (FFT) and sample entropy (SampEn) methods. The noise-robustness of graph features based on the FWHVA, mean degree and mean strength, are investigated using two chaos signals and five groups of EEG signals. Experimental results show that features extracted using the FWHVA is faster than that of SampEn and FFT. The mean strength feature associated with ictal EEG is significantly higher than those of healthy and inter-ictal EEGs. In addition, a 100% classification accuracy for identifying seizure from healthy subjects based on EEG signals shows that the features based on the FWHVA are more promising than the frequency features based on FFT and sample entropy indices for the time series classification.

1.4.3 Investigating the network topologies during sleep

This investigation studies the changes of network topologies from wakeful to deep sleep when temporal complex networks (TCNs) are constructed with EEG signals derived from polysomnography (PSG). The local clustering coefficient (C), mean degree (D), and average shortest path (L) of TCNs are extracted from five individual EEG channels of 28 healthy subjects. The statistics show that brain functions are characterized by the lowest C and the highest D during deep sleep. It is found that C and D associated with the Rapid Eye Movement (REM) stage from occipital region are significantly different to awake and light sleep stages than those from the frontal area. This finding suggests that the TCNs can be an efficient tool for the measurement of sleep quality in clinical settings.

1.4.4 Evaluating functional connectivity in alcoholics based on maximal weight matching

Complex networks are constructed based on synchronized likelihood methods from 61-channel EEG signals and 2-channel EOG signals of an alcoholics' database. A greedy maximal weight matching approach is developed to measure the functional connectivity of the obtained complex networks. The major discovery is that the processing of the repeated and unrepeated stimuli in the γ band in controlled drinkers is significantly more different than that in alcoholic subjects. However, the EOGs are always stable in the case of visual tasks, except for a weak wave when subjects make an error response to the stimuli.

1.4.5 Developing a difference visibility graph constructing algorithm to identify sleep stages

A novel algorithm is developed to identify sleep stages based on the single-channel electroencephalogram (EEG) signal. First, each epoch (30s) EEG signal is mapped into a visibility graph (VG) and a horizontal visibility graph (HVG). Second, a difference visibility graph (DVG) is obtained by subtracting the edges set of the HVG from the edges set of the VG to extract essential degree sequences and to detect the gait-related movement artifact recordings. The mean degrees and degree distributions $p(k)$ on HVGs and DVGs are analysed epoch-by-epoch from 14,963 segments of EEG signals. Then the mean degrees of each DVG and HVG and seven distinguishable degree distribution values of P(k) from each DVG are extracted. Finally, nine extracted features are forwarded to a support vector machine to classify the sleep stages into 2-state, 3-state, 4-state, 5-state and 6-state. The accuracy and kappa coefficients of the 6-state classification are 87.5% and 0.81, respectively. It is found that the mean degrees of the VGs in the deep sleep stage are higher than those in the awake and light sleep stages, and the mean degrees of the HVGs are just the reverse.

1.4.6 Identifying alcoholic EEG and sleep EEG with a graph isomorphism method

An efficient graph isomorphism algorithm based on horizontal visibility graphs is proposed to identify sleep by taking the advantages of two synchronization measuring methods in graph theory: phase locking value (PLV) and visibility graph similarity (VGS). It develops a new linear horizontal visibility graph isomorphism algorithm (HVGI), and tests its feature performance via the sleep stages identification application. Three features from two channel EEG data and one EOG signal are extracted separately from HVGI, PLV and VGS and are forwarded to a support vector machine which classifies the features into sleep-wake state and 6-state. 11,120 data segments are used for the experiments with each segment lasting 30 seconds. The training sets are selected from a single subject and the testing sets are selected from multiple subjects. 10-cross-validation is employed to evaluate the performances of the PLV, VGS and HVGI methods. The HVGI and VGS show significantly different trends from wake to deep sleep, while the PLV is similar to the HVGI in deep sleep stage but shows a large difference in wake.

1.4.7 Unsupervised classifying EEG signals with Multi-Scale K-means

An unsupervised Multi-Scale K-means (MSK-means) algorithm was proposal to distinguish epileptic EEG signals and identify the epileptogenic zone. The ran-

dom initialization of the K-means algorithm can lead to wrong clusters. Based on the characteristics of EEGs, the MSK-means algorithm initializes the coarse-scale centroid of a cluster with a suitable scale factor. The MSK-means algorithm is theoretically proved to be superior to the K-means algorithm on efficiency. In addition, three classifiers: the K-means, MSK-means and support vector machine (SVM), are used to identify seizure and to localize epileptogenic zone using delay visibility graph (JVG) features. The experimental results demonstrate that identifying seizure with the MSK-means algorithm and JVG achieves 4.7% higher accuracy than that of K-means, and 0.7% higher accuracy than that of the SVM.

1.5 Overview of the dissertation

This dissertation consists of 11 chapters. The rest of this dissertation is structured as follows:

Chapter 2 reviews the concepts of the complex brain networks. Spatial complex brain networks and temporal complex brain networks are investigated. The applications of complex brain networks based on EEG signals are summarized in this chapter.

Chapter 3 introduces the experimental EEG signals used in this thesis. Three categories of EEG signals are illustrated: 61-channel EEG and two-channel EOG from alcoholics and controlled subjects, two epileptic EEG data sets, and two sleep EEG databases.

Chapter 4 analyse five types of EEG signals with visibility graph algorithms. The mean degrees, degree distributions and graph entropies are extracted from the VGs associated with the two types of heathy EEGs, two types of inter-ictal EEGs and one type of ictal EEGs. A nonlinear discriminating classifier is applied to identify the seizure from these five EEGs.

Chapter 5 presents a FWHVA algorithm to identify the seizure from epileptic EEG signals in real time. A network topology, mean strength, is introduced to enhance the horizontal visibility algorithm against noise. Theoretical analysis shows that the strength features can identify the spike waves of epileptic EEG signals more efficiently than the degree features. Two chaos signals are simulated to evaluate the speed performance and robustness, and a K-Near Neighbour (K-NN) classifier is applied to identify the seizures based on two features from complex networks. The results compared with those of sample entropy and Fast Fourier Transform features.

Chapter 6 evaluates the multi-channel alcoholic EEG by synchronization likelihood and maximum match. Synchrony likelihood indices are extracted from 61-channel EEG signals and 2-channel EOG signals. These indices are mapped to an adjacency matrix of a graph. The optimal pair channels

are obtained by a greedy maximal weighted matching algorithm. The results show that the synchrony difference between alcoholics and controlled subjects are significant.

Chapter 7 proposes an novel horizontal visibility graph isomorphism (HVGI) for sleep stages classification. Three synchronized methods, HVGI, phase locked value (PLV) and visibility graph similarity (VGS) are evaluated the synchronization among chaos signals and multi-channel sleep EEG signals. Synchrony indies from two channel EEGs and one channel EOG are applied to identify sleep stages. The results show that the performances of HVGI are better than those of PLV and VGS.

Chapter 8 applies CNs to investigate the different network topologies during sleep. There are 42 healthy subjects from two sleep databases to be analysed based on temporal complex network methods. Two local network properties: mean degree, local coefficient clustering and two global network topologies: global coefficient clustering, average shortest path are investigated. These network topologies are evaluated from five channels EEG to check the different trends on different regions.

Chapter 9 reports a difference visibility graph (DVG) to identify the sleep stages based on a signal-channel EEG signals. A DVG is constructed from a VG and a HVG. The features of the mean degrees, degree distributions of a DVG and a HVG are extracted from an epoch of a single-channel EEG. A support vector machine classifier is applied to identify these features into 2-state, 3-state, 4-state, 5-state and 6-state sleep stages. The results are compared with the results reported from existing methods.

Chapter 10 develops an unsupervised Multi-Scale K-means (MSK-means) algorithm to distinguish epileptic EEG signals and identify the epileptic zone. When features from EEG signals are sent directly into a K-means algorithm, the random initialization of the K-means algorithm can lead to wrong clusters. The MSK-means algorithm initializes the coarse-scale centroid of a cluster with a suitable scale factor. In addition, a jump visibility graph method is presented to solve the non-stationary EEG signals. Finally, three classifiers: the K-means, MSK-means and support vector machine (SVM), are used to identify seizures and to localize the epileptogenic zone using jump visibility graph features.

Chapter 11 summarizes the results and findings of the work presented. This chapter also provides the suggestions of further work on temporal complex brain networks.

Chapter 2

Complex Brain Networks

This chapter provides an overview of complex brain networks and their applications in analysing brain functions. Before providing the overview of the complex networks, this chapter begins with Section 2.1 introducing the fundamental concepts of complex networks. Section 2.2 introduces small world networks. Section 2.3 discusses the complex brain networks based on multi-channel EEGs or fMRI data sets. Section 2.4 is devoted to temporal complex networks based on single-channel EEG time series. Section 2.5 explains the known results of complex networks relevant to brain functions during sleep and some brain disorders.

2.1 Basic concepts of complex networks

Complex networks are a subsets of graph theory. A graph $G(V, E)$ consists of a set nodes (or vertices) V and a set of edges E. If the edges are directed, the graph is named a digraph and its E is also named arc A, where an arc at the beginning vertex is called head, and the ending node is named tail. If two nodes v_i and v_j form an edge in an undirected graph (G), this will be denoted as $(v_i, v_j) \in E$. Figure 2.1 illustrates an undirected graph (left) and a digraph (right). The undirected graph has $n = 7$ nodes, $V = \{v_1, v_2, v_3, v_4, v_5, v_6, v_7\}$, and 7 edges, $E = \{(v_1, v_2), (v_4, v_1), (v_2, v_3), (v_2, v_4), (v_2, v_6), (v_3, v_4), (v_3, v_7)\}$. The number of edges is therefore $|E| = 7$. The directed graph of Figure 2.1(b) has $n = 7$ nodes and $|A| = 6$ arcs. An alternative network represented method uses an $n \times n$ adjacency matrix A, where A_{ij} characterizes the connection from node j to node i. If $A_{ij} = 0$, an edge is absent.

Sometimes it is useful to assign a weight to an edge (or an arc) of E (or A in a (di)graph. In other words, the A_{ij} is a numerical value. This (di)graph is called a weighted (di)graph, and the (di)graph is defined with $G(V, E, W)$ (or $G(V, A, W)$). The set W is usually a set of real numbers that indicate the strength, or relative strength, of each edge.

In this thesis, a graph is named as a complex network unless specially defined.

2.1.1 Mean degree and mean strength

In a complex network, the node degree and the degree sequence are two of the basic characteristics of graphs. The degree d_i of node v_i is the number of edges from v_i. For example, let G be Figure 2.1 (a), $d(v_1) = 2$ and $d(v_5) = 0$ are in G. The degree sequence (DS) is the sequence of the degree of a graph, where $DS(G)$ =*(2, 4, 3, 3, 0, 1, 1)*. In general, the degree of a graph is the maximum degree of d_i, such as $d(G) = 4$ in Figure 2.1 (a). The mean degree of a graph with n nodes is defined as:

$$\bar{d} = \frac{1}{n}\sum_{i=1}^{n} d_i \tag{2.1}$$

A weighted graph $G(V, E, W)$ is characterized by a set of weight edges. A strength of a node v_i is defined as follows:

$$S_i = \sum_{j=1}^{n} w_{ij} \tag{2.2}$$

For weighted graphs, according to Barrat et al. (2004), one of the measuring properties of weighted complex networks is mean strength. The mean strength of a graph having n nodes is defined as

$$\bar{s} = \frac{1}{n}\sum_{i=1}^{n} s_i \tag{2.3}$$

Because the computational complexities of calculating mean degree and mean strength are linear, the fast extracted features of complex networks associated with EEG signals are highly significant in a clinic setting. In this thesis, mean degree and mean strength are considered to be two major features for complex networks.

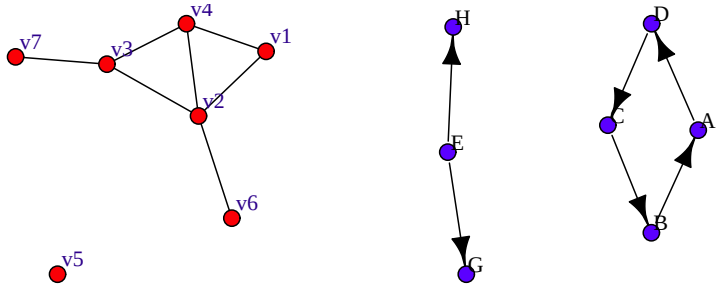

Figure 2.1: Examples of two graphs (a) an undirected graph (b) a digraph

2.1.2 Degree distribution and scale-free networks

Degree distribution (DD) is the linear complexity feature of graphs. The DD is the probability distribution $p(k)$ of k degrees versus k over a graph, which is obtained by counting the number of degrees of k and dividing it by the total number of nodes n. For example, the DD of Figure 2.1(a) is $p(k) = (\frac{1}{7}, \frac{2}{7}, \frac{1}{7}, \frac{2}{7}, \frac{1}{7})$.

In general, the DD of a random graph of $p(k)$ obeys a Poisson distribution. However, the DD of a real network, such as a biological network or social network, always satisfies a power-law distribution (Albert et al. 2000). Mathematically, a nonnegative variable x is considered to have a power-law distribution if its probability distribution satisfies:

$$p(k) = k^{-\lambda} \tag{2.4}$$

where λ is a constant parameter of the distribution known as the exponent or scaling parameter. This phenomenon implies that the most nodes have a small degree, but a few nodes have a larger degree. If a network satisfies a power-law degree distribution, the network is called a scale-free network. Because, if nodes with degree k in the scale-free network increase s times, the probability of nodes with sk degree only decreases $s^{-\lambda}$ as shown in equation 2.5:

$$p(sk) = (sk)^{-\lambda} = s^{-\lambda}k^{-\lambda} = s^{-\lambda}p(k) \tag{2.5}$$

2.2 Small world networks and complex brain networks

2.2.1 Clustering coefficient

The clustering coefficient is an important statistical property of complex networks. It represents the probability that two neighbours of node v_i are also neighbours. If v_i is connected with k_i neighbours ($d(v_i) = k_i$), there are at most $k_i(k_i - 1)/2$ edges between all these neighbours. In a real case, there are only E_i edges, while $E_i = \sum_{j,m} A_{i,j}A_{i,m}A_{m,j}$. The clustering coefficient c_i of node v_i can be calculated by equation 2.6:

$$c_i = \frac{2E_i}{d(v_i)(d(v_i) - 1)} = \frac{2\sum_{j,m} A_{i,j}A_{i,m}A_{m,j}}{k_i(k_i - 1)} \tag{2.6}$$

For a graph G, the mean clustering coefficient of G is the average of the clustering coefficients of all nodes:

$$C = \frac{1}{n}\sum_{i=1}^{n} c_i \tag{2.7}$$

If G is a complete graph, $C = 1$. If G is an isolated graph, $C = 0$. For a random graph, $C \approx O(\frac{1}{n})$. Thus, C of a graph G represents the segregation of the nodes in G. In most real networks, $O(\frac{1}{n}) < C < 1$. For example, the $C_1 = 1$ and $C_3 = \frac{1}{3}$ in Figure 2.1 (a).

2.2.2 Shortest path length

If a graph is connected, for any two nodes v_i and v_j, there exists a path connecting them. Here a path is defined as a sequence of nodes $\{v_i, v_{i+1}, v_{i+2}, \ldots, v_{i+k}, v_j\}$ such that any two subsequent nodes in this list form an edge. Sometimes there is more than one path between two nodes, the shortest path length (or graph distance) $l_{i,j}$ becomes an important factor in measuring the efficiency of information transportation between the two nodes v_i and v_j. The shortest path length of a network is the average $l_{i,j}$ of any two nodes. The definition is shown in equation 2.8.

$$L = \frac{1}{n(n-1)} \sum_{i=1}^{n} \sum_{j=i+1}^{n} l_{i,j} \tag{2.8}$$

In some cases, there exist isolated nodes in a network. Then the L becomes infinite, such as v_5 in Figure 2.1(a). To avoid this case, the first solution is to define $l_{i,j} = 0$ if v_i cannot reach v_j. The second solution is to inverse the path length between nodes as a global efficiency, the definition is listed in equation 2.9.

$$E_g = \frac{1}{n(n-1)} \sum_{i=1}^{n} \sum_{j=i+1}^{n} \frac{1}{l_{i,j}} \tag{2.9}$$

L and E_g are used to measure the overall capacity for parallel information transfer and integrated signal processing. If the L of a network is shorter, the information transported from one node to whole network more quickly. As a result, the global efficiency of the network is higher. In other words, L represents the integration of a network.

2.2.3 Small World Networks

Studies have shown that regular networks have high C and long L, which is efficient for local communications, but inefficient for transporting global information. In contrast, random graphs have low C and short L, making it easy to transport information across an entire network. Wattes and Strogatz (1998) conducted an experiment by connecting the edge with a probability p based on a regular graph G. When $p = 0$, G is regular; if $p = 1$, G becomes a random graph. If C in a G is larger than that in a random graph G_r, and L in G is as long as that in G_r. G has a global efficiency for information transporting but also possesses a local efficiency for communicating with neighbour nodes. This type of network is

named a *small world network (SWN).*

There are at least two methods to determine whether a real network is or is not a small world topology. The first method is defined by the average shortest path length, which indicates that the short path is in the order of the logarithm of the network size:

$$L \propto log(n) \tag{2.10}$$

where n is the number of nodes of G. Another approach is to study C and L of a G by comparing those of a random graph G_r. Let C_r and L_r indicate clustering coefficient the average shortest path length of G_r, respectively. The determination depends on equation 2.11.

$$\begin{aligned} \gamma &= C/C_r \gg 1 \\ \lambda &= L/L_r \approx 1 \end{aligned} \tag{2.11}$$

A more simple scalar measure of small world networks can be defined as $\delta = \gamma/\lambda$. If $\delta > 1$, the network G is a small world network (Humphries et al. 2006).

Many networks exhibit small world network properties. Examples of these are social networks, the Internet, and metabolic networks. Many studies also show that healthy brain functions satisfies the small world network properties (2006). However, it is unclear whether the networks of a disordered brain always obey the properties of small world networks.

2.2.4 Complex brain networks

Complex systems can be studied with a complex network because any complex system can be abstracted as a network. The node of a network can represent a component of a complex system, and the edge of a network represents the relation of two components. The Human brain is one of the most complex systems. Studying the brain system is extremely challenging. Complex networks provide a novel approach for studying brain function, also named complex brain networks.

There are two types of complex brain networks. The first is a structural brain network, which is based on an animal cortical. Thus, it is also named anatomical brain network. Nodes and edges of a structural brain network are defined according to different techniques and scales. A simple method is to map a single neuron into a node, and an edge comes from a common synapse shared by two neurons. However, a human brain has billions of neurons and thousands of synapses per neuron, thus it is impossible to build a complex network based on computers. An alternative approach is to map a group of neurons, such as cortical thickness from a MRI image, into a node. The covariation between two cortical regions is an edge (He, Chen & Evans 2007).

The second is a functional brain network. This method is widely used in EEG signals or fMRI signals. For instance, a node in this network comes from the

average of the blood-oxygen-level dependent (BOLD) fluctuations of a fMRI area or a channel of EEG signals. If two places are statistically coherent, an edge exists.

Both structural brain networks and functional brain networks can be properties of the small-world. For example, structural brain networks associated with MRIs (He, Chen & Evans 2007) reveal a small-world network. Stam et al. (2007) showed that, the functional brain networks from 21 channel EEG signals, satisfy the small world networks. Bassett et al. (2006) found that functional brain networks from MEG signals exhibit the attributes of a small-world network. This evidence support the economical functioning of the brain network (Bullmore & Sporns 2012).

However, because EEG signals are very much interdependent, some edge-based methods may produce many spurious connections (Blinowska & Kaminski 2013). Especially in single-channel EEG signal applications, the edges cannot be mapped from a single-channel EEG or an isolated brain region. Therefore, the conventional complex brain networks cannot be applied in these situations. In this thesis, a novel network is proposed to represent the CNs associated with single-channel EEG recordings. The proposed networks is temporal brain networks (TCNs).

2.3 Spatial brain networks

Spatial brain networks indicate the conventional complex brain networks. The complex brain network concept was formally presented by Bullmore and Sponer (2009). Before this concept appeared, graphs were applied to study brain functions. For example, the networks associated with EEGs from the human brain were shown as small-world brain networks by Bassett and Bullmore (2006). The graph, based on synchronization likelihood from multi-channel EEGs during the sleep, appeared having a small world network structure (Ferri et al. 2007). A team of researchers led by Lee et al. (2011) demonstrated continuous and discrete elements of anaesthetic state transitions through an approach based on mathematical graph theories. After complex brain networks were widely accepted, a brain graph concept was also presented by Bullmore and Bassett (2011). However, it is still unclear whether a brain network is a small world network or a scale-free network (Gallos et al. 2012). Therefore, for clinical applications, brain graphs must be studied in greater depth.

To map the multichannel EEG signals, MEG or fMRI data into a graph G, a channel of EEG, a sensor in MEG, or a voxel of fMRI can be mapped into a node, while the edge of G can be defined by different methods. The edge between pair nodes are defined by a synchrony of pair signals. There are, at most, $n(n-1)/2$ edges obtained from n nodes. Thus, the graph is a weighted graph. A binary adjacent matrix can be obtained by applying a threshold to each edge, then the graph becomes an undirected graph. The following sections describe how to define four types edges between a complex network associated with two time series.

2.3.1 Edge defined by coherence

Coherence is used to measure the dependence between two input signals in a frequency domain. For the same principle, this method can be applied to measure the function connectivity from two brain regions. Two channel EEG signals, or two regions of fMRI, or two time series, x and y can be transferred into X and Y in frequency domain. The coherence of X, Y are defined as

$$Coh(x,y) = \frac{|S_{xy}(f)|^2}{S_{XX}(f)S_{yy}(f)} \tag{2.12}$$

where $S_{xy}(f)$ is the cross-spectral density between X and Y. $S_x(f)$ and $S_y(f)$ present the power spectral density of x and y.

Some studies have been defined the edges of a SCN with coherence methods. For instance, Fallani et al. (2009) used a coherence method to construct brain networks from stroke patients' EEG and Magnetoencephalography (MEG). Peters et al. (2013) used this approach to study brain functional networks in patients with tuberous sclerosis complex (TSC) and autism spectrum disorders.

2.3.2 Edge defined by phase synchrony

Phase synchrony is widely used to study coupled chaotic systems. It is also called phase locked value (PLV) in some literature (Rosenblum et al. 1996, Zhu et al. 2012*b*). Given two time series, $\{x_i\}_{i=1,2,\ldots,n}$ and $\{y_i\}_{i=1,2,\ldots,n}$, their phase synchronization can be measured by the following equation:

$$ps(x,y) = \left|\left\langle e^{i(arg(H(x))-arg(H(y)))}\right\rangle\right| \tag{2.13}$$

where e is Napier's constant, H is Hilbert Transform, arg is the argument function and i is the imaginary unit. If $ps(x,y)$ is equal to 1, signals x and y are perfectly synchronised. When $ps(x,y) = 0$, x and y have no phase synchrony.

The advantage of this method is that $ps(x,y)$ in equation 2.13 only sensitive to the phase of input signals instead of amplifying the input data. Percha et al. (2005) applied phase synchrony to define the edges from epileptic EEG signals. Nicolaou and Georgiou (2014) studied anaesthetic-induced unconsciousness using a phase synchrony method, with the inducement of persistent and reversible widespread γ wave synchrony being most prominent. Edwin et al. (2009) found that the clustering coefficients, and the small world index were negatively correlated with temporal lobe epilepsy duration in the broad frequency band by extended phase synchrony matrix to complex networks. However, this method is limited to frequency bands and fails to process the multimodal spectrum signal (Quiroga et al. 2002).

2.3.3 Edge defined by synchronization likelihood

Unlike coherence and PLV in the frequency domain, synchronization likelihood (SL) is in the time domain. For the two time series $\{x_i\}_{i=1,2,\ldots,n}$ and $\{y_i\}_{i=1,2,\ldots,n}$, their SL with a given probability δ and a Theler window w can be measured by the following steps:

1. Convert the time series $\{x_i\}$ into an m dimensional sequence of a vectors using a time delay λ embedded, X_m by:

$$X_m\{t\} = \{x_t, x_{t+\lambda}, \ldots, x_{t+(m-1)\lambda}\} \; ; \; 1 \leq t \leq (n - m\lambda + 1) \tag{2.14}$$

   where $2 \leq m < n$. Similarly, another embedding Y_m is obtained from the time series $\{y_i\}$.

2. Calculate the autocorrelation of X_m between X_i and X_j with the following equation:

$$C_r = \frac{1}{2w} \sum_{j=1}^{N_e} H(|x_i - X_j|) \tag{2.15}$$

   while $N_e = N - m\lambda$ and H is Heaviside step function, $H(x) = 1$ if $x > 0$, otherwise $H(x) = 0$.

3. Calculate the probability δ of $|Y_i - Y_j| < c_r$ when $|X_i - X_j| < c_r$.

4. Calculate the synchronization likelihood between two signals X_i and Y_i as the following:

$$S_{i,j} = \sum_{k=1}^{Ne} H(c_r - |x_{k,i} - Y_{k,j}) \tag{2.16}$$

$$SL_{i,j} = \frac{1}{2m} \sum_{k=1}^{m} (S_{i,k})(S_{j,k}) \tag{2.17}$$

The range of $SL_{i,j}$ is between 0 and 1. The synchronization matrix is mapped into a weighted graph. When a threshold is assigned to each edge, it makes the weighting of the edge zero or one, the graph becomes an unweighted graph.

Many complex networks defined by synchronization likelihood have been applied to analyse EEG signals. For example Ferri et al. (2007) studied it with sleep EEGs, and Stam et al. (2007) tested the Alzheimer's brain with the SL method.

2.4 Temporal complex networks

The performance of a spatial complex network associated with multi-channel EEG is normally dependent on the number of channels. The number of EEG

Table 2.1: Summary of the definition of nodes and edges in temporal complex networks

Method	Node	Eege
Cycle networks (Zhang & Small 2006)	a cycle	distance between two cycles
Visibility graphs (Lacasa et al. 2008)	a point	visibility between two two points
Horizontal Visibility graphs (Bartolo Luque & Luque 2009)	a point	horizontal visibility between two points
Adaptive nearest neighbor networks (Xu et al. 2008)	a state $x(t)$	distance between two states
Recurrence networks (Marwan et al. 2009)	a state $x(t)$	recurrence of two states

channels in the clinical setting is normally in 19 or 64 as shown in Section 3. In some applications, such as sleep, the number of EEG channels is seldom above three during sleep diagnosis. Joudaki et al. (2012) reported that the size of the EEG-based functional network significantly influences their topological properties. Zhu et al. (2011) showed that complex networks based on eight channel EEG signals are significantly different from those with 64 channel EEG signals. Therefore, studying the complex networks based on single channel EEG signals is an important issue.

A time series, such as EEG signals, climate recordings, or stock market indices, can be transferred to a network representation by means of a suitable algorithm or mathematical mapping. In this thesis, this types of networks are called as temporal complex networks (TCNs). Unlike SCNs, TCNs lose their structural information, but it can be detected through the dynamic behaviour by network topologies if they are applied in biomedical signals.

Zhang et al. (2006) proposed a cycle network for the pseudo-periodic time series. The limitation of this method is that the cycle networks are only suitable for pseudo periodic time series. Marwan et al. (2009) transferred a recurrence matrix of a time series into an adjacency matrix of a recurrence networks. Lacasa et al. (2008) presented a visibility graph method and applied it to characterize chaotic, random and periodic time series. Xu et al. (2008) proposed an adaptive nearest neighbor network. Table 2.1 summaries the definition of nodes and edges in several TCNs. All these methods have potential applications in EEG signal processing. The following section briefly reviews the temporal complex networks in this study.

2.4.1 Visibility graphs

A visibility graph (VG) method proposed by Lacasa et al.(2008) is a powerful tool for time series analysis. Let $G(V, E)$ be a graph, where V and E are the nodes and edges of the graph, respectively. A time series $\{x_i\}_{i=1,2,\ldots,n}$ is mapped into a graph $G(V, E)$, while a data point x_i is converted into a node v_i in G. For any two points $v_i(i, x_i)$ and $v_j(j, x_j)$, the edge between v_i and v_j is connected based on the rule proposed by Lacasa et al. (2008), that is:

$$\forall k \in (i, j); \frac{x_j - x_k}{j - k} > \frac{x_j - x_i}{j - i} \tag{2.18}$$

Figure 2.2 shows how a time series *(7.3, 5.0, 6.2, 6.6, 5.7, 5.0, 9.1)* is transferred into a visibility graph. v_1 is the first node of the graph corresponding to the first point with a value of 7.3. The time series can be characterized with its degree sequence, mean degree, and degree distribution of the VG. For example, the degree sequence of the VG in Figure 2.2 is *(4, 2, 4, 5, 3, 3, 5)*. The mean degree $\overline{d(G)}$ is 3.71 in Figure 2.2.

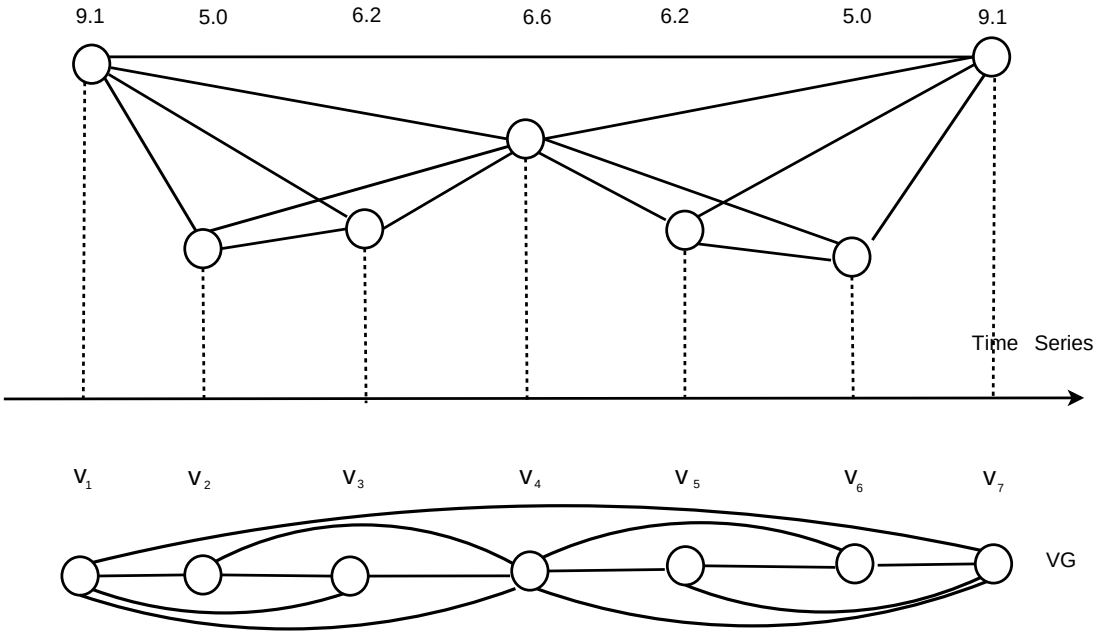

Figure 2.2: Illustration of the time series (a) and the corresponding VG

According to (Lacasa et al. 2008), a periodic time series is normally converted into a regular graph. A random signal is converted into a random graph and a fractal series is mapped into a scale-free graph. Moreover, VGs have also been employed by Shao (2010) to study heartbeat interval signals. Xiang et al. (2012*a*) used it to analyse ECG signals, and Zhu et al. (2012*b*) applied it to study sleep EEGs. However, this method cannot represented the phase space properties.

2.4.2 Horizontal visibility graphs

A horizontal visibility graph (HVG) is a kind of complex network. Normally, a time series $\{x_i\}_{i=1,2,...,n}$ is mapped into a graph $G(V, E)$, where a time point x_i is mapped into a node $v_i \in V$. The relation between any two points (x_i, x_j) are represented as an edge e_{ij} and the value is defined as

$$e_{ij} = \begin{cases} 1, & x_k < x_i \wedge x_k < x_j \\ 0, & otherwise. \end{cases} \tag{2.19}$$

where $e_{ij} = 0$ implies that the edge does not exist; otherwise it does. Figure 2.3 shows a time series as Figure 2.2 and its HVG. the degree sequence of the VG in Figure 2.3 is *(4, 2, 3, 4, 3, 2, 4)* The mean degree in Figure 2.3 is 3.14. It is noted that for the same time series, the nodes in a VG are the same as the nodes in a HVG. Similar to VGs, HVGs are also poorly to represent the phase information in a time series.

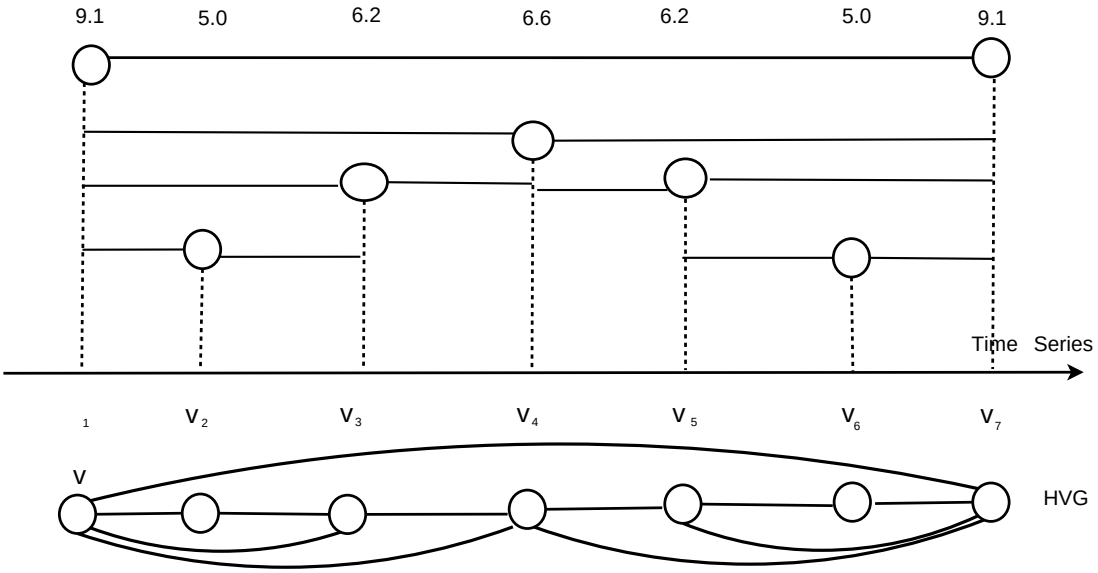

Figure 2.3: (a) An alcoholic EEG (b) and the corresponding HVG

2.4.3 Recurrence networks

Recurrence networks (RNs) encode the underlying system's recurrences in phase space and are based on a fundamental concept in classical physics. It is related to recurrence plot (RP) methods. A RR is applied to visualize the dynamical system behaviour. It calculates the two state vectors in phase space from a time series $\{x_i\}_{i=1,2,...,n}$ using the following steps:

1. Convert the time series $\{x_i\}$ into an m dimensional sequence of vectors

using a time delay λ embedding, X_m by:

$$X_m\{t\} = \{x_t, x_{t+\lambda}, \ldots, x_{t+(m-1)\lambda}\} \; ; \; 1 \leq t \leq (n - m\lambda + 1) \tag{2.20}$$

where $2 \leq m < n$.

2. Calculate the distance between two vector spaces X_i and X_i, with equation 2.21:

$$R_{i,j}(\varepsilon) = \Theta\left(\varepsilon - \|\vec{x}_i - \vec{x}_j\|\right), \tag{2.21}$$

where $\Theta(\cdot)$ is the Heaviside function and $\|\cdot\|$ is a norm.

ε is an experimental value and is used to confirm an area with ε as radius and X_i is the center. If X_j is located in this area, $R_{i,j} = 1$, otherwise $R_{i,j} = 0$. Let a black point to be represented by $R_{i,j} = 1$, the time series $\{x_i\}$ can be visualized with a graph as shown in Figure 2.4, where $\lambda = 1$. Certainly, $R_{i,i} = 1$ always holds, thus the diagonal of matrix R are full of black points.

A recurrence network can be constructed by the recurrence matrix $R_{i,j}$ from a RP, *i.e.,* it is defined as an adjacency matrix of a recurrence network by equation 2.22

$$A_{i,j} = R_{i,j} - \delta_{i,j}. \tag{2.22}$$

$\delta_{i,j}$ is Kronecker delta and is used to remove all points of $R_{i,i} = 1$. Matrix A can be viewed as an undirected graph matrix, thus RNs can be viewed as geometric graphs. Figure 2.5 shows a recurrence network associated with an EEG time series,

Donges et al. (2011) have analysed the paleoclimate with RN methods. Peng et al. (2013) used it to analyse a set of five group EEG signals.

2.5 Applying complex networks to analyse clinical EEG signals

Complex brain networks have been applied to mental health problem and the neurological sciences. From the networks' point-of-view, different brain disorders can be represented by different network topologies of CNs. The following subsections will illustrate some results for Alzheimer patients, Epileptic patients and normal sleep subjects.

2.5.1 Alzheimer's disease

Alzheimer's Disease (AD), a progressive neurodegenerative disorder, is the most common cause of dementia in humans. It slowly attacks nerve cells in brain

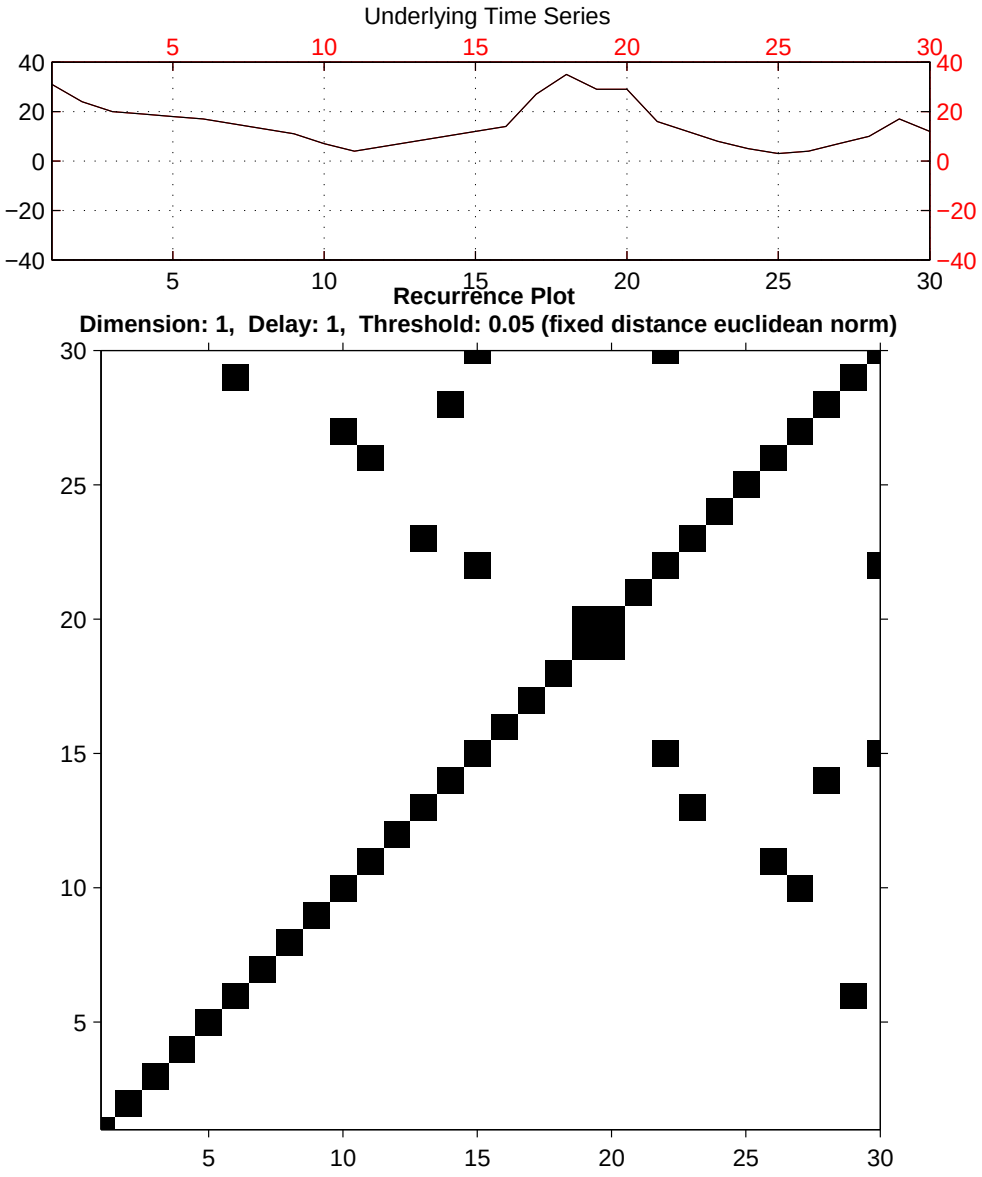

Figure 2.4: (a) An alcoholic EEG and (b) the corresponding Recurrence Plot

centers and surrounding structures, causing a loss of life skills resulting from poor memory and an inability to recognize errors. Some patients with AD will lose all memory and mental function. In Australia (Commonwealth of Australia 2012), the prevalence of dementia is growing and will increase from around 257,000 people in 2010 to just over 981,000 in 2050, with the growth rate expected to peak between 2021 and 2030 as the Baby Boomers age. Research also shows that this disease is more costly to the nation than either heart disease or cancer (Hurd et al. 2013). AD contributes to a staggering rise in health care costs, and the cost is not just monetary as AD patients require full-time 24/7 care. According

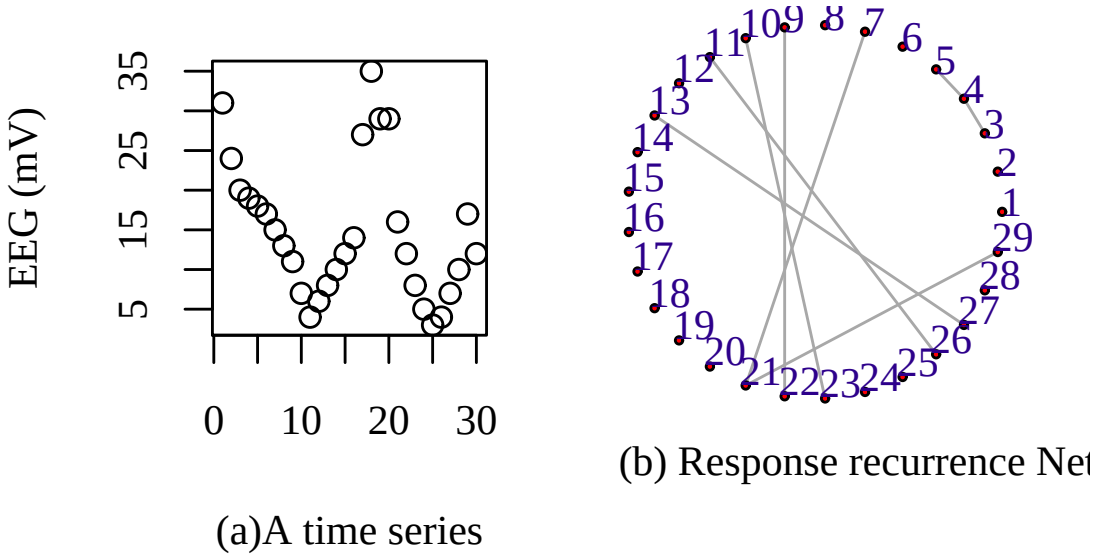

Figure 2.5: (a) An alcoholic EEG (b) and the corresponding RN

to a report from BCC Research (Zutshi 2013), with the percentage of adults over the age of 65 expected to grow worldwide over the next 40 years, the incidence of Alzheimer's Disease is expected to more than double; jumping from 21 million cases in 2010 to 53 million in 2050.

Recently, multi channel EEGs from Dementia have been applied to study brain functions using brain graphs. Adler et al. (2003) employed coherence methods to determine dementia with 87% sensitivity and 77% specificity. The Kogen research group (2001) reported that the EEG changes during long-term treatment with Donepezil in Alzhemer/s patients. Knyazeva et al. (2010) studied the dementia with phase synchrony methods. Stam et al. (2007) showed that the characteristic path length L was significantly longer in AD patients, whereas the cluster coefficient C showed no significant changes. Researchers also found that the Dementia symptoms presented during sleep (Bombois et al. 2010). Brain graphs (Tijms et al. 2013) have been also used to diagnose Dementia.

Complex networks associated with fRMI have also been used to investigate AD patients' brain function. Supekar et al. (2008) showed that a complex brain network of AD has smaller clustering coefficients C, and showed the loss of small-world properties. Buckner et al. (2009) performed an AD-related study using a complex network and fMRIs to address the spatial distribution and the stability of hub regions in intrinsic functional brain networks of humans. Wang et al. (2013) showed an increased path length of frequency-dependent brain networks from an amnestic mild cognitively impaired group.

Existing AD treatments can only offer a brief respite from some of the symptoms in some people. Clinical trials of new therapies in AD patients have, so far, been disappointing. Complex brain networks have illustrated that the AD brain graph is abnormal. Thus, a different therapy may effect the network topologies of the

brain graphs of AD patients. It is still a challenge to evaluate the AD's patients with complex brain networks.

2.5.2 Epilepsy

Epilepsy is a type of brain disorder that takes the form of recurring convulsive or non-convulsive seizures. EEG recordings can provide the information for a better understanding of epilepsy. Before complex networks were applied to study epileptic EEG signals, recurrence plots (PRs) (Ouyang et al. 2008), phase synchrony index (Mormann et al. 2000), and coherence (Takigawa et al. 1996) were applied to detect seizures. These methods, however, have not been successful in identifying seizures. Recently, complex brain networks have been developed as an efficient tool for extracting a number of measurable properties from epileptic patients.

Several studies have used these measures to better understand the properties of the epileptogenic networks. Ponten et al. (2007) applied the synchronization likelihood to find that the clustering coefficient and short path increase during seizure and post-ictal. The network trends to regularity during seizure. Schindler et al. (2008) observed that a concave-like temporal evolution of characteristic path length and cluster coefficient movement from the random towards the more regular, and then back towards to a more random functional topology. They also found that synchronizability is significantly decreased during the seizure state, but increases close to the seizure's ends. Diessen et al. (2014) reported that, the network organization after sleep deprivation in epileptic patients become more regular in the ictal state, and that this might relate to the increased epileptiform abnormalities found in patients after sleep deprivation. All these studies showed that complex networks can be helpful for epilepsy diagnosis.

2.5.3 Sleep quality measurements

Sleep is a basic and necessary human biological process as important as our need for food and drink. Learning and knowledgement is facilitated during sleep (Arzi et al. 2012), but poor sleep can cause significant personal and social problems. Therefore, it is important to evaluate sleep quality. Neural synchrony can be related, for instance, to healthy activity as in the case of the various stages of sleep. Thus, the existing sleep measuring methods are mainly measuring the synchronized, based on time or frequency domain features from EEGs. As for EOG (electrooculogram) and EMG (electromyogram) signals, these poorly studied because both of are in single channel situations in general cases. Complex networks have also used to evaluate the sleep EEG in the work of (Zhu et al. 2012*b*).

The CNs can efficiently represent the deep sleep stages. During deep sleep, the brain activity level changes dramatically. An EEG always appears as slow-wave.

Ferri et al. (2007) showed that there were high levels of synchronization in the slow-wave sleep EEG signals by means of a SL method. By analysing fMRI time series, brain networks have a higher coefficient clustering C in deep sleep than those in wakefulness (Spoormaker et al. 2012). The degrees of complex brain networks based on EEG during deep sleep are low (Bashan et al. 2012). The modularity of SCNs derived from EEG signals during deep sleep is higher than that during the awake state (Tagliazucchi et al. 2013). Boly et al. (2012) showed that the hierarchical organization of large-scale networks are modified into smaller independent modules during NREM sleep.

Some researchers have tried to map the temporal information into SCNs to study brain function (Marzano et al. 2013). However, this types of SCNs cannot work if the spatial information is lost, such as using only EEGs derived from a polysomnography (PSG). PSGs are widely used to measure clinical sleep qualities. Because a PSG contains only two or three channels of EEG signals, a SCN associated with EEG signals from the PSG is difficult to understand due to the presence only two or three nodes. Therefore, it is a challenge to study EEG signals from PSG to measure the sleep qualities with SCNs. This study will explore the individual EEG signals from a PSG with TCNs methods to resolve this challenge.

2.6 The challenges of using complex brain networks to analyse EEG signals

This section briefly reviewed complex brain networks, especially for three temporal brain complex network constructing methods: visibility graphs, horizontal visibility graphs and recurrence networks. These methods have been applied to study multi-channel EEG signals, e.g. epileptic EEGs, and sleep EEGs with various topological characteristics of spatial complex networks. However, there are many technical limitations for spatial complex networks processing EEG signals, such as single-channel EEG signals, environment noise and muscle artifact. An obvious issue is the artifact problem in EEG signals, which includes not only electrical noise, but also eye movement artifacts, such as ECG, or EMG. This issue is discussed in Chapters 5 and 9.

However, the key challenges for complex brain networks associated with clinical EEG signals are how to measure the nodes or edges that represent the biological reality. The edges of known temporal complex networks have some pitfalls, such as the binary nature of the edge. Obviously, the strengths among different functional connectivity from the same subject or the strengths among the same functional connectivity from different subjects are not the same in a real human brain. Thus, the strength should be introduced to represent brain networks. This issue is discussed in Chapters 5 and 7.

Chapter 3

Experimental EEG Data Sets

The research literature contains only one study investigating a single complex brain network (van Diessen et al. 2014, Ouyang et al. 2008), while other studies have focused on the complex brain networks using sleep subjects (Ferri et al. 2007). These studies are not enough to understand the brain function, especially for clinical purposes. For example, brain graphs are used by many researchers to represent small world networks from alcoholic, epilepsy and sleep subjects. What, then, are the differences between these brain functions? If they are the same network topologies, the complex networks are inappropriate for clinical applications. This thesis will investigate the networks between different brain functions from six different EEG databases. All of these databases are briefly described from Sections 3.2 to 3.4.

3.1 Introduction of EEG signals

An EEG signal is a fluctuation in voltage generated by postsynaptic potentials in cortical neurones over the brain scalp (Niedermeyer & da Silva 2005). There are 10^{10} neurons in the human brain, the communication between these neurons occurs by means of some tiny electrical impulses. Sometimes these electrical impulses occur at regular intervals. The electrical impulses can be obtained via two electrodes from the surface of the brain or cortex, which is named as electroencephalographic (EEG). The first EEG recording in humans was performed by Hans Berger in 1924, and this discovery was published in 1929 (Berger 1929). More and more studies began to apply EEG signals to analyse brain function for clinical or research purposes. The EEG has been widely used in epileptic diagnosis, sleep scoring and anaesthetic monitoring.

Because an EEG recording is continuous over time, the EEG measures voltage changes over time and space. There are some terms related to EEGs, such as amplitude, channel, epoch and montage. In generally, the amplitude of an EEG is measured in microvolts. The channel is the recorded voltage fluctuations be-

tween a pair of electrodes. For example, Figure 3.1 shows an EEG recording demonstration.

However, diagnosis of clinical EEG remain a challenges in sleep quality measurements (Brigo et al. 2013) and in epilepsy prediction (Mormann et al. 2007). Because EEG records are non-stationary and non-randomness signals, these non-stationary or non-randomness characteristics may be a useful physiological marker for the Epilepsy diagnosis. For example, Andrzejak et al. (2012) showed that the EEG signals from epileptogenic brain areas are less random, more nonlinear-dependent, and more stationary compared to signals recorded from nonepileptogenic brain areas. This chapter will introduce four types clinical EEG signals. All of these signals are analysed from Chapter 4 to Chapter 10 as experimental data.

3.2 Alcoholic EEG

The alcoholic EEG data used in this thesis were obtained from the University of California, Irvine Knowledge Discovery in Databases Archive UCI KDD (Bache & Lichman 2013). The data were collected from 122 subjects. Each subject completed 120 trials with three types of stimuli as shown by Zhang et al. (1997). $S1$ (one stimulus presentation), $S2M$ (one picture stimulus twice) and $S2N$ (the second test picture is different from the first time). In the case of $S2M$ and $S2N$, subjects were tasked with deciding whether the second picture was the same as the first stimulus (Zhang et al. 1997). If the decision was incorrect, the data was marked as $S2Merr$, $S2Nerr$, respectively.

Two datasets from the alcoholic EEG database were used in this study: training set *SMNI_CMI_TRAIN* and testing set *SMNI_CMI_TEST* . Each data set contains two groups of subjects: 300 records of alcoholic drinkers and 300 records of controlled drinkers. Therefore, there are 1,200 records in total, with each recorded containing the signals from 64 electrodes caps.

Figure 3.1: EEG equipment demonstration

The data sets were collected with 64 EEG electrode caps, the recording system had 61 channel EEG signals, two channel EOG siganls, and one reference electrode. The sampling frequency of these data was 256 Hz. It is not necessary to analyze all channels in all cases. Palaniappan (2002) used a genetic algorithm to select the eight optimal channels (Pz, P7, O2, FPz, TP7, P6, C1, FCz) to classify the alcoholics and controlled drinkers based on datasets TRAIN and TEST in γ band. Some studies (Rangaswamy et al. 2004, Hayden et al. 2006) used the channels: $FP1$, $FP2$, $F74$, $F3$, Fz, $F4$, $F8$, $T7$, $C3$, Cz, $C4$, $T8$, $P7$, $P3$, Pz, $P44$, $P8$, $O1$ and $O2$ for the specified measurement. Sample EEG signals from the $C3$ channel in this database are shown in Figure 3.2. $S1$ is one stimulus presentation, $S2M$ is one picture stimulus twice and $S2N$ is the second test picture and is different from the first time.

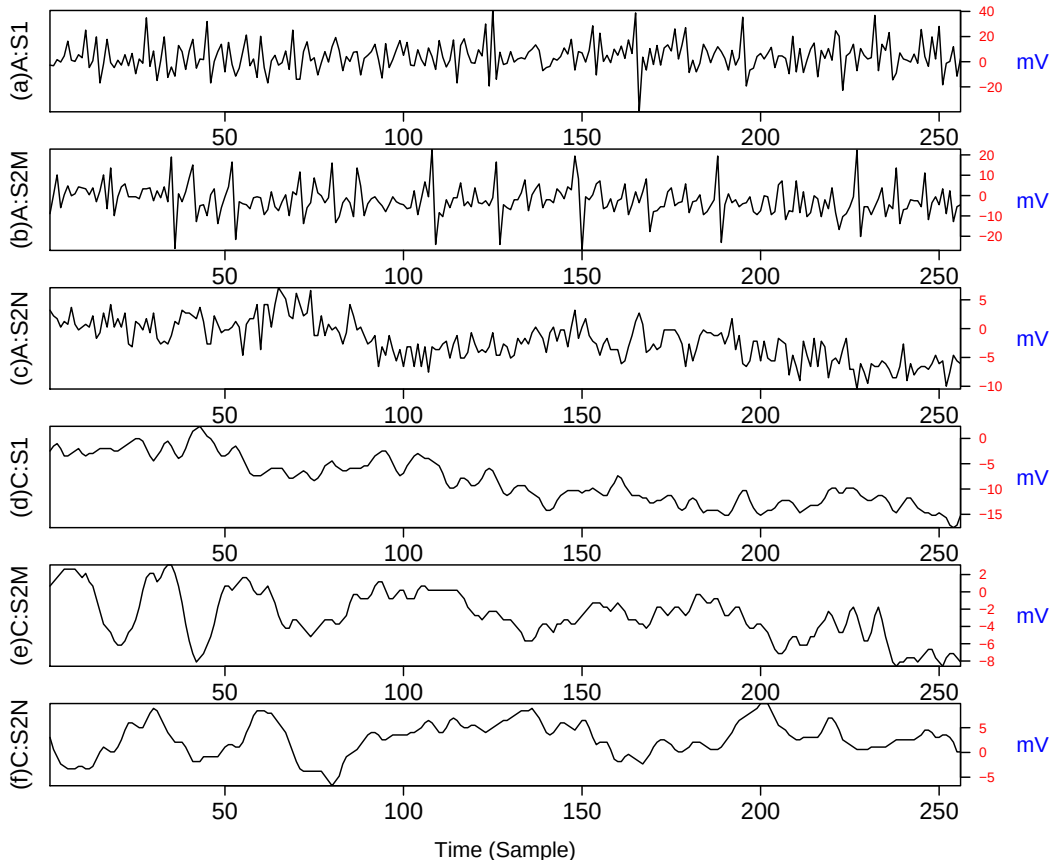

Figure 3.2: The EEG wave of alcoholic EEG (A:) and controlled drinkers (C:)

3.3 Epileptic EEG

3.3.1 Small epileptic EEG database

This thesis uses a small epileptic public EEG database which can be obtained from http://www.meb.uni-onn.de/epileptologie/science/physik/eegdata.html. The dataset

was described by Anndrzejak et al. (2001). The EEG data were digitised in 173.61 samples per second, obtained from a 12-bit A/D converter. The band-pass filter settings were at 0.53-40Hz. The whole EEG dataset consists of five groups of data sets (denoted set A-E) and each group contains 100 recordings. Sets A and B were recorded from five healthy volunteers with eyes opened and eyes closed, respectively. Sets C and D were recorded from five epileptic patients during seizure-free intervals from the opposite hemisphere of the brain and within the epileptogenic zone, respectively. Set E contains only the seizure activity EEGs. Sample recordings of five class EEG signals are shown in Figure 3.3. The total samples are 1000. Figure 3.3(a) is healthy subjects with eyes open (Set A), Figure 3.3(b) is healthy subjects with eyes closed (Set B), Figure 3.3(c) is inter-ictal on non-epileptic zone (Set C), Figure 3.3(d) is inter-ictal on epileptic hemisphere (Set D) and Figure 3.3(e) is a seizure EEG time series (Set E).

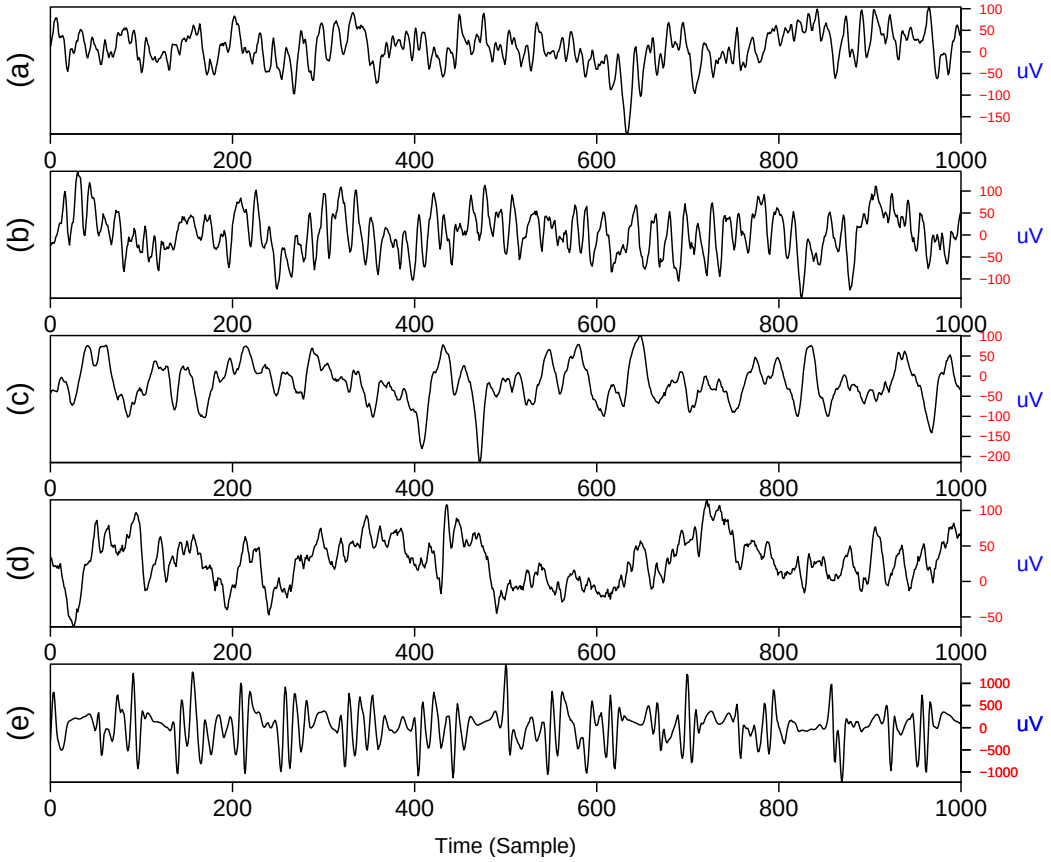

Figure 3.3: Small epileptic EEG database has five sets (set A-E)

3.3.2 Bern-Barcelona EEG database

An iEEG dataset was obtained from the public Bern-Barcelona EEG database (Andrzejak et al. 2013) collected from five patients with pharmacoresistant epilepsy. The database includes two distinct sets: one comes from EZ (denoted as Set F) and the other was recorded from brain areas that were not involved in seizure

onset (denoted as Set N). The sampling rate was 512 Hz if the number of the recording channels was less than 64. Otherwise, it was 1024 Hz.

Each dataset contains two signals: signal x is the focal EEG channel and signal y is the neighboring channel in EZ or NEZ, respectively. Each signal in each recording has 10240 data points. There is a total of 7500 recordings in the database. The detailed description and usage of this database can be found in Andrzejak et al. (2012).

3.3.3 CHB-MIT database

The seizure detectors were evaluated using the CHB-MIT database, which includes the scalp EEG recordings of 23 pediatric patients, and is available online at PhysioNet (Goldberger et al. 2000). All patients of the dataset were included in our study except for one. In the case of the exception, the entire electrode montage was altered during the recording process. The number of channels were changed in the case of some other patients as well. In these cases, 18 channels were considered and they remained unchanged throughout the whole duration of the recording. For the remaining patients, all 23 channels of the electrode montage were used. Our dataset, therefore, consists of the scalp recordings of 22 patients. A second dataset was recorded 1.5 years after the first recording of Patient 1. This recording was handled separately, resulting in 23 distinct datasets. A total of 131 seizures were recorded during 892 h of monitoring. The data were sampled at 256 Hz and a bipolar electrode montage was used. A detailed description of the dataset can be found online through the link (http://www.physionet.org/physiobank/database/chbmit).

3.4 Sleep EEG

Sleep is important for physiological functioning and mental processing. The classification of sleep stages is traditionally performed by experts based on the visual interpretation of the PSG according to Rechtschaffens and Kales ($R\&K$) recommendations (EA 1969) or a new guideline developed by the American Academy of Sleep Medicine (AASM) (Iber 2007). There are two basic sleep stages in healthy adult sleep according to $R\&K$ rules, one is nonrapid eye movement (NREM) sleep, the other is rapid eye movement (REM) sleep. The 3-state stage includes awake (AWA), NREM and REM. A 4-state stage divides the NREM into light sleep and deep sleep. The deep sleep is also named as slow wave sleep (SWS). A 5-state sleep stage sperates the light sleep into stage 1 (S1), stage 2(S2). The 6-state sleep stages in $R\&K$ standard consists of AWA, S1, S2, stage 3 (S3), stage 4 (S4) and rapid eye movement (REM). In this case, stages S1, S2, S3 and S4 are denoted as non-rapid eye movement (NREM). While in the AASM standard, the NREM is divided into stage N1, stage N2, and stage N3 (deep or delta-wave sleep).

EEG is well established for assessing the functional states of the human brain. During deep sleep, the brain activity level change dramatically. The various sleep stages can be identified using EEG signals. The literature shows that the most progresses has been made in the frequency-domain and/or time-domain. For the sleep stages classification, S1 stage is characterized by alpha (8-12.5 Hz) and theta (4-8Hz) frequency components of the EEGs, as well as some slow, rolling eye movements. S2 stage is easing recognized by recognizing the spindles and K-complexes (12-14Hz) in the EEG waves. Stages S3 and S4 are similar and combined as a SWS, appeared in the frequency of 0-4Hz. All of these four sleep stages are also named as NREM, REM sleep stage occurs during dreaming. The *R&K* standard also includes a special sleep stage marking as REM plus movement (MVT) sleep stage. Sample recordings of sleep EEG signals are shown in Figure 3.4.

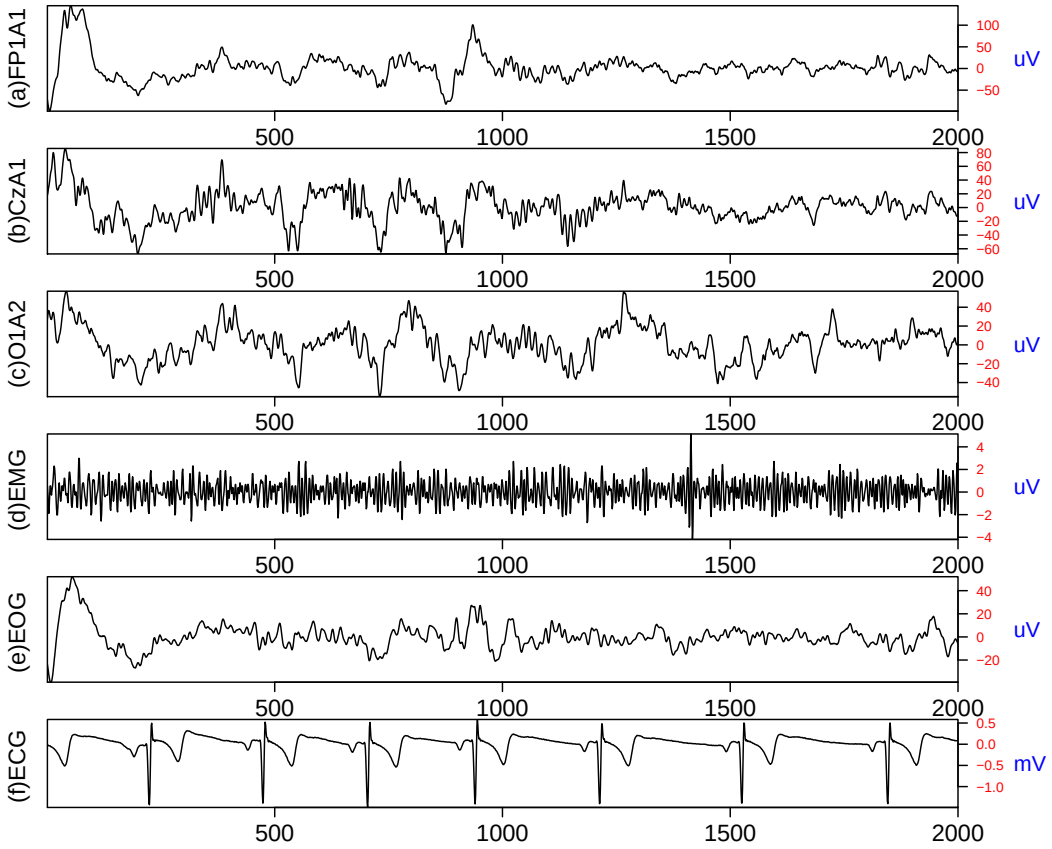

Figure 3.4: The structure of the Sleep EEG

The experimental data used in this thesis was obtained from two public sleep EEG databases. The database records were derived from PSG devices.

3.4.1 Sleep EDF databases

The Sleep-EDF database (Kemp 2013, Kemp et al. 2000) is part of Physionet data bank (Goldberger et al. 2000). Data recordings from eight subjects in this database were used across the thesis. The first four data were recorded in 1989 from ambulatory healthy volunteers and the last four data were recorded in 1994 from subjects suffering from mild problems failling asleep. The recording data of each subject is saved in an EDF-File (Kemp et al. 1992) and each file of the sleep recordings includes one horizontal EOG, and two EEG channels (FpzCz and PzOz). The sampling frequency was 100Hz. Band-pass filters were set as 0.0350 Hz.

The information from the sleep subjects are summarized in Table 3.1. Because the hypnogram was generated by experts every 30 seconds, the interval of each segment (or epoch) in this study was defined as 30 seconds, and thus each signal in one segment contains 3000 data points. The original sleep stages of these segments are labeled with one of the eight classes: AWA, S1, S2, S3, S4, REM, MVT and UNS (unknown states).

3.4.2 Dream Sleep databases

The second EEG dataset was acquired at a sleep laboratory of a Belgium hospital using a digital 32-channel polygraph (BrainnetTM System of MEDATEC, Brussels, Belgium), named the Dream sleep EEG database (DEVUYST, 2013). Polysomnographies were recorded from 20 healthy subjects through one whole night. Three EEG channels (CzA1, Fp1A1 and O1A1) were used. The standard European Data Format (EDF) (Kemp et al. 1992) was used for storage. The sampling frequency was 200Hz. Band-pass filters were set as 0.1670 Hz. These recordings were specifically selected for their clarity and the volunteers were free of medication. Table 3.2 summarizes the test subjects in this database.

Table 3.1: The information of subjects in Sleep EDF database

Subject	Night	Age	Sex	LightsOff	Subject	Night	Age	Sex	LightsOff
0	1	33	F	0:38	21	1	51	F	23:28
0	2	33	F	21:57	21	2	51	F	23:59
1	1	33	F	22:44	22	1	56	F	23:47
1	2	33	F	22:15	22	2	56	F	23:14
2	1	26	F	22:50	23	1	50	F	0:51
2	2	26	F	22:57	23	2	50	F	0:32
3	1	26	F	0:02	24	1	54	F	23:22
3	2	26	F	0:24	24	2	54	F	22:50
4	1	34	F	23:12	25	1	56	F	0:32
4	2	34	F	23:35	25	2	56	F	23:49
5	1	28	F	1:22	26	1	51	F	23:39
5	2	28	F	0:35	26	2	51	F	0:20
6	1	31	F	0:16	27	1	54	F	23:41
6	2	31	F	22:44	27	2	54	F	22:58
7	1	30	F	0:36	28	1	56	F	23:55
7	2	30	F	0:41	28	2	56	F	0:13
8	1	25	F	23:35	29	1	51	F	22:38
8	2	25	F	23:37	29	2	51	F	23:04
9	1	25	F	23:02	30	1	50	M	0:09
9	2	25	F	23:01	30	2	50	M	0:20
10	1	26	M	22:59	31	1	54	M	23:44
10	2	26	M	23:07	31	2	54	M	23:14
11	1	26	M	23:00	32	1	57	M	0:48
11	2	26	M	1:14	32	2	57	M	0:15
12	1	26	M	0:50	33	1	60	M	22:58
12	2	26	M	1:03	33	2	60	M	22:55
13	1	27	M	0:14	34	1	54	M	23:03
14	1	27	M	22:55	34	2	54	M	22:30
14	2	27	M	23:22	35	1	57	M	0:02
15	1	31	M	23:56	35	2	57	M	23:30
15	2	31	M	23:38	36	2	51	M	23:59

Table 3.2: The information of subjects in Dream Sleep databases

Subject	Age	Sex	Duration
subject1	23	F	08:00:40
subject2	47	F	08:12:30
subject3	24	F	08:24:20
subject4	48	F	08:46:30
subject5	46	F	08:51:30
subject6	65	F	08:18:40
subject7	45	F	08:26:00
subject8	22	F	08:05:00
subject9	21	F	09:18:40
subject10	20	F	08:36:20
subject11	30	F	08:24:10
subject12	54	F	08:00:40
subject13	23	F	09:15:40
subject14	57	F	08:22:10
subject15	20	F	07:00:00
subject16	27	F	08:03:50
subject17	23	M	08:18:30
subject18	27	M	08:30:40
subject19	27	M	08:36:50
subject20	20	M	09:32:30

Chapter 4

Analysing Epileptic EEG Signals with Visibility Graph Algorithms

This chapter analyzes the human Epileptic Electroencephalogram (EEG) based on a visibility graph algorithm. An EEG time series is mapped into a visibility graph (VG). Then a mean degree, a degree distribution and one graph entropy are extracted from each VG. The chapter shows that the mean degrees on VGs associated with epileptic EEG signals are larger than those associated with healthy subjects. Similar to mean degrees, the graph entropies of VGs associated with healthy subjects is lower than those associated with epilepsy. The number of nodes v_i with $d(v_i) = 5$ on a VG from healthy subjects are significantly different from those of epileptic subjects. The mean degree, graph entropy and the number of nodes with $d(v_i) = 5$ or $d(v_i) = 8$ are used as features to discriminate the ictal EEG signal from healthy EEGs with eyes opened, healthy EEGs with eyes closed, two inter-ictal EEGs.Experimental results demonstrate that the features of VGs can achieve a high classification accuracy allowing the identification of seizures based on EEG signals. The related work was presented in Zhu et al. (2012*a*) and Wang et al. (2014).

This chapter is organized as follows: the known results of previous seizure identification work. represented in the literature is briefly introduced in the next section. A brief for graph entropy and A nonlinear discriminant classifier are introduced in Section 4.2. Section 4.3 presents the experiment results from this study. The existing results of healthy subjects, inter-ictal EEGs and ictal EEGs are compared with the proposed VG method. Finally, the discussion is presented in Section 4.4.

4.1 Introduction

At some stage of their lives, approximately 1% of the world's population will suffer from Epilepsy, a disorder of the brain. Electroencephalogram (EEG) could help to

diagnose the symptoms of Epilepsy. Epilepsy symptoms have two categories: ictal symptoms, which are an expression of the actual seizure; inter-ictal symptoms, when patients are not having any seizures. Traditional ictal detection using EEGs is very time consuming because seizures are occur randomly and produce huge volumes of EEG data. Thus, automatic seizure detection is an important tool in the diagnosis of Epilepsy.

It is difficult to identify the seizure using EEG data directly because the EEG data is in high dimension. The raw EEG data are needed to extract the lower dimension features to send into a classifier to enable the identification the seizure or ictal. Osorio et al. (1998) reported that any attempts at detecting seizures must be based on the recognition of power and frequency features from the EEGs. Polat et al. (2007) used the power spectrum density (PSD) features to distinguish the healthy EEGs and ictal EEGs for a 98.72% accuracy with a 10-fold cross-validation. Using the same data, Iscan et al. (2011) combined PSD and cross-correlation to increase the accuracy to 100%. Subasi et al. (2005) used a wavelet transform to classify the EEGs of healthy subjects and seizure activity with a 93% accuracy. Nonlinear features, such as Lyapunov exponents (Güler et al. 2005, Adeli et al. 2007), permutation entropy (Nicolaou & Georgiou 2012), have also been used to discriminate healthy subjects, the ictal and the inter-ictal EEGs. The Lyapunov exponents method resulted in a 96.79% accuracy. The permutation entropy method provided 100% accuracy for healthy and seizure subjects. Siuly et al. (2011) used a clustering technique for feature extraction, classifying healthy versus ictal with 99.9% accuracy, and classified the healthy versus the inter-ictal with 84.9% accuracy.

In contrast, with conventional power and frequency methods, this study uses the degree distribution features based on a visibility graph method to detect the seizures. VG methods were proposed by Lucasa et al. (2008). A VG is mapped from a time series signal into a graph according to geometric visibility features. A periodic time series can be converted into a regular graph, a random signal into a random graph and a fractal series into a scale free graph. VG methods have been widely used to study multifractal stochastic processes (Ni et al. 2009) and the nonlinear properties of financial data (Yang et al. 2009). Moreover, VG methods have been used to analyse human heartbeat dynamics by Shao (2010). Shao (2010) has shown that the degree distribution ($p(k)$) of the heart beat interval based VGs satisfied the power law. In other words, $p(k) = k^{-3}$. Dong and Li (2010) claimed that it was not easy to identify a healthy from a congestive heart in the long time series with a VG method. In our previous our study (Zhu et al. 2012*a*), mean degree and degree distributions of VGs have been applied to identify seizures. However, the graph entropy and variants of degree distributions of VGs have never been used in epileptic EEG analysis although other graph-based methods have been used to study epileptic EEGs (Reijneveld et al. 2007). This study shows that the ictal EEGs can be identified with the graph entropy and the variants of degree distribution of VGs.

4.2 Experimental data and methods

The automatic epileptic classification diagram is shown in Figure 4.1. It is noted that the raw EEG signals are mapped directly into a VG without any frequency domain preprocessing.

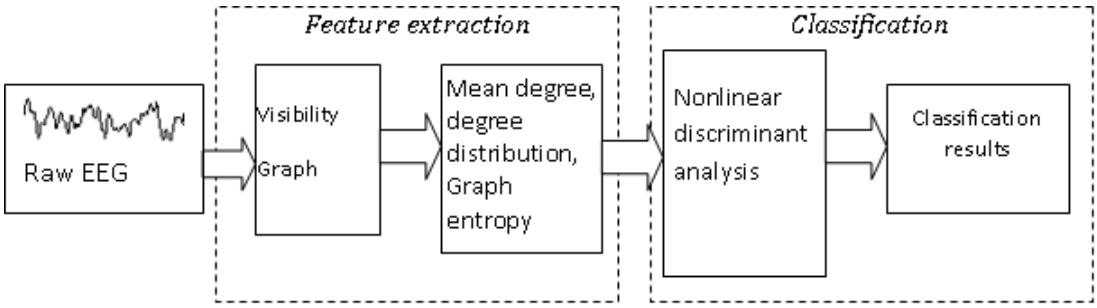

Figure 4.1: Block diagram of the proposed VG methods for EEG signal classification.

4.2.1 Experimental data

The epileptic EEG datasets described by Andrzejak et al. (2001) were used in this chapter. This EEG dataset used, was introduced in Section 3.3.1. This chapter used all five sets of data: Set A to Set E. Each data set contained 100-single channel EEGs for 23.6s from five healthy volunteers and five epileptic patients. The size of a segment of each EEG is 4097 points.

4.2.2 Mean degrees and degree distributions of epileptic EEGs

In this chapter, the mean degree of a VG and its degree distribution (DD) are extracted as key features for seizure detection. The mean degree definition can be referred to Chapter 2. The DD is the probability distribution $p(k)$ of k degrees versus k over a graph, which is obtained by counting the number of degree k and dividing it by the total number of nodes N. Futher detail can found in Section 2.1.2.

According to Bullmore and Sporns (2009), the DD of a complex network does not not appeared as a pure power-law distribution on low degree nodes. Therefore, the low degree nodes can be used to classify ictal EEG signals from health signals and inter-ictal EEG signals. This chapter will investigate the mean degree, variants of the DD of VGs from set A to set E.

4.2.3 Graph entropy

There are several graph entropies based on graph vertex or edges (Dehmer & Mowshowitz 2011). This study defines the graph entropy (GE) with the Shannon's entropy formula (2001) measurement as follows:

$$h = -\sum_{k=1}^{n} p(k) log(p(k)) \tag{4.1}$$

where $p(k)$ is the degree distribution of graph G. However, a graph has only one GE value but has variants of degree distribution.

4.2.4 Nonlinear discriminant analysis

The linear discriminant analysis (LDA) is a method for classifying a set of observations into predefined classes. Because LDA assumes that the probability density functions of the extracted features satisfy a normal density, the accuracy of LDA to classify EEG signals normally show a poor performance compared to the support vector machine (Garrett et al. 2003). However, Subasi and Gursoy (2010) reported that the accuracy of identifying Set A from Set E is 100% by a LDA classifier. In this study, equation 4.2 which is used to identify seizure sets from other sets, is in the form of:

$$L = w_1 * \bar{d} + W_2 * p(5) + w_3 * p(8) + w_4 * GE \tag{4.2}$$

where $\bar{d}$ is the mean degree, $p(5)$ and $p(8)$ are the DD values when the node degrees are five and eight, and GE is the graph entropy. However, L_1 is not in a high score for Sets C, D and Set E.

To improve the performance of identifying seizure from inter-ictal EEG signals, a quadratic discriminant analysis (QDA) was selected to distinguish Set E from Sets A, B, C, and D. Let X be the vector features of a VG (including GE, mean degree and DDs), the optimal classifier which can be derived from equation 4.3.

$$Q(x) = (X - \bar{X_1})L_1^{-1}(X - \bar{X_1}) - (X - \bar{X_2})L_2^{-1}(X - \bar{X_2}) + log|L_2^{-1}L_1| \tag{4.3}$$

while $L = \{L_1, L_2\}$ is the pooled sample covariance matrix of equation 4.2. Therefore, equation 4.2 is mainly used to classify Set A versus Set D; and Set A versus Set E. In this study, the LDA and QDA were conducted using an R package: MASS (Ripley et al. 2012).

4.2.5 Accuracy, sensitivity, specificity, precision, recall and F-value

In order to evaluate the performances of the methods proposed in this chapter, the accuracy (AC), sensitivity (SE), and specificity (SP) are assessed for the EEG classification. These parameters are defined below:

$$SE = \frac{TP}{TP + FN} \tag{4.4}$$

$$SP = \frac{TN}{TN + FP} \tag{4.5}$$

$$AC = \frac{TN + TP}{TN + FN + FP + TP} \tag{4.6}$$

Where TP=correctly classified seizure EEG, TN=correctly identified non-seizures EEG, FP=falsely identified ictal EEG and FN=falsely recognized non-seizure EEG. There are another measure methods for the classification, such as precision, recall and F-value. Although it isn't used widely in EEG signals classifying, these paraments still are considered to outcome the novel algorithms in this thesis.

$$PR = \frac{TP}{FP + TP} \tag{4.7}$$

$$RE = \frac{TP}{FP + FN} = SE \tag{4.8}$$

$$F_v = \frac{2PR * RE}{PR + RE} \tag{4.9}$$

Where PR used to indicate the probability that the patient really has the seizure during a seizure test, which is also named as positive predictive values. RE measures the proportion of actual positives which are correctly identified as seizure, which is the same as SE. and F_v is uses to measure the test's accuracy, which is also named as F-Score or F-Measure.

4.3 Results

To evaluate the performances of the VG method and the features discussed in Section 4.2, the algorithm is implemented with R programming language in Windows 7 with 3.0G Hz Inter CoreTM Duo E8400 processor and 4GB of RAM. The total segments from sets A to E are 5000. The experiments consist of three parts:

1. The calculations of the mean degrees on Sets A, B, C,D and E;
2. The statistical analysis of the graph entropy of Sets A, B, C, D and E;.
3. The analysis of the degree distributions of Sets A, B, C, D and E.

4.3.1 Mean degrees of VGs from epileptic EEGs

The maximal value, minimal value and mean value of degrees on a VG from each dataset are calculated and the box statistical plot is presented in Figure 4.2. The left is healthy subjects with eyes open (Set A), next is healthy subjects with eyes closed (Set B), inter-ictal of non epileptogenic zone (Set C), inter-ictal of epileptogenic zone (Set D) and ictal (Set E).

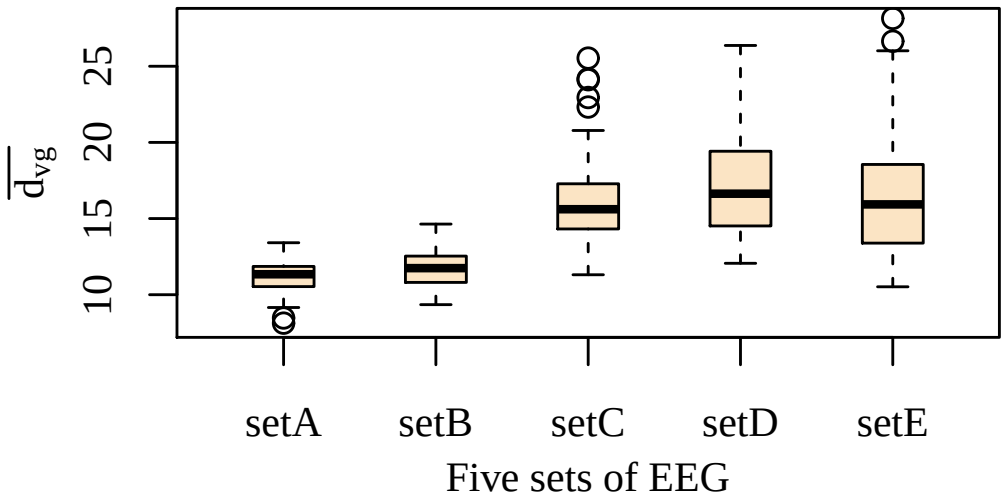

Figure 4.2: The mean degree of VGs associated with five type EEGs

Figure 4.2 shows that the statistical degree values of the mapped VGs of Sets A-E. It is clear that the mean degree of Set A is significantly different from Sets C, D and E. However, Sets C, D and E only have a slight difference.

4.3.2 Graph entropies of VGs from epileptic EEGs

Next, the GEs of five types of EEG signals are investigated. Figure 4.3 shows the statistical graph entropy of VGs associated from Sets A-E. The left is healthy subjects with eyes open (Set A), followed by healthy subjects with eyes closed (Set B), inter-ictal of Set C, inter-ictal of Set D and ictal (Set E). Figure 4.3 clearly shows that the GEs of VGs associated with Set D are significant larger than those of other sets. In contrast to Figure 4.2, the lowest GE of the five sets is Set B instead of Set A in Figure 4.3.

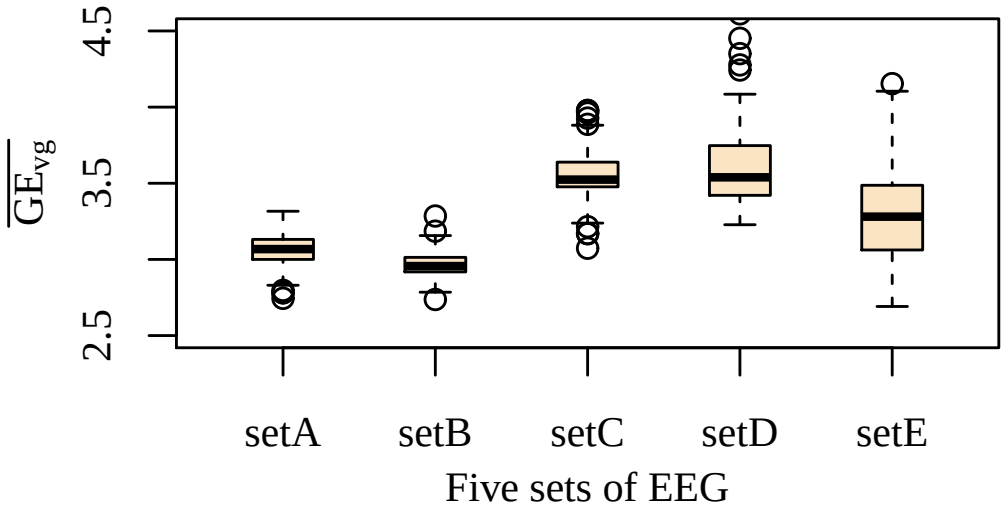

Figure 4.3: The mean degree of VGs associated with five EEG signals

4.3.3 Degree distribution on low degree nodes

Figure 4.4 shows the DDs from $d(v_i) = 4$ to $d(v_i) = 8$ of VGs associated with five groups of EEG signals. It is clear that the nodes with a small degree do not satisfy the power-law, agreeing with the conclusion reported by Bullmore and Sporns (2009) that physically embedded networks often do not have pure power degree distributions. It is obviously that the DDs for those of degrees less than three are not significantly different. The degree from five to eight of DD in Set A is more different from those of other sets as shown in Figure 4.4.

4.3.4 Classification results

The extracted features from five types of EEG sets were spilt into one training set and a testing set during classification. There were 100 channels of data made up of 4097 points for each class in total. Half (50*5=250) of them were used as the training data and the remaining (250) were used as the testing data.

The agreements in identifying Set E from other four groups of EEGs between a manual scoring and LDA, QDA two automatic methods are shown in Table 4.1. The average agreement with an expert is 97.3%. The highest classification obtained between set A and set E from Table 4.1 is 100%.

It is clear that the accuracies using QDA are better than those of LDA when the two groups' data are of equal size, but the accuracies of the former are lower than those of latter when the two group proportions different, especially to detect the Set E from Sets A, B, C and D. These results demonstrate that QDA is more suitable than LDA for classifying unbalanced EEG data sets. It is also shown

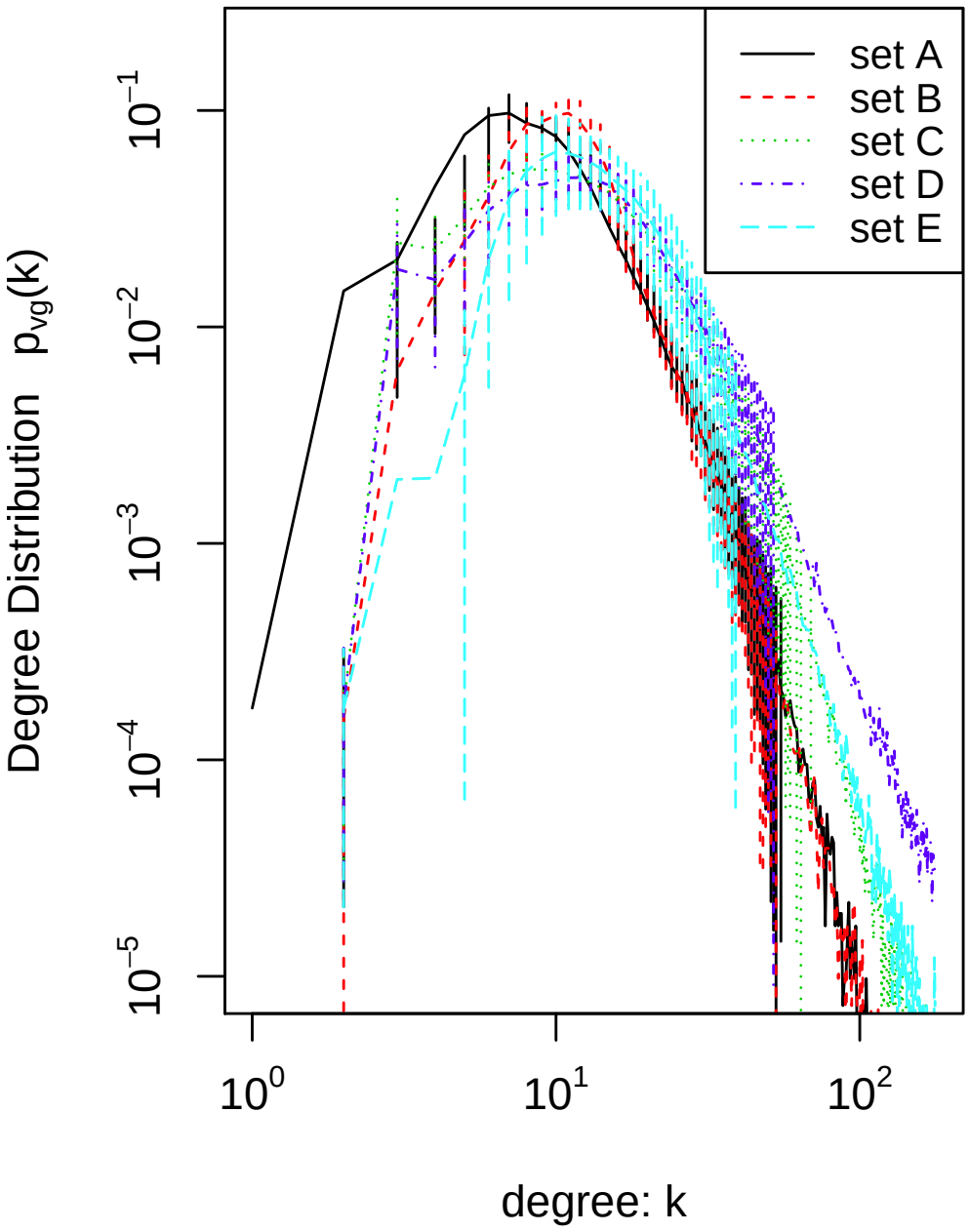

Figure 4.4: The illustration of the mean DD from sets A, B, C, D and E

that the seizure can be efficiently identified from the healthy EEG groups even the subjects closed their eyes.

The computation times extracted the GE and mean degree based on the VG

Table 4.1: The classification accuracy of Set E vs Sets A,B,C,D and (A,B,C,D) with 4097 data points per segment and LDA, QDA classifier.

Data group	*LDA*				*QDA*			
	SE	SP	AC	F_v	SE	SP	AC	F_v
Set A vs Set E	0.97	1.00	98.5%	0.99	1.00	1.00	100%	1.00
Set B vs Set E	0.87	1.00	93.0%	0.93	0.99	0.99	99.0%	0.99
Set C vs Set E	0.95	1.00	97.5%	0.98	0.99	0.98	98.5%	0.98
Set D vs Set E	0.89	0.96	92.0%	0.92	0.93	0.94	93.5%	0.93
Sets (A, B, C, D) vs Set E	0.92	0.98	92.6%	0.82	0.98	0.69	90.2%	0.91

method for 500 segments (2000 seconds) EEG records is 42.92 seconds, which can be accepted for off-line analysis. The experiments are implemented on a computer with 3.2G Hz Inter Xeon(R)W5580 eight processor, 24GB of RAM and 64 Windows 7. However, one second EEG recoding needs 21 ms processed isn't suitable for real time analysis.

4.4 Discussions

4.4.1 Network topology changes with seizure

These phenomena suggest that the performances of the classification for Set E vs Set A and Set E vs Set C are better than the classification performance for Set E vs Set D. This explains why the existing research has shown that the accuracy of identifying Set E from Set A is higher than that from Set D (2011, 2012*a*).

As shown in Figure 4.4, when degree $k > 8$, three DDs exhibit the power law behaviour. The power law exponents of Set A is about -3, and the power law exponents of Set D and Set E is about -2.5. However, when degree $k < 9$, a strong wave was shown in Set E. These phenomena imply that the number of nodes with a very small degree or a very large degree is lower than the number of nodes with degree between five and 15.

Let us show how well the number of nodes with a small degree can be used to classify the seizures and healthy subjects. In Figure 4.4, $p(k)$ of Set A based on a VG from $k = 8$ is clearly lower than those from Set D and Set E. However, Set D and Set E could not be easily classified after the degree is larger than 12, as shown in Figure 3. Therefore, it is necessary to use a nonlinear discriminant analysis to classify these two cases. The degree of VG in seizure onset is lower than those in the inter-ictal state, which is also consistent with the known results

in Kolaczyk and Kirsch (2008).

4.4.2 Compared to other existing methods

To verify the classification performances with the degree parameters on a VG graph, we compare the results of our proposed algorithm with the existing results shown in Table 4.2.

Table 4.2: Classification accuracies from the literature and the proposed VG method for the same datasets

Researchers	Features	Classifier	Datasets	Accuracy	Epoch length
Subasi and Gursoy (2005)	Wavelet	LDA with SVM	A, E	100%	4096
Polat and Gne (2007)	PSD	Decision Tree	A, E	98.72%	256
Guo et al. (2011)	DWT	ANN	A, E	99.6%	4098
Zhu et al. (2013)	Entropy	MSK-means	A, E	100%	1024
Nicolaou and Georgiou (2012)	PE	SVM	A, E	93.42%	1024
			C, E	88.83%	1024
Fernandez-Blanco et al.(2012)	Star graph	ANN	A, E	99.95%	2048
			B, E	96.58%	2048
			(A,B,C,D), E	97.8%	2048
The proposal method	MD and DD of VG	QDA	A, E	100%	4097
			B, E	99.0%	4097
			(A,B,C,D), E	90.2%	4097

The classification (accuracy for seizure and healthy subjects) by the proposed VG method is 100% as shown in Table 4.2. The classification accuracy for Set B and Set E of all methods is also higher, 99.0%.

4.5 Chapter Summary

In this chapter, the graph entropy and degree parameters of a visibility graph method have been used to identify ictal EEG signal from other signals. The mean degree, graph entropy and degree distribution of a VG have been employed to study the differences between two groups of healthy EEG signals, two groups of inter-ictal EEG signals and one type of seizure activity EEGs. The experiments have shown that the mean degrees and graph entropy from healthy EEGs are significantly different from the epileptic EEGs. The experimental results showed that the DDs of a VG on healthy and epileptic EEGs approximately satisfy the power-law. However, the nodes with a small degree of VG from healthy subjects illustrate a significant different from those from epileptic patients. Based on the study results, the inter-ictal and seizure activity EEGs could be distinguished from the low DDs with a nonlinear discriminate analysis. The optimal features are used for the classification. A higher accuracy of 99.0% between healthy subjects with eyes closed and seizure patients is obtained. Because recording EEG are always a boring and long procedure, subjects can easily close their eyes to rest them. The method presented in this chapter better identifies the seizure from the healthy even when subjects close their eyes. However, the speed of constructing VG graphs from one second EEG record is still slow. Chapter 5 will introduce the linear speed of an algorithm to construct a time series to a graph.

Chapter 5

A Fast Horizontal Visibility Graph Algorithm

Chapter 4 proposed a VG based method for identifying ictal EEG from healthy EEG with 100% accuracy. However, the speed is unacceptable slowly for real time applications. This chapter proposes a linear complexity weighted horizontal visibility graph constructing algorithm (FWHVA) to identify epileptic EEG signals. The performance of the FWHVA is evaluated by comparing with Fast Fourier Transform (FFT) and sample entropy (SampEn) methods. The graph features, mean degree and mean strength, is investigated using two chaos signals and five groups of EEG signals. Experimental results show that features extracted using the FWHVA are faster than those of SampEn and FFT. The mean strength features associated with ictal EEG are significantly higher than those of healthy and inter-ictal EEGs. In addition, a 100% classification accuracy for identifying seizure from epileptic EEG shows that the features based on the FWHVA are more promising than the frequency features based on FFT and entropy indices based on SampEn for time series classification. Related work was presented in (Zhu, Li & Wen 2014*b*).

This chapter is organised as follows: the feature extraction of EEG signals is presented in the next section. The FWHVA method is illustrated in Section 5.2. Section 5.5 investigates the computing speed and robustness of against-noise. The performances of the FWHVA are tested by two types of chaos signals in Section 5.5 and applied to identify epileptic EEGs in Section 5.6. The discussions of the advantages and disadvantages of the proposed method are illustrated in Section 5.7.

5.1 Introduction

Feature extraction is an essential procedure for analysing and classifying time series, especially for EEG signals (Guo et al. 2011). There are two main methods

for extracting features from a given time series: linear and nonlinear methods. Conventional linear methods are based on frequency domain (Srinivasan et al. 2005) or time domain (Ansari-Asl et al. 2006). Fast Fourier Transform (FFT) has been widely applied in time series analysis, especially for epileptic EEG signal classification. The power spectral density (PSD) feature (Polat & Güneş 2007) based on FFT can be identified seizure efficiency. However, frequency domain is not sufficiently robust enough to represent inter-ictal epileptic signals because the raw EEGs are chatic and nonlinear (Pritchard et al. 1995).

The human brain consists of many nonlinear neuron cells. The neuron system is complicated and nonlinear. As a result, many researchers have begun to consider the nonlinear method to extract the nonlinear features from EEG signals. Correlation dimension features from ictal signals (Andrzejak et al. 2001, Adeli et al. 2007) are smaller than those from inter-ictal EEG signals. A series of entropies (Bai et al. 2007, Nicolaou & Georgiou 2012) are widely applied in epileptic EEG detection. The largest Lyapunov exponent (Adeli et al. 2007) from healthy EEG signals are larger than those of inter-ictal signals. Recurrence plot features (Thomasson et al. 2001, Ouyang et al. 2008) are also employed to identify ictal signals. Tang et al. (2013) analysed visibility graphs (VGs) from higher band frequencies of seizure EEGs and showed that the performance of the VGs based approach is better than that of the simple entropy method. Zhu et al. (2012*b*) also implemented VG based features to identify the ictal EEGs from healthy EEGs with a 100% accuracy. However, many nonlinear feature extraction algorithms are slower than the FFT method, which making them hander to implement in real time applications.

This chapter presents a fast weighted horizontal visibility algorithm (FWHVA) to classify epileptic EEG signals in linear complexity. Similar to the PSD features based on FFT from frequency domain, strength and degree features are investigated based on the FWHVA from the graph domain. Two chaos signals, with white noise added, are also applied to evaluate the robustness and computing speed by the features from FWHVA, FFT and SampeEn. Five groups of EEG signals: two groups of normal EEGs, two categories of inter-ictal EEG signals and one type of ictal EEGs, are used to investigate the classifying performance when features are extracted from the graph, frequency and time domain separately.

5.2 Methodology and experiment of design

This chapter uses a small epileptic EEG database, which was described in Section 3.3.1. Five sets analysed in this chapter. Sets A and B were recorded from five healthy volunteers with eyes open and eyes closed, respectively. Sets C and D were recorded from five epileptic patients during seizure-free intervals from the opposite hemisphere of the brain and within the epileptogenic zone, respectively. Set E contains only seizure activity EEGs.

The automatic epileptic EEG detection method is shown in Figure 5.1. It is

a two-stage classification procedure. The first stage involves feature extraction, which maps a raw EEG signal into a WHVG. At this stage, two features, the mean degree and mean strength, are obtained from each graph. The second stage involves the classification, which uses the K-NN classifier to identify the seizures.

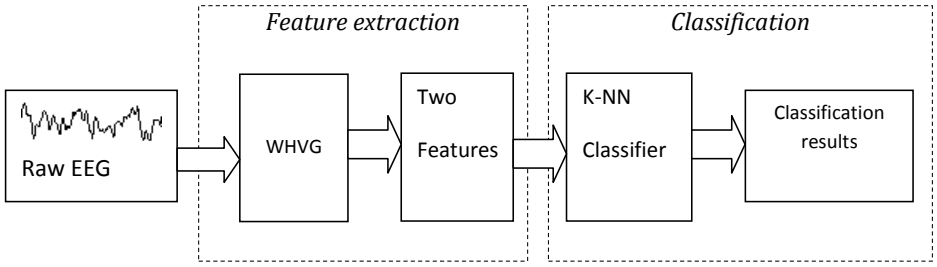

Figure 5.1: Block diagram of epileptic EEG classification with FWHVA

5.2.1 Limitation of horizontal visibility graphs

A horizontal visibility graph (HVG) is a type of a complex network proposed by Luque et al. (2009). It has been widely used in time series analysis, as shown in Section 2.4.2. However, its ability to distinguish between monotonic (consistently increasing or decreasing) time series and a constant time series is limited.

As shown in Figure 5.2, the first five data points $Y1 = \{-310, 93, 494, 789, 798\}$ increase and last three data points $Y2 = \{106, -326, -623\}$ decrease. But $DS(Y1) = \{1, 2, 2, 2, 2\}$ and $DS(Y2) = \{2, 2, 1\}$, which make HVG of increase time series is similar to those of decrease sequence. The degree sequence of Figure 5.2 (b) shows that HVGs cannot be used to distinguish between monotonic (consistently increasing or decreasing) time series and a constant time series. In fact, seizure EEGs always include many spike waves, as shown in Figure 5.2(a). Therefore, it is necessary to introduce improved graph features to enhance the performance of spike waves identification.

5.2.2 Weighted horizontal visibility graph

This section introduces a weighted graph to help to discriminate between monotonic increase (or decrease) time series and constant time series as shown in Figure 5.2. A weighted horizontal visibility graph associated with a time series $\{x_i\}_{i=1,2,\ldots,n}$ is denoted as $G(V, E, W)$. The weight W_{ij} of edge E_{ij} between nodes

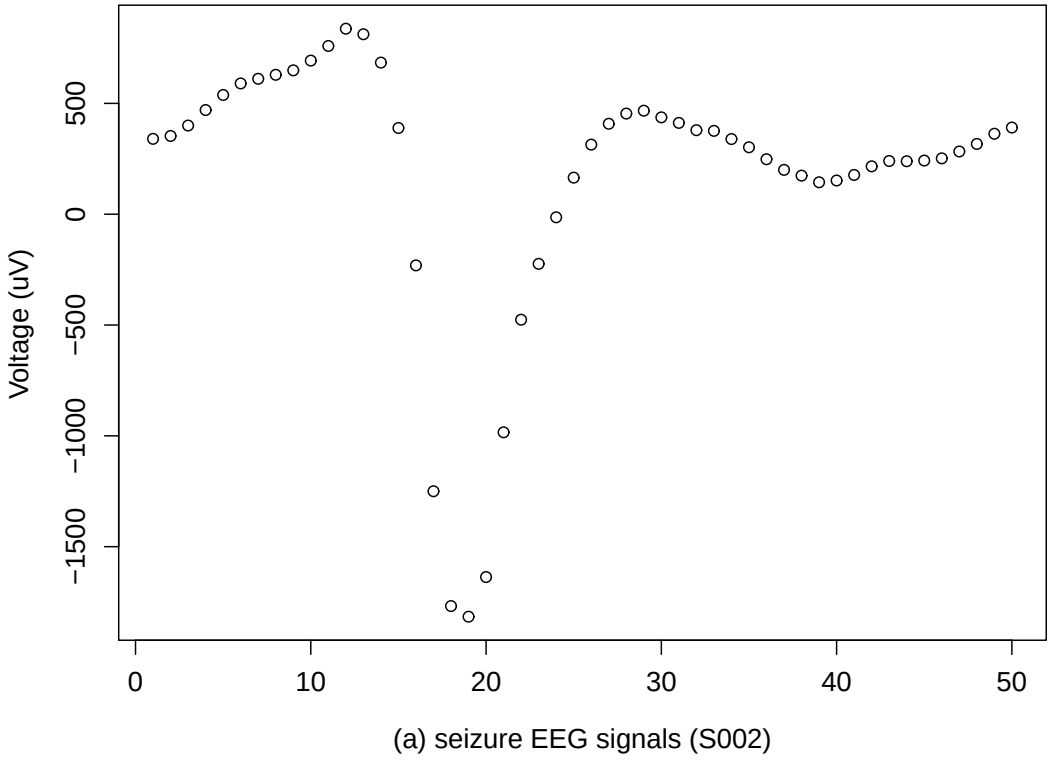

(a) seizure EEG signals (S002)

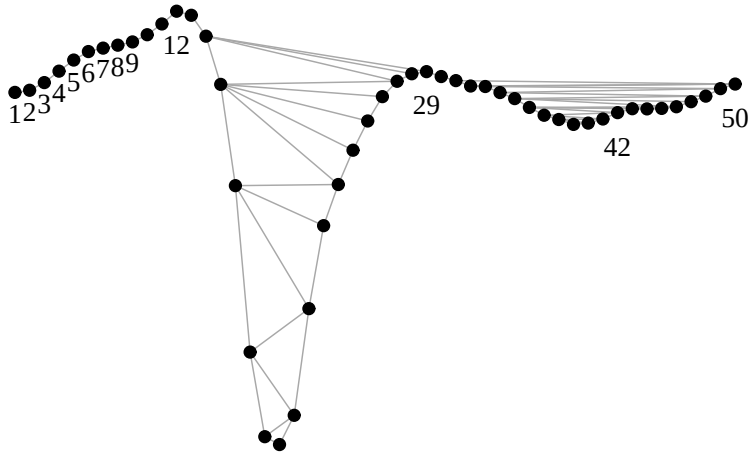

(b) Corresponding HVG of (a)

Figure 5.2: (a) A segment of an EEG time series with seizure (b) A HVG corresponding to the signal in (a).

V_i and V_j is defined as Equation 5.1:

$$w_{ij} = \begin{cases} |(x_i - x_j)(i-j)| + 1, & x_k < x_i \wedge x_k < x_j \\ 0, & otherwise. \end{cases} \tag{5.1}$$

A weighted graph is characterized with the concept of *strength*. The strength of node v_i is defined as Equation 5.2:

$$s_i = \sum_{j=1}^{n} w_{ij} \tag{5.2}$$

The parameter can be used to distinguish a monotonic increase (or decrease) time series from a constant time series. Let us consider the time series in Figure 5.2 again. The strength sequence of the WHVG associated with the first five data points of $Y1$ is $\{404, 806, 698, 306, 257\}$. The strength sequence of the WHVG associated with the last three data points of $Y2$ is $\{666, 731, 298\}$. It is obvious that the two strength sequences are different.

There are many measuring parameters in complex networks, such as clustering coefficient, average path, etc (Newman 2003). The mean degree and degree distribution (DD) are two linear complexity features of graphs. For weighted graphs, according to Barrat et al. (2004), the measuring properties of weighted complex networks are mean strength, weighted clustering coefficient etc. The mean strength of a graph having n nodes is defined as:

$$\bar{s} = \frac{1}{n} \sum_{j=1}^{n} s_j \tag{5.3}$$

Based on graph theoretical analysis, the computation complexities of finding a clustering coefficient, counting triangles (Schank & Wagner 2005), and the average shortest path (Goldberg & Radzik 1993) are $O(n^2)$, which is low efficient when applied in real time applications. In this chapter, mean degree and mean strength are considered because the computational complexities of calculating mean degree and mean strength are linear.

5.2.3 Peak frequency and power spectral density

Given a time series $\{x_i\}_{i=1,2,\ldots,n}$, it can extract the frequency domain features $\{X(\omega_j)\}_{i=1,2,\ldots,N}$ by Fast Fourier Transform (FFT), where $N \geq n$ is the power of 2. In general, two features are widely studied in EEG signal processing. The first one is the peak frequency f_p, which is defined as

$$f_p = \{\omega_i | X(\omega_i) = max(\omega_{j=1\ldots n})\} \tag{5.4}$$

The second one is power spectral density (PSD), which defines the energy distribution of a signal over the time-frequency domain. PSD refers to the amount of power per unit frequency as a function of frequency. Different algorithms are used for the estimation of the PSD. A simple method is calculated by using the

equation below:

$$p_\theta = \frac{1}{N}\sum_{i=1}^{N}|X(\omega_i)| \tag{5.5}$$

This study used the peak frequency f_p between 4-40Hz and the mean PSD P_θ over frequency band 0.5 to 40Hz to compare with the mean strength over all degrees. In this study, the PSD algorithm is calculated by the R package SeeWave (Sueur et al. 2008).

5.2.4 Sample entropy

Entropy is used to measure the complexity of a time series. It has been widely applied to EEG signal processing. Sample Entropy was proposed by Richman and Moorman (2000). Bai et al. (2007) used approximate entropy (AE) and sample entropy (SE) to analyse epileptic EEG signals, and found that SE is more suitable for identifying seizures than approximate entropy. A SampEn algorithm used in this study to estimate the SE is available from Physione website (http://www.physionet.org/physiotools/sampen/). The algorithm of SampEn has three input parameters, (1) m: the embedded dimension, (2) r: the similarity criterion, (3) n: the length of a time series $\{x_i\}_{i=1,2,\ldots,n}$. In this study, two SE features (Se_1: m=2, r=0.15, and Se_2: m=2, r=0.2) of each epoch of EEG signals are extracted.

5.2.5 K-nearest neighbour

The K-NN algorithm is a traditional pattern recognition method (Cover & Hart 1967), and is a statistical supervised classification. K-nearest neighbour (K-NN) classifiers are commonly used in epileptic EEG signal processing because they are known to be very sensitive to the curse-of-dimensionality (Wang et al. 2009). However, a K-NN classifier can achieve a good performance when the dimension of features is low (Wang et al. 2009). The dimension of extracted features in this study is three at most. A K-NN classifier is, therefore, applied to compare the performances of the features using SampEn, HVG and WHVG. The K-NN is that, given a new test data t, the algorithm obtains the K nearest neighbours from the training set Y based on the distance between t and Y. The distance used in this study is neighbor Euclidean distance as shown in Equation 5.6:

$$dst(x_t, y) = \sqrt{\sum_{i=1}^{n}(y_i - x_t)^2} \tag{5.6}$$

The most dominant class amongst these K neighbours is assigned as the class

of t. In this study, the K-NN algorithm is implemented in R package FNN (http://cran.r-project.org/web/packages/FNN/index.html), where K is 3.

5.3 HVG constructing algorithm

To implement Equation 2.19 of the HVG in Section 2.4.2, the iterative implementation algorithm is shown in Algorithm 1.

Algorithm 1: Constructing HV from a time series x

```
Data: input: x[1...n]
Result: HVG(V,E)
  for i=2;i < n; i++ do
    for j=1; j < i ; j++ do
      flag=True
      for k=j+1; k < i and flag==True; k++ do
        if x[k] stratify conditions of Equation 2.19 then
          flag=False
        end if
      end for
      if Flag then
        V[i] and V[j] are connected
      end if
    end for
  end for
```

Algorithm 1 looks simple, however it needs to iterate three variables (i, j and k), which means that the worst-case execution time to obtain a degree sequence of a HVG for a time series with n data points is $o(n^3)$. Thus, Algorithm 1 is difficult apply to real time applications. For instance, Xia et al. (2013) showed that the computing time for HVG constructor increased from 0.04 seconds to 2.28 seconds when the input size of data points increased from 1000 to 8000.

5.4 FWHVG constructing algorithm

To improve the constructing time, firstly k in Equation 2.19 should be eliminated. The idea is based on Equation 5.7,

$$w_{ij} = \begin{cases} 1, & x_j > max(x[(j+1)\dots(i-1)]) \\ 1, & j+1 = i \\ 0, & otherwise. \end{cases} \tag{5.7}$$

Logically, Equation 5.7 is similar as Equation 2.19 but without the iterative loop of k. Second, to minimize iteration j in Algorithm 1, only the maximal value among $x[1 \dots i-1]$ needs to be considered. A vector *SortList* is used to store maximal values of $x[1 \dots i-1]$. Following Equation 5.7, this study improves Algorithm 1 into a FWHVA algorithm which is shown in Algorithm 2:

Algorithm 2: Constructing WHVG from a time series x

Data: input: $x[1 \dots n]$
Result: WHVG(V,E,W)

```
1:  SortList.push(1)
2:  for i=2;i < n; i++ do
3:     V[i] and V[i-1] are connected
4:     W[i] = |x[i] − x[i − 1]| + 1
5:     if x[i] >= x[i − 1] then
6:        repeat
7:           j=SortList.pop()
8:           if j ≠ i − 1 then
9:              V[i] and V[j] are connected
10:             W[i] = |(x[i] − x[j]) × (i − j)| + 1
11:          end if
12:       until SortList is not empty and x[j] < x[i]
13:       if x[j] > x[i] then
14:          SortList.push(j)
15:       end if
16:    end if
17:    SortList.push(i)
18: end for
```

Algorithm 2 uses two loops, while the execution time of the inner repeat (line 6) is equal to the average depth of the stack. An algorithm based on HVGs developed in our previous study (Zhu et al. 2012*b*) was similar to this one, but it did not include the weighted portion. Gutin et al. (2011) showed the worst case of the numbers of edges in a HVG as follows.

Lemma 1. *(Gutin et al. 2011): The maximum number of edges in a HVG on $n > 1$ vertices is $2n - 3$, which represents the time series in the form of $\{\dots, 8, 6, 4, 2, 1, 3, 5, 7, 9, \dots\}$ or $\{\dots, 9, 7, 5, 3, 1, 2, 4, 6, 8, \dots\}$.*

Because a WHVG is a subset of a HVG, the average number of the edges is the same as the HVG. Now let us consider the computational complexity of the FWHVA algorithm.

Lemma 2. *The complexity of constructing a FWHVA is $O(n)$.*

Proof. It is clear that the worst case is decided by the execution time of a loop at line 12 of Algorithm 2: FWHVA, when its WHVG has the maximum number of edges. According to Lemma 1, the average execution time of each node of a HVG

is at most 2. It implies that the executing time at line 8 is less than $2 * (2n - 3)$. Therefore, the time complexity is $O(n)$. Since SortList at line 17 is n at most, the space complexity is also $O(n)$. ■

5.5 Simulation analysis with chaos signals

To verify Lemma 2 in Section 5.4, the proposed FWVHA and SampEn are implemented in C program language, while the FFT, PSD and statistical analysis are implemented by R package SeeWave (Sueur et al. 2008). The experiments include two parts: (a) analysing and classifying two chaos signals with added noise based on the HVGs, PSD and sample entropy; (b) evaluating the computing time by comparing SampEn and the FWHVA.

5.5.1 Statistical analysis of noise-robustness and stability of WHVGs

The stability and noise-robustness of the proposed method are two important factors in pattern classification. Two chaos signals: Hénon map, and Logistic map, are used to evaluate the performance. The Hénon map is defined in Equation 5.8:

$$\begin{aligned} x_{i+1} &= 1.4 - x_i^2 + 0.3u_i \\ y_{i+1} &= 1.4 - (Cx_i + (1-C)y_i)y_i + Bv_i, \\ u_{i+1} &= x_i, v_{i+1} = y_i \end{aligned} \tag{5.8}$$

While the Logistic map uses following Equation 5.9

$$x_{t+1} = \alpha x_t(1 - x_t) \tag{5.9}$$

The same amount of Gaussian white noise (GWN) is added to both of the above chaos signals to evaluate the performance of robustness against noise. Because the aim of this study is to classify EEG signals, and the duration of the epileptic EEG signals are limited from one second (Barlow 1985) to five seconds (Ouyang et al. 2008, Ouyang et al. 2012), the size of these chaos signals is 1024. The parameters in equations 5.8 and 5.9 are assigned as $a = 4$, $B = 0.3$, $C = 0.2$. 20 test-runs are conducted in the experiments with initial values x_0, y_0, u_0 and v_0 are randomly assigned between $(0, 1)$.

Figure 5.3 illustrates six features: mean degree $\bar{d}$, degree distribution of degree two ($DD[2]$), mean strength $\bar{s}$, sample entropy Se_1, peak frequency F_p and mean PSD p_θ extracted from two chaos signals with added white noise. There are 20 executions times. Distances between Logist and Lotist+WGN, or Henon and Henon+WGN of Figure 5.3(c) are smaller than those of Figure 5.3(b), Figure 5.3(e) and Figure 5.3(f).

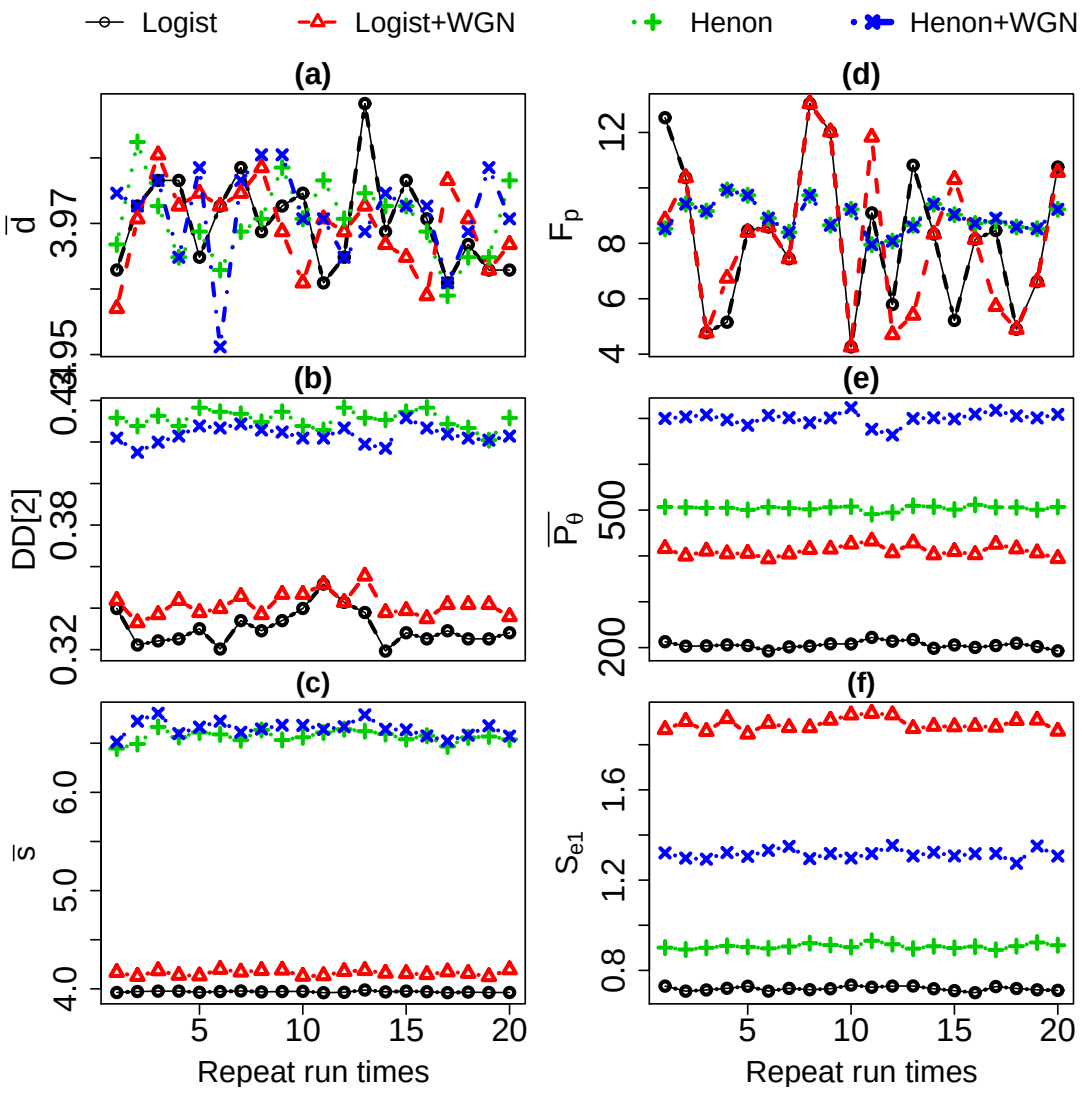

Figure 5.3: Results for $\bar{d}$, DD[2], $\bar{s}$ of WHVGs, Se_1 of sample entropy, F_p and p_θ of frequency domain (ordered from a, b, c, d, e, and f)

It is found that $\bar{d}$ of the HVGs (Figure 5.3 (a)) and the Fp from frequency domain (Figure 5.3 (d)) are sensitive to the initial values of Chaos signals, while $DD[2]$, Se_1, and $\bar{s}$ are kept steady against the initial values. It is observed that $\bar{s}$ is more robust than $DD[2]$, Se_1 and p_θ based on the distances between chaos signals and the chaos signals with noise. Therefore, mean strength is more robust against noise than other features.

5.5.2 Comparing computational time based on the HVA, SampEn, PSD and FWHVA

This section compares computation speeds of the HVA, SampEn, PSD and FWHVA methods. All algorithms are run on a 3.20G Hz Intel@Xeon W5580 CPU pro-

cessor machine with 24G RAM. The operating system is Windows 7.0 64 bits. The average execution times for the four algorithms: HVA, SampEn, PSD and FWHVA are shown in Figure 5.4. Figure 5.4(a) and Figure 5.4(b) are in a different scale. The execution times of the HVA and SampEn rise rapidly when the size of input data n increases, while the execution time of the FWHVA exhibits a slower growth rate than that of PSD. The ratio of the execution times between SampEn and the FWHVA is 76 times when $n = 4000$, and it is more than 3.8 times faster than PSD when $n = 4000$.

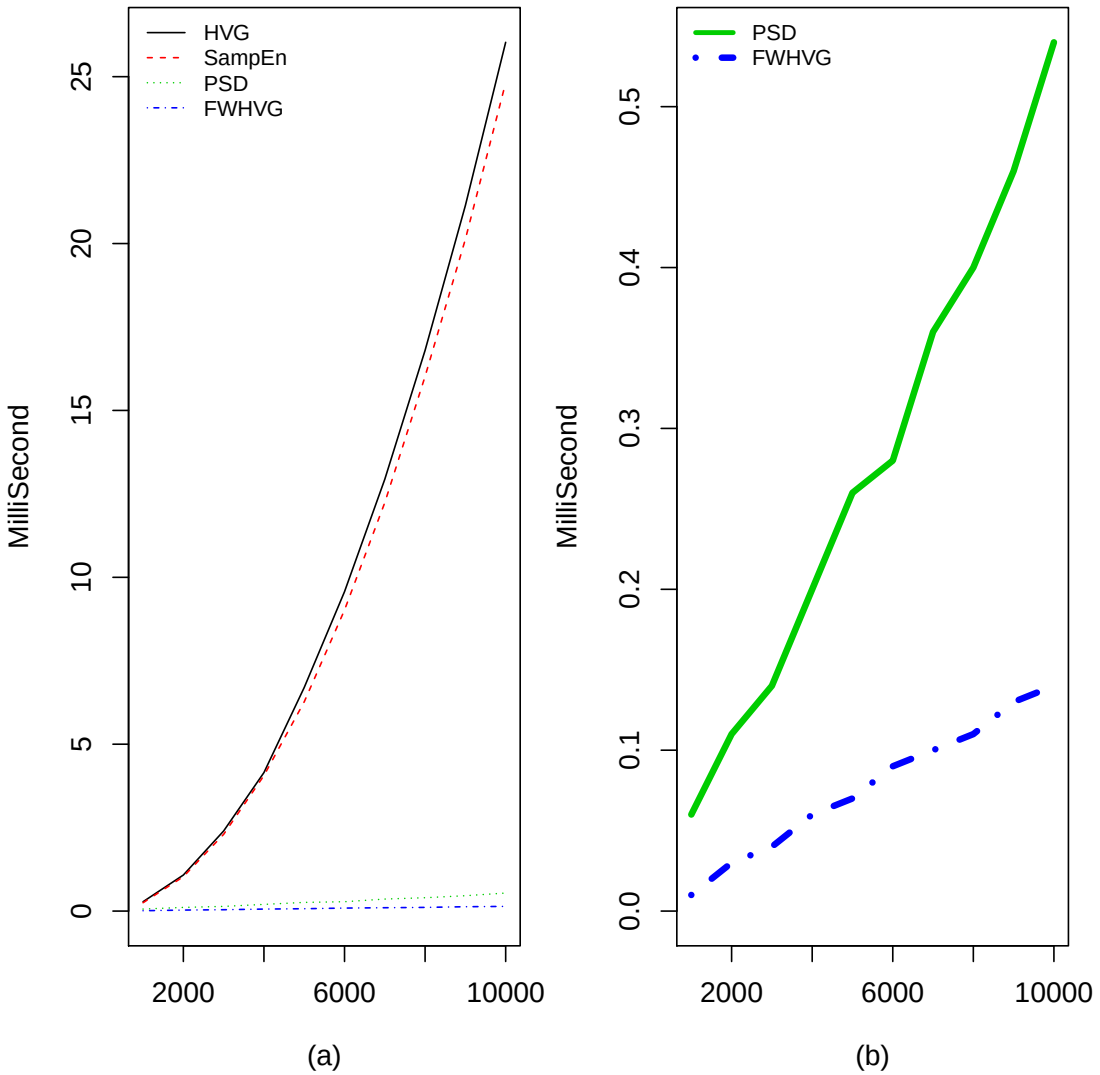

Figure 5.4: Execution times versus data points from 1000 to 10,000 for HVA, SampEn PSD and FWHVA in (a), the PSD and FWHVA in (b)

5.6 Epileptic EEG classification application

To evaluate the performance of the extracted features for pattern classification, four parts of experiments are included: (1) analysing and classifying epileptic

Table 5.1: $\bar{d}$, F_p and Se_1 for the five groups of signals

Data group	$\bar{d}$	F_p	Se_1
Set A	3.80 ± 0.041	4.37 ± 0.33	1.01 ± 0.174
Set B	3.86 ± 0.034	4.80 ± 1.37	0.91 ± 0.184
Set C	3.71 ± 0.093	4.37 ± 0.56	0.68 ± 0.158
Set D	3.70 ± 0.085	4.32 ± 0.45	0.61 ± 0.201
Set E	3.89 ± 0.051	4.35 ± 0.27	0.48 ± 0.155
p-value	< 0.0001	< 0.0001	< 0.0001

EEGs based on the mean degrees of the HVGs; (2) analysing and classifying epileptic EEGs based on $\bar{d}$ and $\bar{s}$ of the WHVG; (3) classifying the EEGs using HVGs, SE and PSD methods with the same EEG segment size; (4) classifying the EEGs using HVGs, SE and PSD methods with different sizes of EEG segments. For experiments (1) and (2), each EEG recording is divided into four equal epochs and each epoch contains 1024 data points. For experiments (3) and (4), every EEG recording is separated into 23, 8, 4, 2, and 1 equal epochs, and each epoch has 173, 512, 1024, 2048 and 4096 data points, respectively. The 10-fold cross validation is used to demonstrate the mean accuracy of 10 times K-NN classification. The whole set is divided into 10-subsets, one of 10 subsets is used as a test, and the other subsets are put together to conduct a training set.

5.6.1 Statistical analysis of the features: $\bar{d}$ of HVGs, F_p of FFT and Se_1 of SampEn

In order to evaluate the performances of the different features, $\bar{d}$ of HVG is tested and compared with Se_1 (m=2, r=0.15) and F_p of the peak frequency $4-40Hz$ in this section. $\bar{d}$, Se_1 and F_p are extracted from a 1024-point segment of an EEG signal, respectively. Table 5.1 shows the statistical results of these three features. Each recording was divided into four 1024 points per segment, and each feature comes from one epoch. A one way ANOVA test was conducted for all groups.

Figure 5.5 shows the results of $\bar{d}$ from HVGs associated with the five sets of epileptic EEG signals. Each group includes 400 recordings and each recording has 1024 data points. The error bar has 95% confidence interval. It is found that $\bar{d}$ of the HVGs associated with the ictal EEG (Set E) is the highest among those from other EEGs. $\bar{d}$ of the HVGs associated with Set D is the lowest, and those of the healthy EEG (Set A) is in the middle level.

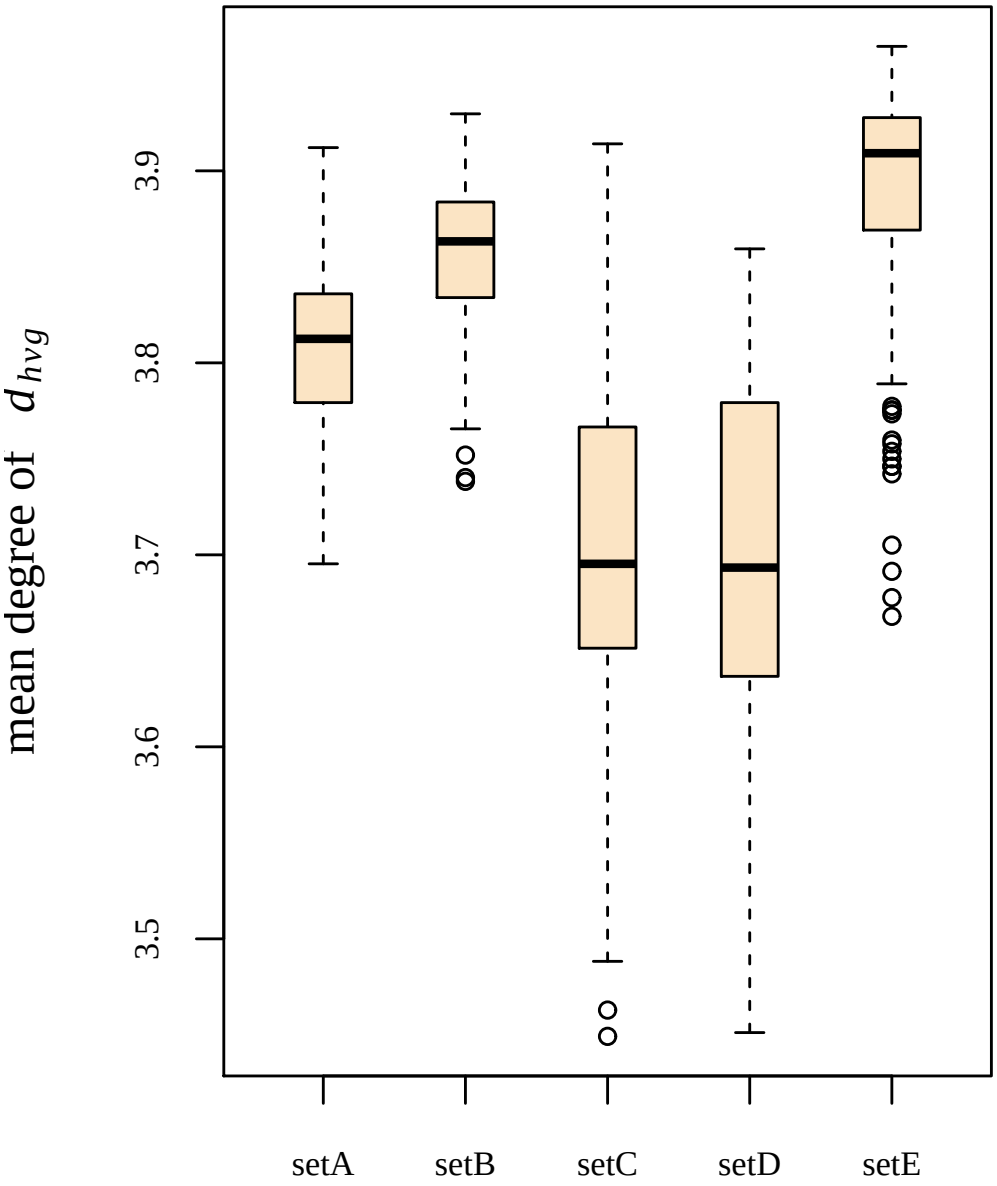

Figure 5.5: $\bar{d}$ of HVGs associated with the five sets EEGs

5.6.2 Statistical analysis of features: $\bar{s}$ of HVGs, P_θ of PSD and Se_2 of SampEn

This section investigates the statistical differences using WHVGs. Table 5.2 shows that the statistical results of the three features: $\bar{s}$ of the WHVGs, Se_2 of SampEn and P_θ of the PSD, where each recording was separated into four 1024 points per segment. Each feature comes from one epoch. A one way ANOVA test was conducted for all groups

Figure 5.6 shows the mean strength among the five sets of epileptic EEG datasets. Figure 5.6(a) and Figure 5.6(b) are in different scales. Each group has 400 record-

Table 5.2: $\bar{s}$, P_θ and Se_2 for the five sets of the EEG signals

Data group	$\bar{s}$	P_θ	Se_2
Set A	307 ± 78.2	$1.9x10^5 \pm 8.7x10^4$	1.23 ± 0.196
Set B	490 ± 152.1	$6.5x10^5 \pm 5.2x10^5$	1.09 ± 0.233
Set C	316 ± 169.1	$2.3x10^5 \pm 2.3x10^5$	0.84 ± 0.196
Set D	653 ± 1288.8	$4.6x10^5 \pm 1.1x10^6$	0.76 ± 0.249
Set E	2564 ± 1341.24	$2.0x10^7 \pm 2.0x10^7$	0.56 ± 0.177
p-value	< 0.0001	< 0.0001	< 0.0001

ings and each recording has 1024 data points, and the error bar has 95% confidence interval. Compared to Figure 5.5, the mean strength of the WHVGs associated with Set E has the highest value, while $\bar{s}$ of the WHVGs associated with Set A is the lowest, and those associated with Sets B and D are in the middle. Figures 5.5 and 5.6 indicate that the performance of $\bar{s}$ of the WHVGs could not be represented by $\bar{d}$ of the HVGs.

5.6.3 The classification using the HVGs, SE and PSD with the same EEG segment size

To evaluate the performance, a K-NN classifier is used to distinguish the seizure EEG from the other sets of EEG data. First, one single feature is used to conduct the classification, where odd numbers of epochs are in the training set and the others are in the testing set. The results with 1024 data points per segment and a K-NN classifier are shown in Table 5.3.

Second, the performances of identifying seizure EEGs are evaluated with the same groups of two dimensional features: $\bar{d}$ and $\bar{s}$ of from HVGs, two SE features: Se_1 and Se_2, and two frequency domain features: F_p and P_θ, separately. The results with 1024 data points per segment and a K-NN classifier are illustrated in Table 5.4.

The classification accuracy with $\bar{d}$ and $\bar{s}$ features showed in Table 5.4 are higher than those with Se_1 and Se_3, and those based on F_p and P_θ when classifying Set E from Sets A, C, and D, respectively. Comparing to Table 5.3, the classification accuracy using $\bar{d}$ and $\bar{s}$ in Table 5.4 increases significantly ($p = 0.04$), while the accuracy of agreement with Se_1 and Se_2 has no significant difference ($p = 0.11$).

Therefore, $\bar{d}$ and $\bar{s}$ from the WHVGs are much better features for the EEG signals classification than sample entropy features or the PSD extracted features, especially for using the unlbalanced data sets as the example set E vesus sets

Table 5.3: The classification accuracy of Set E vs Sets A,B,C,D and (A,B,C, D) using only one feature

Data group	$\bar{d}$				Se_1				F_p			
	SE	SP	AC	F_v	SE	SP	AC	F_v	SE	SP	AC	F_v
Set A vs Set E	0.89	0.75	82%	0.82	0.98	0.96	97%	0.97	0.47	0.66	56%	0.56
Set B vs Set E	0.76	0.67	71%	0.70	0.98	0.92	95%	0.95	0.58	0.55	56%	0.56
Set C vs Set E	0.86	0.85	85%	0.85	0.63	0.66	65%	0.64	0.67	0.51	59%	0.59
Set D vs Set E	0.92	0.92	92%	0.92	0.66	0.62	64%	0.63	0.71	0.58	64%	0.64
Sets (A, B, C, D) vs Set E	0.97	0.58	89%	0.78	0.90	0.42	80%	0.66	0.99	0.01	79%	0.49

Table 5.4: The classification accuracy of Set E vs Sets A,B,C,D and (A,B,C, D) using two features

Data group	$\bar{d}, \bar{s}$				Se_1, Se_2				F_p, P_θ			
	SE	SP	AC	F_v	SE	SP	AC	F_v	SE	SP	AC	F_v
Set A vs Set E	1.0	0.99	99%	0.99	0.99	0.98	99%	0.98	1.0	0.99	99%	0.99
Set B vs Set E	0.99	0.96	97%	0.97	0.92	0.92	92%	0.92	0.92	0.89	90%	0.90
Set C vs Set E	0.98	0.99	98%	0.98v	0.87	0.89	88%	0.88	0.96	0.97	97%	0.98
Set D vs Set E	0.89	0.97	93%	0.93	0.78	0.84	80%	0.80	0.93	0.95	94%	0.94
Sets (A, B, C, D) vs Set E	0.98	0.94	97%	0.96	0.94	0.75	90%	0.84	0.97	0.85	95%	0.91

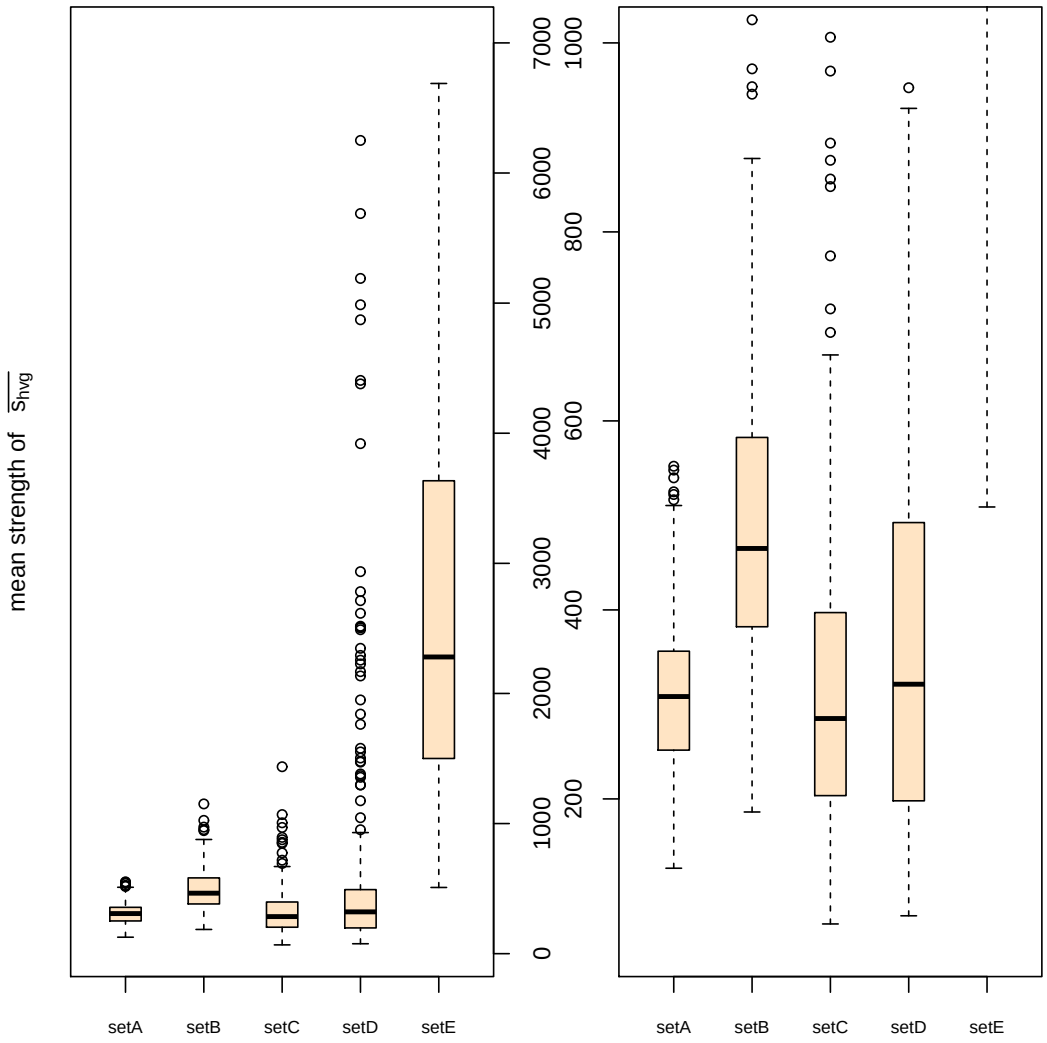

Figure 5.6: $\bar{s}$ of WHVGs for the five sets EEGs

A,B,C and D.

5.6.4 Evaluating the classification performance using different sizes of an EEG segment

In this section, the classification accuracies for identifying Set E from Set A and from Set (A, B, C, D) with the K-NN classifier are evaluated using five different sizes of an epoch. Each epoch contains 173, 512, 1024, 2048 and 4096 data points, respectively. The extracted features based on the WHVG and SampEn are forwarded to a K-NN classifier to conduct the classification, respectively. The average accuracies using five different lengths of odd epochs using a 10-fold cross-validation by the k-NN classifier are listed in Table 5.5 when one epoch has 173, 512, 1024 and 4096 data samples, separately.

Table 5.5: The classification accuracies on training set using 10-fold cross-validation

	Epoch size	173	512	1024	2048	4096
Set A vs Set E	$\bar{d}\&\bar{s}$	99.1%	99.5%	99.8%	100%	100.0%
	$Se_1\&Se_2$	95.3%	97.3%	98.0%	98.5%	98.0%
	$Fp\&P_\theta$	96.9%	98.5%	99.3%	99.0%	99.0%
Set (A,B,C,D) vs Set E	$\bar{d}\&\bar{s}$	96.2%	96.5%	95.0%	95.4%	93.6%
	$Se_1\&Se_2$	87.0%	87.8%	84.8%	90.6%	90.4%
	$F_p\&P_\theta$	94.4%	95.1%	95.7%	96.6%	97.2%

5.7 Discussions

5.7.1 Using linear complexity graph features to characterize epileptic EEGs

It is observed that $\bar{d}$ associated with chaos signals in Figure 5.3 and associated with epileptic EEG signals in Table 5.1 are close to 4. This result agrees with those reported by Luque et al. (2012) that the mean degree of a periodic time series (period is T) satisfies the following equation:

$$\bar{d} = 4(1 - \frac{1}{2T}) \tag{5.10}$$

Equation 5.10 implies that $\bar{d}$ is close to 4 if period T of a time series is large enough, which implies that the accuracy classifying with $\bar{d}$ will decline for long-period time series. However, Table 5.4 illustrates an increased accuracy in identifying seizures when the EEG segment size grows. The evidence strongly supports the notion that EEG signals are nonstationnarity.

In addition, based on Table 5.1 and Figure 5.5, the HVGs with 1024 points of ictal and inter-ictal EEGs satisfy $\bar{d} < 3.9$ and $\bar{d} < 3.72$, respectively. In contrast, $\bar{d} > 3.95$ from two chaos signals with added noise are shown in Figure 5.3. These phenomena agree with the results reported by Pritchard et al. (2005) that the inter-ictal EEGs are not low-dimensional chaos. From a physiological point-of-view, the linear complexity features based on $\bar{d}$ and $\bar{s}$ present that EEG signals during seizures are more chaotic. The results are also consistent with the results reported by Hu et al. (2004).

5.7.2 Feature extraction methodology and performance

This study uses the FWHVA method to extract $\bar{d}$ and $\bar{s}$ from the WHVG for detecting seizures. Compared with the FFT and entropy methods, this method has the following advantages:

1. It is a simple and fast calculation method, faster than FFT as shown in Section 5.5.
2. It is suitable for applications in classifying a short term time series, especially non-stationary EEG signals, such as epileptic EEGs and sleep EEGs (Zhu et al. 2012*b*). Because the strength feature is more suitable for identifying spike-waves, the epileptic diagnosis can be more efficient by the FWHVA on these types of EEGs.
3. The strength feature is better for characterising the epileptic EEGs than the PSD, as shown in Figure 5.6 and Table 5.4.
4. The strength feature extracted by the FWHVA is more robust against Gaussian white noise, as shown in Figure 5.3.
5. The WHVGs can map EEG recordings onto a different set of edges (by defining different weights and relations).

Therefore, thousands of parameters can be deduced from the graph features, such as mean and probability distributions of nodes or edges. It is relatively easier to obtain those key features to identify seizure or inter-ictal EEGs, as shown in Section 5.3. While other nonlinear methods, such as sample entropies, cannot extract significant features by just changing their parameters.

The proposed algorithm only requires one parameter, the input signals, which is not affected by the sampling frequency. In other words, it is independent from the frequency domain. Unlike the FFT algorithm, the window size should be the power of 2, while the FWHVA algorithm has no limit to the length of input data or window size. Therefore, the algorithm is more robust and easily to be applied to any size of data. Similarly, as frequency bands can be divided into different sub-frequency bands, the WHVGs can enhance the performance by adjusting different degree distributions. For example, Zhu et al. (2012*a*) used degree distributions to identify epilepsy. Unfortunately, this method is not suitable for long-period stationary signals, especially using $\bar{d}$ feature, due to periodic limitations in Equation 5.10. For example, the classification accuracy between Set (A, B, C, D) and Set E by using $\bar{d}$ and $\bar{s}$ features is less 3.6% for 4096 data points per segment, but it is 1.8% larger for a 173 data point segment compared with F_p and P_θ, as shown in Table 5.4. Thus, a further study is needed to investigate other graph features for long-term signals.

5.7.3 Bottleneck of the computation speed for classifying epileptic EEGs

As shown in Figure 5.1, there are two stages in EEG classification. The computation times for Set A and Set E with five different epoch sizes are presented in Table 5.6. The size of the input data in the classification stage in Figure 5.1 is the number of features, while that in Stage 1 is the EEG samples. Therefore, Stage 1 introduces the bottleneck of the computation for EEG signals classification due to the large size of recordings. The FWHVA algorithm is an important factor of speed when faster classifiers, such as the K-NN classifer, are applied in classifying EEGs.

Table 5.6: The classification accuarcy compared with other existing methods with the same epiletic EEG data sets.

		Epoch size(E) and the number of epochs (n)				
Stages	Methods	E:173 n:2300	E:512 n:800	E:1024 n:400	E:2048 n:200	E:4096 n:100
Stage 1	FWHVA	5.07	3.90	3.67	3.61	3.49
	PSD	7.81	10.15	14.50	21.80	38.80
	SampEn	10.53	17.72	30.38	56.73	112.01
Stage 2	FWHVA	0.21	0.02	0.01	0.01	0.01
	PSD	0.19	0.02	0.01	0.01	0.01
	SampEn	0.17	0.03	0.02	0.02	0.02

From a clinical point-of-view, the size of a segment of epileptic EEG signals is less than five seconds (Ouyang et al. 2008, Ouyang et al. 2012). In fact, Barlow (1985) suggested that a better segment period is 1 second. In addition, when the epoch size is 173 (1 second) as shown in Tables 5.5 and 5.6, the classification performance with features based on the WHVGs is 8.9% higher than those based on the SamEn, and 1.5 higher than that of the PSD, while the speed of the FWHVA is faster than those of PSD or SampEn. Therefore, the FWHVA is an efficient tool for real time epileptic EEG signal processing.

5.7.4 Comparison with other methods

The classification accuracies for the epileptic EEG database from different literature are presented in Table 5.7.

According to Table 5.7, the accuracy of classification between Sets A and E is 0.4% different from the best result by Srinivasan et al. (2005) based on frequency

Table 5.7: The classification accuracy by the MSK-means and other existing methods

Researchers	Features and classifier	Datasets	Epochs length	Accuracy	Feature dimension
Srinivasan et al. (2005)	PSD & Elman network	A, E	1024	99.6%	5
Polat and Gne (2007)	PSD & Decision Tree	A,E	256	98.72%	129
Guo et al. (2011)	DWT & ANN	A, E	4097	99.6%	2.32
Nicolaou and Georgiou (2012)	PE & SVM	A, E	1024	93.42%	1
		D, E	1024	88.83%	1
Siuly et al. (2011)	Clustering & SVM	A, E	4096	99.9%	9
		D, E	4096	93.6%	9
Zhu et al. (2012*a*)	Entropy& MSK-means	A, E	4097	100%	11
Orhan et al. (2011)	DWT and K-means & ANN	A, E	4097	100%	4
		(A,B,C,D), E		99.6%	18
The proposal method	Weighted HVG & K-NN	A, E	2048	100%	2
		D, E	20 48	100%	2
		(A,B,C,D), E	2048	96.0%	2

Table 5.8: The computing time (seconds) for 2000 seconds EEG records

Methods	The proposal method	PSD	SE	VG
	1.51	1.73	48.11	42.92

domain, for Sets D and E it is 0.6% different from the best result by Siuly et al. (2011). The classification of Sets (A,B,C,D) and E classification are close to clinic requirement, though is just little less compared with the PSD method.

However, our proposed method uses only two dimension features, and the speed is much faster than the PSD. In fact, according to Table 5.3, the classification accuracy between focal inter-ictal EEGs and ictal EEGs with the HVG feature $\bar{d}$ is higher than those from the peak frequency features F_p and SampEn feature Se_1. The 92.0% classifying accuracy on Set D and Set E only with one feature $\bar{d}$ is higher than the 83.13% accuracy with one permutation entropy feature and a SVM by Nicolaou and Georgiou (2012).

In addition, to compare the computation times of FWHVA algorithm, the feature extracted time of SE, PSD, VG and FWHVA are listed in the Table 5.8. The input segments of EEG records are 500, and each segment has 4096 points, which is four seconds. Therefore, the total 500 segments contains 2000 seconds EEG records. The experiments are implemented on a computer with 3.2G Hz Inter Xeon(R)W5580 eight processor, 24GB of RAM and 64 Windows 7.

According to Table 5.8, the FWHVA is the fastest than others,which use 0.76 ms to deal with one second EEG signals, this speed can be accepted in real time applications.

5.8 Chapter summary

The chapter presents three main contributions. First, two novel features: $\bar{d}$ and $\bar{s}$ from WHVGs are proposed to identify ictal EEGs from healthy EEGs with a 100% accuracy when a segment EEG has 2048 or 4096 data points. $\bar{d}$ and $\bar{s}$ from ictal EEGs are found to be significantly higher than those for healthy and inter-ictal EEG, which explains that ictal EEGs are more chaotic. Second, $\bar{s}$ of a graph is more robust against noise than the PSD in frequency domain and sample entropies in time domain. The strength feature is also more stabile for the initial value of chaos signals than the latter two features. Last, a linear complexity of the FWHVA algorithm is proposed and tested. Compared with the sample entropy and FFT, the computational efficiency of the FWHVA is 76 times faster than

sample entropy and is 3.8 times faster than the FFT when the size of signals is more than 4000 data points. In addition, this study can also be applied to other time series analysis.

Chapter 6

Evaluating Functional Connectivity in Alcoholics Based on Maximal Weight Matching

EEG-based applications face the challenge of multi-modal integrated analysis problems. In Section 2.3, three methods for defining the functional connectivity of a brain graph were discussed. This chapter will introduce one method, synchronization likelihood, to study different complex brain networks between alcoholics and controlled drinkers. A greedy maximal weight matching approach is applied to measure the functional connectivity associated with EEG and EOG signals. The major discovery is that the processing of the repeated and unrepeated stimuli in the γ band in controlled drinkers are significantly different from those in alcoholic subjects. However, the EOGs are always stable in the case of visual tasks, except for a weak wave when subjects make an error response to the stimuli. The related work was presented in (Zhu et al. 2011).

To study the functional connectivity between five regions of the cortex, the raw data were processed in four steps. First, a filter technique for short data samples as described in Section 6.2. Second, the calculation of the autocorrelation problem with short time series is discussed. The coupled Hénon system is used as a reference to verify the approach. Third, the synchronization matrix of each recording is mapped into a weight graph G and the greedy maximal weight matching M of G is obtained for alcoholics and controlled drinkers, respectively. The electrode pairs of M are encoded according to the electrode pairs' directions and regions. Lastly, the average of the maximal weight matching both for alcoholics and controlled drinkers is calculated separately. The maximal weight matching on 8, 19, and 61 channels are computed and are used to evaluate which directions and regions of synchronization are enhanced or decreased when different stimuli are applied.

6.1 Introduction

In recent years, electroencephalograms (EEGs) have been widely used to evaluate the dysfunction of the brain of alcoholic people. Researchers have focused mainly on four frequency bands, θ (4-8 Hz), α (8-12.5 Hz), β (12.5-28.5Hz) and γ (28.5-45Hz). In the θ band, heavy drinkers have better synchronization than controlled subjects with 62 tin electrodes (de Bruin et al. 2004). In the α band, alcoholics have lower activity in the left anterior cortex than in the right anterior cortex (Hayden et al. 2006). Michael et al. (1993) also found that the α coherence increases at the central region. Winterer and Goldman (2003) found that the posterior coherence of alcoholics are significantly increased, both in α band and β bands. Moreover, heavy drinkers have higher synchronization in γ band (de Bruin et al. 2004). However, an optimal brain function has a high synchronization which is different from the increased coherence of alcoholics (Keller et al. 2007). In fact, increasing the coherence of alcoholics is also in contrast to the study on a public 61-channels EEG alcoholics dataset with two electrooculogram (EOG) signals.

By the event related potential (ERP) technique, it was found that the right hemisphere of alcoholics is depressed, unlike that of controlled drinkers (Zhang et al. 1997). Moreover, using a synchrony visualization method, Sakkalis et al. (2007) found that alcoholics had impaired synchronization in α band and low β synchronization compared to controlled drinkers. Therefore, increased or decreased synchronization was the result of inconsistency in the alcoholics databases, meaning there is no efficient way to study functional connectivity of the human brain using multi-channel and multi-modal data. In fact, supporting muti-modal data integration and fusion is one of challenges in EEG-based applications. This chapter will use graph theory to study this challenge and investigate the functional connectivity when EEG and EOG are combined.

Graph theoretical methods have been employed to study EEGs for about a decade. A popular approach is based on a small-world network (Watts & Strogatz 1998). The functional connectivity of the human brain has been proved to be a small-world network by some researchers (Humphries et al. 2006, Micheloyannis et al. 2006). The approach is to map a synchronization matrix into a binary graph G, in which the nodes of G are mapped from electrodes, and the weight of each edge of G is the synchronization value between two electrode pairs. However, the properties of a small-world network only describe the clustering and small-world effect in the whole graph. The graph cannot be used to analyze the functional connectivity between pair-wise nodes.

The aim of this study is to investigate the visual stimuli of the different brain regions of alcoholics with that of the different brain regions of controlled drinkers, with maximal weight matching on multi-modal datasets. The data set in this study includes $11,035$ EEG recordings where $7,014$ trials are alcoholics, while the rest are controlled drinkers.

6.2 Methodology

6.2.1 The alcoholic data set and the optimal channels

The experimental data used in this chapter were obtained from the University of California, Irvine Knowledge Discovery in Databases Archive UCI KDD (Bache & Lichman 2013). The database was discussed in Section 3.2. Because these EEG data sets were collected with 63 electrode caps, it is not necessary to analyze all channels in general case. Palaniappan and Omatu (2002) used a genetic algorithm to select the eight optimal channels (Pz, P7, O2, FPz, TP7, P6, C1, FCz) to classify the alcoholics and controlled drinkers on the basis of dataset TRAIN and TEST in γ band. Some studies (Rangaswamy et al. 2004, Hayden et al. 2006) have used the channels: $FP1$, $FP2$, $F74$, $F3$, Fz, F4, F8, T7, C3, Cz, C4, T8, P7, P3, Pz, P4, P8, O1 and O2 for the specified measurement. This study uses the maximal weight matching method to evaluate the performance of these optimal channels.

6.2.2 Filtering and autocorrelation

This section discusses two key processing techniques for short time series with each signal having 256 points being recorded in one second. One key process is to filter out the data from the lower band and another is to extract the attractor from the short time-series EEGs.

Filtering is a necessary preprocessing step to separate the band from the raw EEG data. For example, to extract the γ band from the raw data, the digital butterworth filter was used in Ravi and Palaniappan (2006), and a band-pass filter construct with low-pass filter and high-pass filter was used in Palaniappan and Omatu (2002). The filtering results greatly affected the process of EEG, especially on the low frequency band.

Figure 6.1 illustrates a case of the band-pass filter on the lower frequency signals. Figure 6.1(a) is a segment EEG from a alcoholic, Figure 6.1(b) is the α wave of Figure 6.1(a), Figure 6.1(c) is a segment EEG from a controlled drink, and Figure 6.1(d) is the β wave of Figure 6.1(c). To obtain α (8.5–12Hz) from channel $C3$ of $co2a000364$ subject and $co2c0000338$ subject in 0 trial, the θ waves and β waves, shown in Figure 6.1, were employed after it was filtered using the following SCILAB IIR filtering method:

$$[lisys] = iir(4,'bp','cheb1',[0.014, 0.031],[0.01, 0.06]);$$

It is easy to observe that both filtered signals are smoothed from zero to five points, which increase the coherence if these two time series are analyzed. Therefore, the first and last four points are ignored and only 248 points were used.

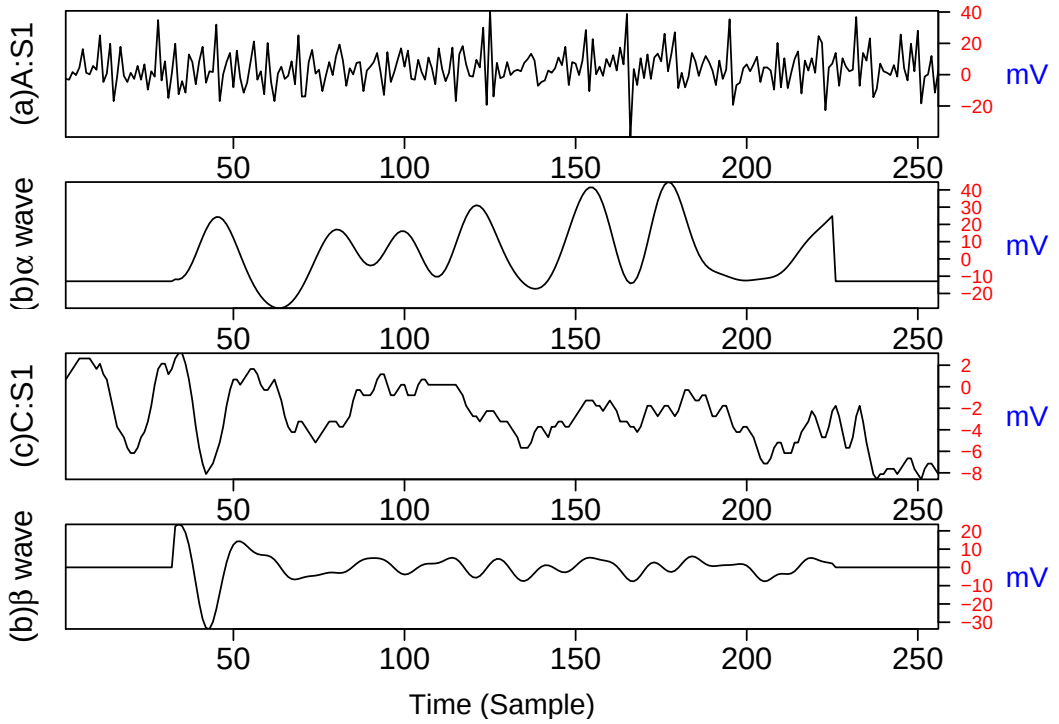

Figure 6.1: An example of the filter effect on the EEG signals

EEG signals can be viewed as a nonlinear dynamical system that can be extracted by the attractor in the phase space (Theiler 1986). To classify single trial EEG, time series $\{x_i\}_{i=1,2,\ldots,n}$, $\{x_i\}$ can be converted to a m-dimensional embedding vector $X \in R^m$:

$$X_m\{t\} = \{x_t, x_{t+\tau}, \ldots, x_{t+(m-1\tau}\} \; ; \; 1 \leq t \leq (n - m\tau + 1) \tag{6.1}$$

where $i = 1, 2, \ldots, N_e = N - m\tau$ and τ is the time delay. Then, the autocorrelation factor of the time series can be obtained from the phase space X by employing the Theiler method (Theiler 1986). However, the Theiler algorithm is more complex and does not work well on short time series data. So, a simple approach is used in this study to obtain the autocorrelation factor C_r, which is calculated using equation 6.2:

$$C_r = \frac{1}{N_e + 1} \sum_{j=i+w}^{N_e} \sigma(|X_i - X_j|), i \in [1..N_e] \tag{6.2}$$

where w is Theler window, σ is Heavisible function, $\sigma(x) = 1$ if $x > 0$; otherwise $\sigma(x) = 0$. It is noted that equation 6.2 is more efficient than the probability approach in Stem and Dijk (2002), because the probability step is ignored in this equation.

C_r is sensitive to w and m in a short time series. Sanz-Arigita et al. (2010) illustrated an example to set up the parameters for a smaller data set, where

$m = 6$ and $w = 6$. However, according to Takens's idea (Takens 1981), $m > 2d$, where d is the dimension of the system on the attractor. Therefore, $d < 3$ when $m = 6$, which should not be a real feature of the attractor for the EEG series. In this chapter, the parameters are as follows: $lag = 1$, $m = 26$ and $w = 64$, which are suitable for extracting the attractor from the 256 EEG points.

6.2.3 Mapping a synchronization matrix into a graph

Synchronization Likelihood (SL) was discussed in Section 2.3.3. It is clear that the range of $SL_{i,j}$ is between 0 and 1. In general, the synchronization matrix is mapped into a binary graph (Sanz-Arigita et al. 2010). Because $SL_{i,j} = SL_{j,i}$, let $SL_{i,i} = 0$, SL is a symmetric and can be represented as an adjacency matrix of a graph, where nodes represent channels, and edges are the synchronization value between two channels. Therefore the synchronization matrix is mapped into a weighted graph in this study.

To verify the SL method, an identical Hénon system is used in this chapter, which was also used in (Stam & Van Dijk 2002):

$$\begin{aligned} x_{i+1} &= 1.4 - x_i^2 + 0.3u_i \\ y_{i+1} &= 1.4 - (Cx_i + (1-C)y_i)y_i + Bv_i, \\ u_{i+1} &= x_i, v_{i+1} = y_i \end{aligned} \tag{6.3}$$

where x_0, y_0, u_0 and v_0 are initialized to random values. Figure 6.2 is a graph mapped from the coupled Hénon system with parameters $B = 0.3$ and $C = 0.6$ to 0.8, where SL parameters are $l = 1$, $m = 26$, $w = 64$ and $N = 256$. For simplification, the weights less than 0.02 are ignored.

6.2.4 Greedy maximal matching on the regions of the brain

A matching in graph G is a subset of pair-wise non-adjacent edges. That is, no two edges share a common vertex. A greedy weight matching M is the one for which the sum of the weights of the edges of M is maximal with a greedy method. For example, Figure 6.2 has a greedy weight matching $M = \{x = 0.8, y = 0.8\}, \{x = 0.7, y = 0.7\}, \{x = 0.6, y = 0.6\}$. The total weight is $w(M) = 1.73$ and the highest weight edge $\{x = 0.8, y = 0.8\}$ belongs to M.

Maximum matching problems are well-known problems in graph theory and have been proved to be solved with a complexity of $O(n^3)$ (Gabow 1976). Certainly, there exists an optimal algorithm for processing EEGs. For example, the optimal pairing of signal components are separated by comparing with a greedy approach (Tichavsky & Koldovsky 2004). However, maximum weight matching does not always include the highest weight edges (Tichavsky & Koldovsky 2004). Therefore, the greedy algorithm is used to ensure that the highest weight edge is always

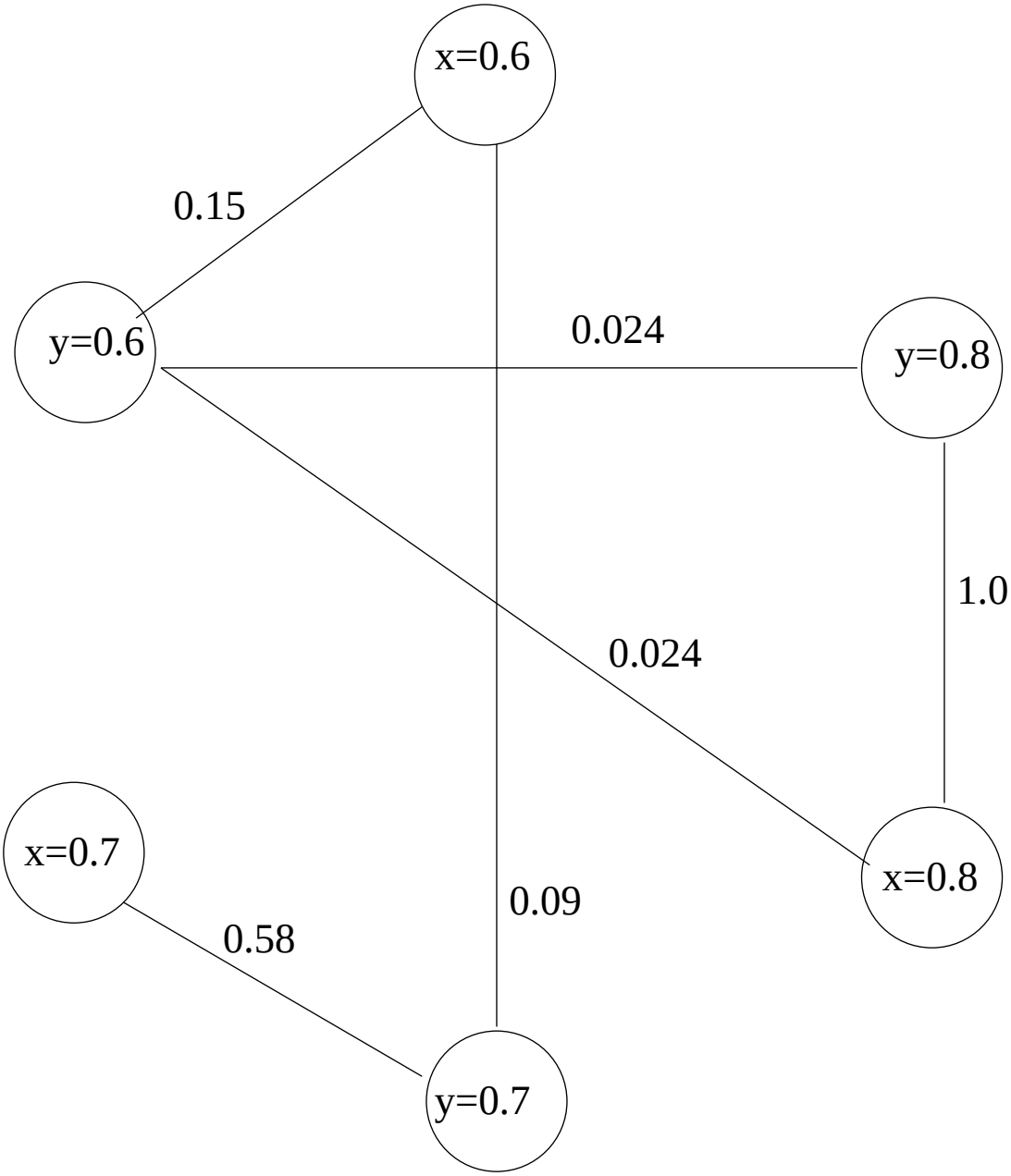

Figure 6.2: A graph of the Hénon system (B=0.3)

included in the matching.

In this chapter, the algorithm is greedy and recursive. First, the largest weight edge e is selected from G into M, then e and the two connected nodes are removed from G, and this procedure is repeated until the number of remaining nodes is less than two. The details of the greedy algorithm is presented in (Dapena & Castedo 2003).

To measure the effect of the pairwise electrodes, the brain is divided into six regions: Frontal (F), Central (C), Parietal (P), Occipital (O), Temporal (T) and EOG regions. The first five regions include the electrodes following the rules in

Zhang et al. (1997). The F region consisted of $FP1$, $FP2$, FPz, $AF1$, $AF2$, $AF7$, $AF8$, AFz, $F1$, $F2$, $F3$, $F4$, $F5$, $F6$, $F7$, $F8$ and Fz. The C region consists of $Fc1$, $Fc2$, $Fc3$, $Fc4$, $Fc5$, $Fc6$, $C1$, $C2$, $C3$, $C4$, $C5$, and $C6$. The P region consists of $Cp1$, $Cp2$, $Cp3$, $Cp4$, Cpz, $P1$, $P2$, $P3$, $P4$ and Pz. The O region consists of $Po1$, $Po2$, $Po7$, $Po8$, Poz, $O1$, $O2$, and Oz. The T region consists of $T7$, $T8$, $Tp7$, $Tp8$, $Cp5$, $Cp6$, $P7$ and $P8$. The EOG region consists of X and Y electrodes. To more precisely evaluate the affect on the left or right hemisphere, three groups are defined: left(L) , right(R) and join(J). For example, the matching $M_1 = \{F3, F7\}$ is encoded $F.L$ implying that the pair-wise electrodes belong to the left fontal region, $M_2 = \{P4, P8\}$ is $P.R$ implying that the pair-wise electrodes belong to the right parietal region, $M_3 = \{O1, O2\}$ is $O.J$ implying that the pair-wise electrodes belong to the left and right occipital regions.

6.3 Results and Discussions

6.3.1 Verifying the optimal channel numbers using greedy maximal weight matching

Three different channel numbers: 8, 19 and 63 are analyzed using the greedy maximal weight matching in γ band, which are shown in Figures 6.3 to 6.5. Figures 6.3 and 6.5 indicate significant differences between alcoholics and controlled drinkers. However the differences between alcoholics and controlled drinkers are smaller in the case of the 19-channel EEG, as shown in Figure 6.4. For instance, controlled drinkers have a higher pair-wise $\{O2, P6\}$ than alcoholics, in the case of the 8-channel EEGs and the pair-wise $\{FCz, Pz\}$ is never shown in the $S2$Nerr of controlled drinkers. On the other hand, the controlled drinkers have a higher SL value in $F.R$ than alcoholics do, on a 63-channel EEGs and EOGs (Figure 6.5). However, it is difficult to divide the controlled drinkers and alcoholics from Figure 6.4 because the values of $F.L$ and $F.R$ on $C.S1$ are lower than $A.S2Nerr$.

To evaluate the complexity of 8 optimal channels based on Palaniappan and Omatu (2002), the basic 19-channel based on Rangaswamy et al. (2004) and Hayden et al. (2006), and the 63-channel in this study, the running time of the three types of channels are listed in Table 6.1.

6.3.2 The synchrony of EEG signals between alcoholics and controlled drinkers

The results of this study on the average of SL are different from the results in de Bruin et al. (2004). 77 alcoholics and 45 controlled drinkers of FULL datasets are analyzed by applying three different stimuli. The analysis results of FULL

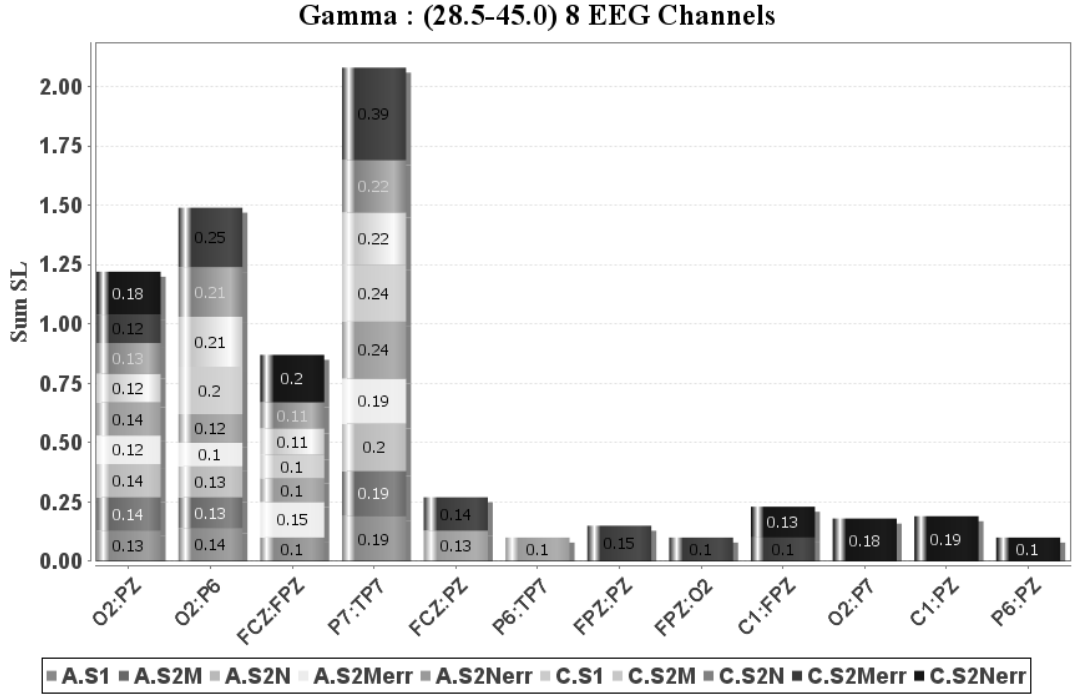

Figure 6.3: Full Dataset with 8 channels

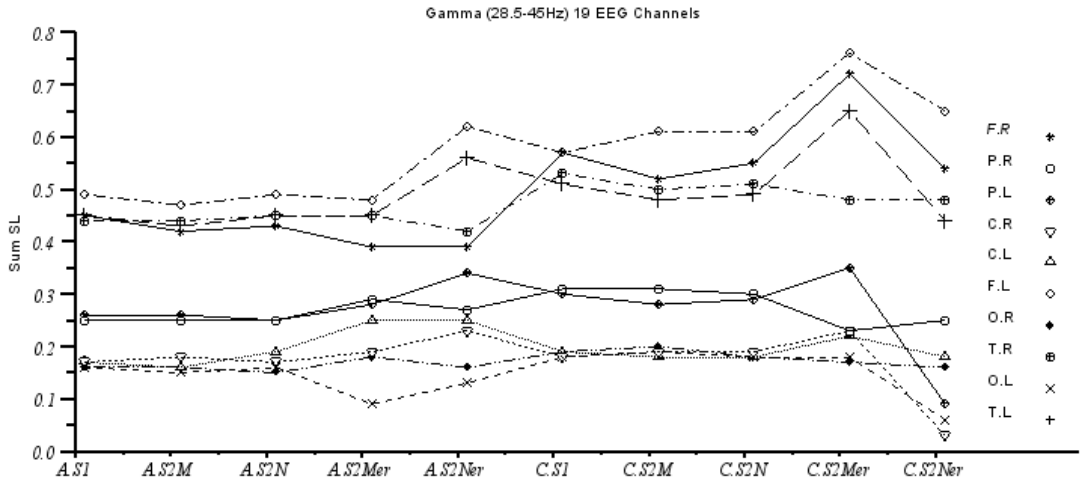

Figure 6.4: Full Dataset with 19 channels

dataset are shown in Table 6.2, where a indicates alcoholics and c means controlled subjects. In the case of γ band, the average synchronization in alcoholics is less than that in controlled drinkers, which is consistent with the result in (Ravi & Palaniappan 2006), but is different from the result in de Bruin et al. (2004), This is because the test data do not include data about the eye and body movements (Zhang et al. 1997). On the other hand, in the α band, the alcoholics have a better synchronization than controlled drinkers do, which agrees with the α band result in de Bruin et al. (2004).

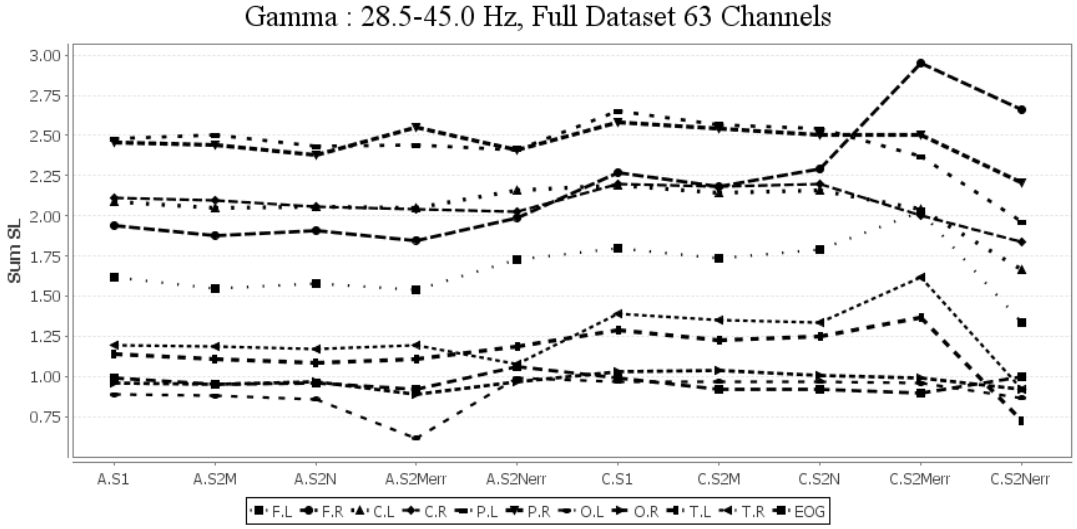

Figure 6.5: Full Dataset with 61 EEGs and 2 EOGs

Table 6.1: Running time for the number three types of channels

Databases	Trials	8 Optimal channels	19-channel	63-channels
TEST	600	8.5	13.5	25.5
TRAIN	600	8.5	13.6	25.7
FULL	11035	17.31	258.7	761

Furthermore, an interesting discovery is that the left cortex of alcoholics is different from that of controlled drinkers in the γ band. These results are shown in Table 6.3. The synchronization of the left and right brain of subjects are always increased during β, α and θ bands. Conversely, the synchronization of the left cortex of alcoholics and controlled drinkers are stable in γ bands in 4.6 and 4.9 respectively, and the synchronization value of the right cortex are decreased from 4.73 to 4.7 in alcoholics but are slightly increased in controlled drinkers. Therefore, the abnormal synchronization of γ bands on the left and right hemisphere imply that the alcoholics process the repeated and unrepeated stimuli differently from the controlled drinkers. The next section will use maximal weight matching to enhance these results on all wave bands.

6.3.3 The functional connectivity during repeated and unrepeated stimuli

Although both Figures 6.3 and 6.5 show a good synchronization of γ band in the parietal region of alcoholic and controlled drinkers, the $S2$Merr and $S2$Nerr of

Table 6.2: Average of 11,035 trials SL on FULL database

Stimul	$S1$ Obj		S2 Match		S2 Nomatch	
Hz	a	c	a	c	a	c
γ	0.188	0.200	0.184	0.196	0.182	0.198
β	0.239	0.251	0.233	0.236	0.240	0.244
α	0.265	0.275	0.273	0.275	0.279	0.278
θ	0.308	0.314	0.308	0.307	0.310	0.313

Table 6.3: Mean and SD of the left and right on Full database, M:S2M. N:S2N

		Alcoholics		Controlled drinkers	
B	T	L	R	L	R
γ	M	4.6 ± 1.55	4.73 ± 1.59	4.9 ± 1.57	5.11 ± 1.65
	N	4.6 ± 1.59	4.7 ± 1.57	4.9 ± 1.5	5.13 ± 1.66
β	M	5.85 ± 2.04	6 ± 2.11	5.86 ± 2	6.17 ± 2.13
	N	6 ± 2.08	6.17 ± 2.16	6.06 ± 2.05	6.33 ± 2.1
α	M	6.86 ± 2.46	7.11 ± 2.57	6.89 ± 2.38	7.21 ± 2.42
	N	6.96 ± 2.4	7.27 ± 2.51	6.97 ± 2.41	7.29 ± 2.54
θ	M	7.75 ± 2.25	8.01 ± 2.29	7.72 ± 2.22	8 ± 2.36
	N	7.81 ± 2.29	8.07 ± 2.3	7.87 ± 2.2	8.16 ± 2.25

alcoholics and controlled drinkers show significantly different trends. For instance, except for $P.R$, $T.R$ and EOG, all regions are decreased from S2Merr to S2Nerr in controlled drinkers, but they are stable or slightly increased in alcoholics. This implies that the functional connectivity are different while repeated and unrepeated stimuli are applied in alcoholics and controlled drinkers.

Figures 6.6 to 6.8 demonstrate these results in β, α and θ wave bands . For example, for the controlled drinders, (in Figure 6.6) for the β band, except $P.R$, all areas decrease from S2Merr and S2Nerr, and $P.R$, $C.R$, $F.R$, $F.L$, $T.L$ and EOG increase for the alcoholics. In contrast, it is noted that the α band are different from γ and β bands, as shown in Figure 6.7. Only $O.L$ and $F.L$ are decreased from S2Merr to S2Nerr in the case of alcoholics, while the other regions are increased. However, only half the regions of controlled drinkers are increased, while the other half is decreased. In Figure 6.8, all regions of controlled drinkers are decreased, but $F.L$ is slightly decreased on alcoholics. Furthermore, the synchronization

of the α band is higher than that of the other bands in the parietal regions, which is consistent with the results in Sakkalis et al. (2007); and the ratio of α band synchronization in the left to that in the right regions is higher than the synchronization of other bands. The $P.R$, $C.L$ are larger than $P.L$, $C.R$ in $S2$Nerr for the controlled drinkers; but are approximately equal in alcoholics. These EEG phenomena imply that there are different processing procedures in different regions of alcoholics and controlled drinkers with the repeated stimuli and unrepeated stimuli.

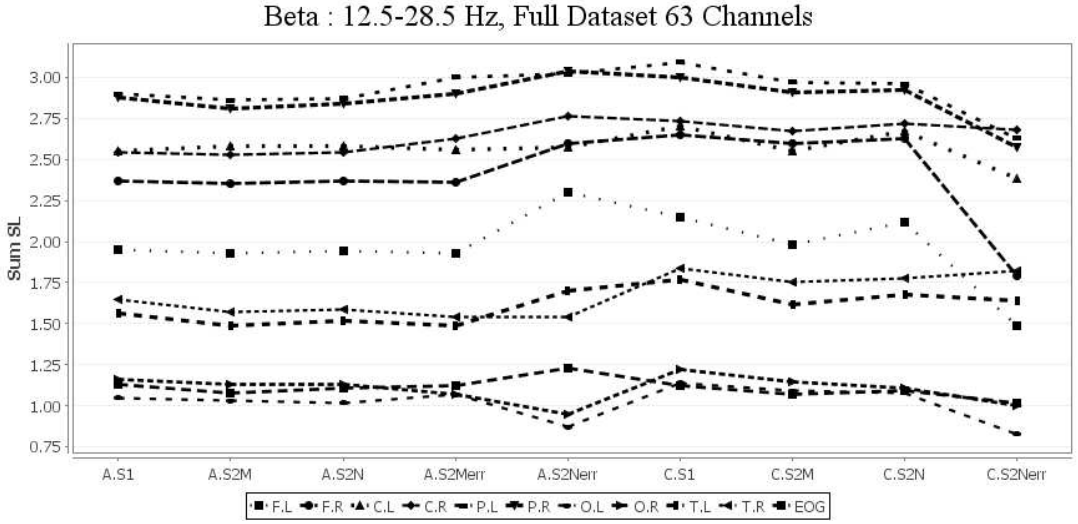

Figure 6.6: β on Full Dataset with 61 EEGs and 2 EOGs

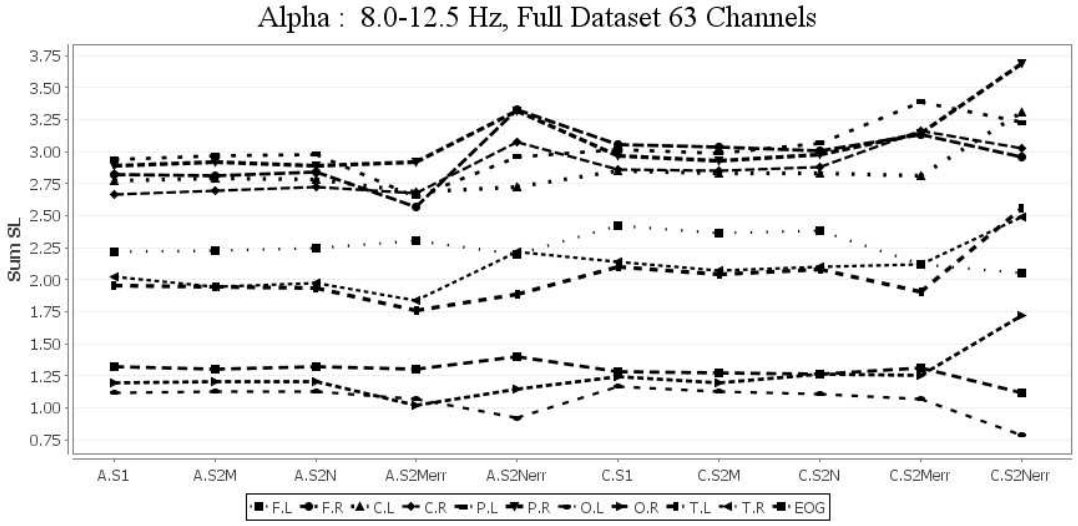

Figure 6.7: α on Full Dataset with 61 EEGs and 2 EOGs

There is an interesting finding in this dataset: the EOG is very stable from Figures 6.3 to 6.8, irrespective of whether on alcoholics or on controlled drinkers, with only a weak decrease in $S2$Nerr in the case of controlled drinkers. These results imply that the alcoholics are not affected by the EOG signal, because the EOG does not represent the response to visual stimuli.

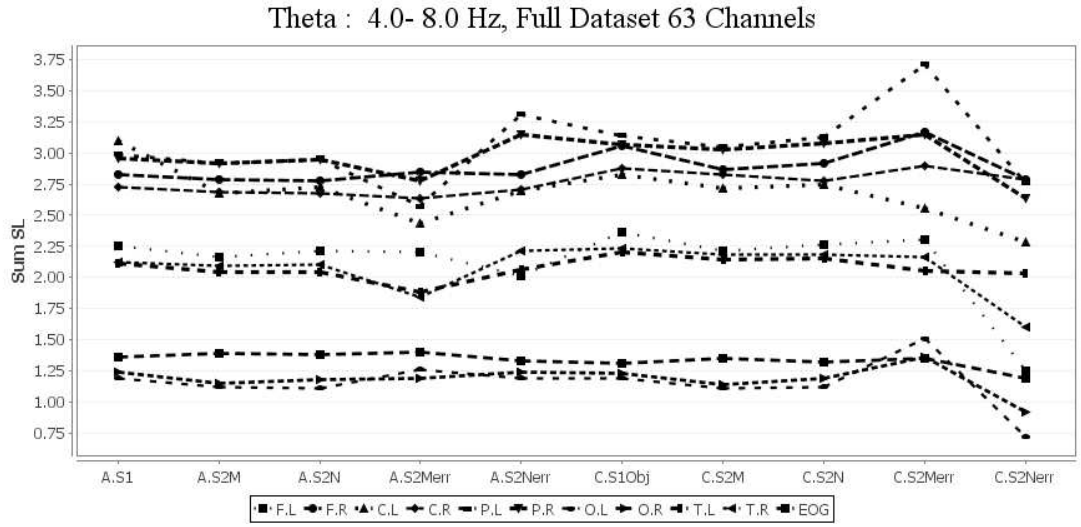

Figure 6.8: θ on Full Dataset with 61 EEGs and 2 EOGs

6.4 Chapter Summary

In this chapter, the greedy maximum weight matching analysis on the functional connectivity in the human brain is proposed. This is the first time that the functional connectivity between EEG and EOG is investigated. It is also the first time that a classical graph algorithm is used to study the synchronization of EEG phenomena. Compared with the modem small-world graph theories, this approach can classify the repeated and unrepeated stimuli on controlled drinkers, and can be used as a testbench for the selection of optimal channel numbers. Moreover, this study indicates that maximal weight matching combined with synchronization can be a useful tool to evaluate the abnormal EEG signals. It is also found that the different functional connectivity between processing repeated stimuli and unrepeated stimuli in the controlled drinkers is larger than that in the alcoholics. Moreover, it shows that the *EOG* is not sensitive with the alcoholics.

Chapter 7

Studying Multi-channel sleep EEG based on Graph Isomorphism

Based on the fast weighted horizontal visibility algorithm in Chapter 5, this chapter presents an efficient horizontal visibility graph isomorphism algorithm (HVGI) by taking advantage of two synchronization measuring methods: phase locking value (PLV) and visibility graph similarity (VGS). Four sleep subjects are tested with three synchrony methods. Three synchronized indices between two channel EEGs and one EOG signal are extracted with each method. Analysis results shows that HVGI indices increase from wake stage to deep sleep. These extracted features are forwarded into a support vector machine to classify the sleep stages. 11,120 data segments are used for the experiments with each segment lasting 30 seconds. The training sets are selected from a single subject and the testing sets are selected from others subjects. Wake-sleep stage classification is used to evaluate the performances of the PLV, VGS and HVGI methods. The experimental results show that features based on the HVGI algorithm are better than those based on PLV and VGS. The sensitivity of the 6-state sleep stage classification shows that the HVGI feature is suitable for light sleep stage identification. In addition, the speed of the HVGI is 39 times faster than the VGS algorithm. Some results were presented in (Zhu et al. 2012*b*) .

This chapter is organized as follows: the synchrony studied on sleep EEG are briefly introduced in the next section. The proposed HVGI algorithm and other several synchronization measuring methods, such as PLV, VGS, are introduced in Section 7.2.2. Section 7.3 presents the experiment results.

7.1 Review of sleep stages classification with synchrony methods

Sleep is a spontaneous, reversible brain state. People spend about one-third of living time in sleep. During sleep, the body will be recovered and information on memory will be integrated. Sleep deficiency increases the risk of heart disease (Walters & Rye 2009), hypertension (Gangwisch et al. 2006), and suicidal thoughts (McCall & Black 2013). Therefore, measuring sleep quality is an important issue for healthy life style evaluation.

Synchronization is a common phenomenon in the human brain. Several synchrony measurements based on electroencephalography (EEG) signals have been presented in recent years. Cross correlation (Apostol & Creutzfeldt 1974, Abdullah et al. 2010) and coherence function (Knapp & Carter 1976) are two simple and linear methods to measure the interdependency between two channels of EEGs in both time and frequency domains. Nonlinear synchronization approaches, such as phase locking value (PLV) (Rosenblum et al. 1996), synchronization likelihood (SL) (Stam & Van Dijk 2002) and visibility graph similarity (VGS) (Ahmadlou & Adeli 2012), appear more powerful in solving the problems of time series signals.

Coherence and synchrony analysis have been widely applied in sleep EEG analysis. For example, Achermann and Borbély (1998) showed that coherence between homologous interhemispheric derivations was high in the low frequency range and declined with increasing frequencies during sleep. Mölle et al. show (2004) that learning increases human electroencephalographic coherence during subsequent slow sleep oscillations. Ferri et al. (2007) showed that there were high levels of synchronization in the slow-wave sleep EEG signals by means of the SL method. Aijun He et. al (2007) proposed the PLV method for sleep stages identification. Aksahin et al. (2012) used a coherence function to classify the sleep apnea syndromes. However, few works identified sleep stages with synchrony methods. Although Zhu et al. (2012*a*) presented a similar horizontal visibility directed graph to identify seven sleep stages with four subjects, the accuracy was not enough higher. The PLV or SL methods are limited in sleep stage classification because clinical sleep EEG signals are always recorded from PSGs, which are normally less three channel EEG signals. The three channel signals can only extract a complex network with three nodes, which hardly extract meaningful necessary features to conduct sleep classifications.

This chapter proposed an efficient horizontal graph isomorphism (HVGI) method to identify the sleep stages within three biomedical siganls. The horizontal graph isomorphism is proved in linear speed. To evaluate the performance, three synchrony measuring methods, PLV, VGS and HGI, are applied to test sleep stage classification. For each of the three algorithms, first, two channel EEG signals (Fpz-Cz and Pz-Oz) and one EOG (the horizontal) signal are used and filtered in delta, theta and alpha bands. Second, the synchronization matrix is calculated by HVGI, PLV and VGS respectively. The synchronization matrix is extracted and forwarded as the input to a support vector machine algorithm to classify the

seven sleep stages. There are 1390 segments of data forming the training set, and a total of 11120 segments of data from four subjects are used for testing. Finally, the classification accuracy and the computing speed of the PLV, VGS and HVGI algorithms are then compared in the end.

7.2 Data and methodology

The procedure of the proposed method is shown in Figure 7.1. The synchronized indices PLV, VGS and HVGI, associated with two channel EEGs and one channel EOG was mapped into three complex networks. The classification of sleep stages involves the training stage and the testing stage, with the size of training data is only 12.5% of the size of testing sets.

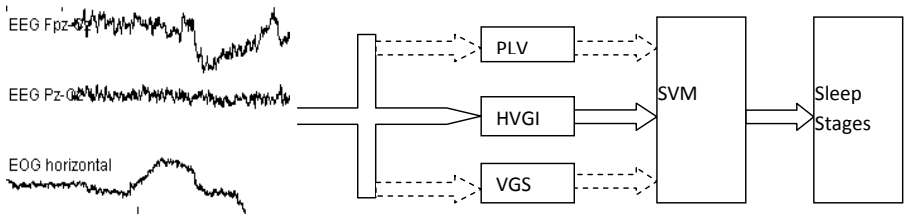

Figure 7.1: Processing Diagram by HVGI, PLV and VGS

7.2.1 Experimental data

The experimental data used in this chapter were obtained from the public Sleep-EDF database as shown in Section 3.4.1, which is also used in Chapter 9. Only four data recordings from subjects: sc4002e0, sc4012e0, sc4102e0 and sc4112e0, are used in this chapter. In addtion, this study only uses the segments from 1 to 2780 for all four subjects, with a total of 11,120 data segments. The processing diagram for two sleep EEG signals and one EOG signal is shown in Figure 7.1.

7.2.2 Visibility graph similarity method

The Visibility Graph Similarity (VGS) algorithm was introduced by Ahmandlou and Adeli (2012) based on the visibility graph algorithm. Like the PLV algorithm, it is used to measure the generalized synchronization among multiple signals. It is divided into three steps. First, any two input time series signals,$\{x_i\}_{i=1,2,...,n}$ and $\{y_i\}_{i=1,2,...,n}$, are mapped into two VGs, G_x and G_y. The second step is to calculate the degree sequences of DS_x and DS_y, respectively. Last the synchronization of

x and y is calculated based on the degree sequences using their cross correlation:

$$S(x,y) = \frac{Cov(DS_x, DS_y)}{\sigma_{DS_x}\sigma_{DS_y}} \tag{7.1}$$

where $Cov(x,y)$ is the covariance of x and y, and $\sigma(x)$ is the standard deviation of x. The value of $S(x,y)$ are in the range of [0..1]. The index of the VGS algorithm is the average of S in each channel.

Although the VGS algorithm has been proved to be more powerful than the coherence method or the SL method for analyzing certain types of Chaos signals (2012), there are two obvious drawbacks of VGS. The fist is that the VGS algorithm is based on the Algorithm 1. As time complexity for constructing a VG is $O(n^3)$, the VGS algorithm is also slow in $O(n^3)$. The other drawback is that the VGS algorithm yields an incorrect result for the synchronization between two signals. Considering two time series signals, $x = \{7,1,2,4,2,1,7\}$ and $y = \{6,2,1,4,1,2,6\}$, their degree sequences of the VG are the same: $DS_x = DS_y = \{4,3,3,6,3,3,4\}$. From calculating equation 7.1, we have: $S(x,y) = 1$. This result indicates that x and y are exactly synchronized with each other - which is not true in this case.

7.2.3 Horizontal visibility graph isomorphism

This study proposes a graph isomorphism algorithm to overcome the pitfalls in Section 7.2.2. To improve the speed of constructing graphs, the FWHVA algorithm is used. To measure the difference between two graphs, graph isomorphism is employed. Graph isomorphism is a bijection between two graph G and H. If all edges of G and H can be mapped by one to one with the a same labeled DS, the G and H are exactly isomorphic. Because Cook (1971) shows that graph isomorphism could not be solved in polynomial time unless $P = NP$, this study applies a linear time method to measure this problem between the two HVGs. Given two degree sequences DS_x, DS_y of two HVGs G_x, G_y, the horizontal visibility graph isomorphism index (HVGI) of two graphs is measured as following:

$$HVGI(G_x, G_y) = 1 - |\frac{DS_x - DS_y}{DS_x + DS_y}| \tag{7.2}$$

If G_x and G_y are isomorphic, the $HVGI(G_x, G_y)$ is one, otherwise if G_x and G_y are different, then the $HVGI(G_x, G_y)$ is small. If one graph is empty, then the $HVGI(G_x, G_y)$ is zero. It is noted that equation 7.2 only holds for HVGs because the HVGs from the same time series have the same DS.

7.2.4 Multiclass support vector machine classification

A support vector machine (SVM) was applied to perform the multiple sleep stages classification. SVMs have been used in sleep stages classification by other researchers (Zhu et al. 2012*b*, Mourad Adnane & Yan 2012, Vatankhah et al. 2010). Using a SVM classifier, it is possible to conduct a linear space discrimination or nonlinear classification by choosing a kernel function. There are four kernel functions: linear, polynomial kernel, radical basis function (RBF) and sigmoid. It was included in an R package e1071 (Karatzoglou et al. 2006), the RBF kernel was applied and the control parameter γ for the RBF kernel of SVM is fixed to 0.33.

7.3 Results and discussions

To evaluate the performances of the three synchronization methods: PLV, VGS and HVGI, the experiments were conducted with R programming language, PLV was described in Section 2.3.2. The sleep EDF-file data mentioned in Section 3.4.1 was converted into the ASCII format.

7.3.1 Analysing HVGI on whole sleep processing

Figure 7.2 shows three channels HVGI index among 2800 epochs from subject *sc*4012*e*0. Three obvious cases are determined from Figure 7.2. First, that sleep is more synchronized than awake on all pairs of channels, which indicates that the EEG signals during sleep stages are more synchronized than those during awake. Second, that the HVGI of REM is lower than that of SWS, which also agrees that the REM is desynchronized than NREM.

According to existing results, such as (Ferri et al. 2007) and (Mölle et al. 2004), the synchrony between EEG signals in sleep is stronger than those in wake stages. The HVGI measuring results agree with this evidence.

7.3.2 Compared with HVGI, PLV, and VGS

Figure 7.3 shows the three synchronized indices of three channels among six sleep stages. It is obvious that the HVGI are the highest indices. The HVGI of pair channel FpzCz–PzOz and pair channel PzOz–EOG increase stably from AWA stage to S4 stage, while the HVGI of pair channel PzOz–EOG just maintain growth from the AWA stage to the S3 stage, the HVGI of S4 stage drops just above S2 stage. Compared to HVGI, the increasing trends of PLV are only similar FpzCz–PzOz case, only the PLV of AWA is larger than that of S1. Both PLV

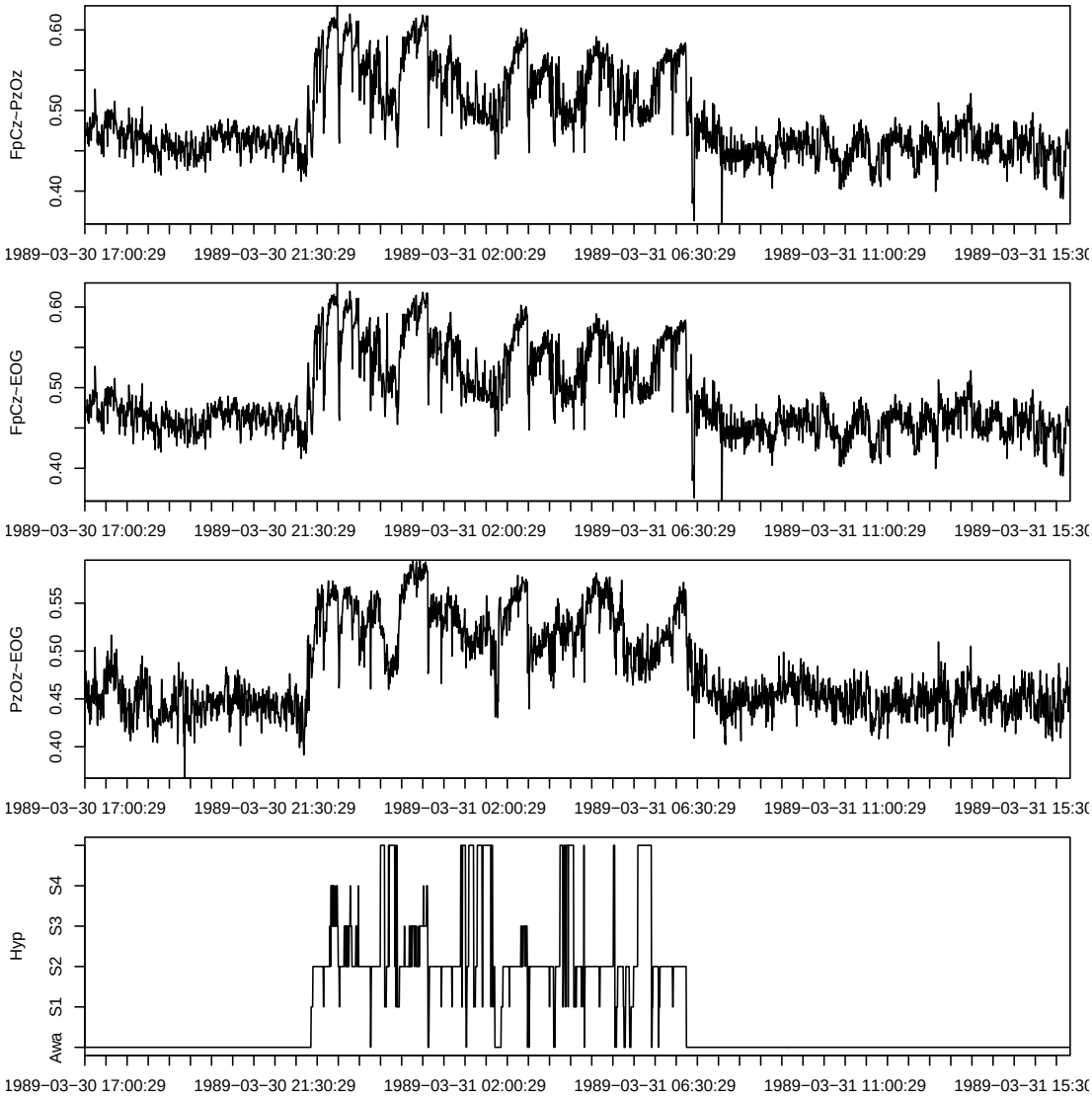

Figure 7.2: HVGI associated with two EEG channel (FpzCz and PzOz) and one EEG channel

between EEG and EOG fluctuate in each sleep stage. Unlike HVGI, the lowest PLV indices of three pair channels are located in sleep stages S1, S2 and S2 respectively. Like PLV, the VGS between EEG and EOG remain steady in each sleep stage. Only the VGS of pair FpzCz–PzOz is appear as a wave curve, where the VGS of AWA is lowest. However, the lowest PLV of S1 is deviation from the biological view. Thus, HVGI is more suited to representing synchronized indices during the sleep.

On the other hand in Figure 7.3(b) and (c), all HVGI of the REM stage are lower than the deep sleep stage more like the S1 sleep stage. Similar to HVGI and PLV of REM stage also drops to the same level as S1 stages. In contrast, VGS of the REM stage is higher than the other stages. These phenomena show that the different synchronized indices of sleep stage are significantly different, especially on the synchronized indices between EEG and EOG signals.

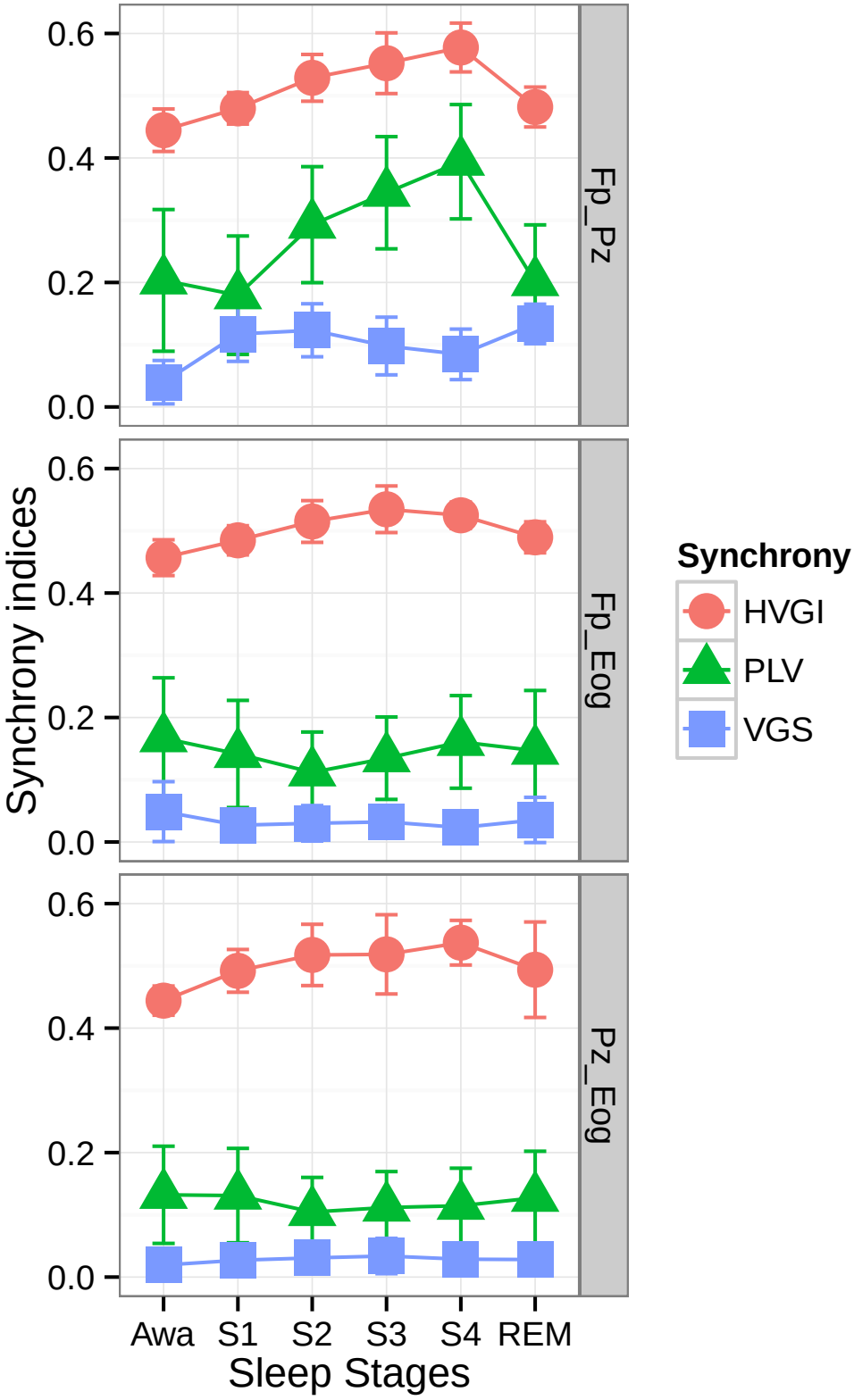

Figure 7.3: Three synchronized indices and the sleep stages

7.3.3 Classifying Sleep EEGs

First, the sleep-wake sleep state classifications are conducted with PLV, VGS and HVGI methods. The accuracies are listed in Table 7.1, where the training data set is from subject sc4012e. Symbol * in Table 7.1 indicates that the training data are from that subject *sc*4012*e*0. The results using the four subjects were compared. The highest classification accuracy of 96.02% was obtained for both subjects *sc*4012*e*0 and *sc*4002*e*0 by HVGI. However, as for the subject *sc*4112*e*0, it is found that sleep identification possesses highest specificity 60% based on PLV which is better than those based on VGS and HVGI.

Table 7.1: Sleep-wake classifying accuracies with the PLV, VGS , HVDS

Subject	PLV			VGS			HVGI		
	SE	SP	AC	SE	SP	AC	SE	SP	AC
sc4002e0	0.90	0.62	80%	0.89	0.93	87%	0.94	0.99	96%
sc4012e0	0.85	0.52	74%	0.94	0.94	94%	0.96	0.96	96%
sc4102e0	0.80	0.29	62%	0.82	0.89	83%	0.93	0.80	88%
sc4112e0	0.94	0.60	85%	0.97	0.48	85%	1.00	0.16	79%
average	0.87	0.51	76%	0.91	0.78	87%	0.96	0.73	90%

Second, the confusion matrix of six-sleep state with *sc*4002*e*0 classified with HVGI is shown in Table 7.2. The training set is *sc*4012*e*0. The confusion table is shown in Table 7.2. The accuracy of Table 7.2 is 81.0%.

Table 7.2: The confusion matrix and sensitivity on 6-state sleep stages with HVGI

		Expert's scoring					
		AWA	S1	S2	S3	S4	REM
The proposed method	AWA	1754	2	1	1	3	11
	S1	1	0	0	0	0	0
	S2	43	12	325	90	179	38
	S3	0	0	0	1	20	0
	S4	0	0	0	0	0	0
	REM	28	45	47	2	1	166
Sensitivity		96.1%	0.0%	87.1%	0.01%	0.0%	77.2%

According to Tables 7.1, the accuracy for individual subjects is only slightly affected by a different training set for the HVGI methods. In contrast, the accuracies of the PLV and VGS are strongly affected by a different training set. According to Table 7.2, The average accuracy of the HVGI is closer to the accuracy rate by an expert's evaluation, which is $83 \pm 3\%$ (Chapotot & Becq 2010). The HVGI with SVM also has a higher accuracy than the power spectral density with an artificial neural network method (Ronzhina et al. 2012), which is at most 76.40% on six sleep stages for the same Sleep EDF dataset.

The computation times using the three synchronization measuring methods are evaluated and shown in Table 7.3, which does not include the SVM running time. All experiments are implemented on a computer with 3.0G Hz Inter CoreTM Duo E8400 processor and 4GB of RAM. From Table 7.3, it can be observed that the HVGI method is 39 times faster than the VGS, but 5 times slower than the PLV due to the running time in HVGI including the executing cross correlation time. Each 30-second of a segment only needs 8.03ms for obtaining its sleep stage with the HVGI algorithm.

Table 7.3: Computational time for feature extracting

Algorithms	PLV	VGS	HVGI
Running time	0.42s	95.09s	2.41s

7.4 Chapter Summary

Although synchronization methods, such as the PLV and VGS, are widely used to study the EEG signals, the application for multi-sleep stages classification by these methods are not previously reported in the literature. This chapter is the first time the HVGI has been applied to analyse sleep EEG signals. This chapter is also the first report of PLV accuracy for classifying sleep stages. To efficiently identify the isomorphism between two horizontal visibility graphs, a linear complexity algorithm is presented based on FWHVA algorithm as shown in Chapter 5. This chapter compares three synchrony measuring methods: PLV, VGS and HVGI, with a SVM to identify sleep-wake sleep stages classification and 6-state sleep stages scoring with 11120 segments. It is shown that the brain signals during sleep are always higher synchronized than those of awake. The results show that the accuracy of the HVGI classification method is the highest among those of the VGS and PLV, and the accuracy of the HVGI is only slightly affected by a different training data. These results suggest that the proposed HVGI method is promising and can be used for online sleep stages classification.

Chapter 8

Analysis of Network Topologies during Sleep

Over the last few years, studies multi-channel EEG signals with complex brain networks have grown rapidly. Chapter 2 reviewed the complex brain networks of sleep by means of multi-channel EEG signals and graph analysis. However, the network topologies associated with individual sleep EEG signals are poorly understood. This chapter investigates the changes of network topologies from wakefulness to deep sleep when temporal complex networks (TCNs) are associated with EEG signals derived from polysomnography (PSG).

The local clustering coefficient (C), mean degree (D), and average shortest path (L) of TCNs are extracted from five individual EEG channels of 28 healthy subjects. The statistics shows that brain functions are characterized by the lowest C and the highest D during deep sleep. It is found that C and D, associated with rapid eye movement (REM) stage of the occipital region, are significantly different from those of stages awake and light sleep of the frontal area. This finding suggests that the TCNs can be an efficient tool for the measurement of the sleep quality in clinical situations. However, the identification of sleep stages from EEG electrodes from human brain's central, parietal and occipital regions is better than that from frontal zone.

The remaining sections in this chapter are organized as follows: The temporal complex networks and their network topologies are introduced in Section 8.2. Section 8.3 presents the experiment results, and some existing results are compared with the network topologies associated with multi-channel EEGs in Section 8.3. Finally, conclusions are drawn in Section 8.5.

8.1 Introduction

Complex networks are a subset of graphs which are represented as nodes that connected by edges. Complex networks have been proven to be a powerful approach to quantifying important patterns of brain dynamics. Recently, as shown in Chapter 2, two typical functional complex networks were widely applied in brain function study. The first are spatial complex networks (SCNs). A node in a SCN is a brain region, or a voxel (Hayasaka & Laurienti 2010) or an EEG channel (Ferri et al. 2007), and an edge of a SCN is presented when there is an anatomical connection or a functional correlation between the two nodes. SCNs help researchers understand how the brain function works in a system level (Bassett & Bullmore 2006, Bullmore & Sporns 2009, He, Chen & Evans 2007, Reijneveld et al. 2007). Human brain functional networks show the properties of small world networks (SWNs) (Bassett et al. 2006), which have a high local clustering coefficient (C) (Watts & Strogatz 1998) and a short average path length (L). Complex brain networks (Bullmore & Sporns 2009) are an examples of SCN.

The second are temporal complex networks (TCNs) from one channel EEG signals. A node of a TCN is a data point from an EEG time series or a phase space of an EEG time series, and an edge of a TCN is defined by the geometric relationship between two nodes. Visibility graphs (VGs) (Lacasa et al. 2008) are one type of TCN and have been applied to study brain dynamics from EEG time series (Dong & Li 2010, Zhu, Li & Wen 2014*a*).

Complex networks have attracted growing interest in brain function analysis. SCNs have been also applied in sleep function analysis. For example, networks during sleep, based on multi-channel EEGs, appeared having a higher C and a lower L phenomenon (Ferri et al. 2007). By analysing fMRI time series, brain networks have a higher C in deep sleep than those in wakefulness (Spoormaker et al. 2012). The degree of SCNs based on EEG during deep sleep are low (Bashan et al. 2012). The modularity of SCNs derived from EEG signals during deep sleep is higher than those of wakefulness (Tagliazucchi et al. 2013). Some researchers have tried to map the temporal information into SCNs to study brain functions (Holme & Saramäki 2012), however, this type of SCNs cannot work if the spatial information is lost (such as using only EEGs deriving from PSGs). A SCN associated with EEG signals from PSG has only two or three nodes because a PSG contains two or three channel EEG signals. Therefore, the three SCNs cannot represent sleep qualities.

This study focuses on the TCNs from individual EEG signals, especially those from PSGs. Then a natural question rises, how do TCNs differ between the awake and sleep EEG signals compared with SCNs?

8.2 Materials and methodology

8.2.1 Preprocessing sleep databases

Two sleep databases are applied in this chapter as shown in Table 8.1. The distribution of proportions from each sleep stage on two database are not the same. To minimise the sleep stages, difference of the two database, stages S1 and S2 in both databases were combined as a LS stage. The concatenated method is the same as the existing literatures (Hsu et al. 2013, Berthomier et al. 2007). In same principle, stages S3 and S4 are combined as deep sleep (DS). There are no significant differences in subjects' age or gender between these two databases (see Table 8.1).

Table 8.1: Summary of the EEG data information

Databases	Subjects Age	Gender (male/female)	Electrodes	Epochs (AWA/LS/DS/REM)
Sleep-EDF	28.4 ± 5.3	4/4	FpzCz,PzOz	3589/2935/721/1415
Dream	33.5 ± 14.6	4/16	Fp1A1, CzA1, O1A2	1324/10608/1717/2995
p-Values	0.66	0.42	Na	Na

8.2.2 Mean degree, clustering coefficient and average path

Figure 8.1 (a) shows how a sleep EEG signal X is transferred into a visibility graph. Here X comes from a subject, *subject1*, with 40 points in the Dream sleep database (DEVUYST, 2013) from the second epoch. Two nodes are connected if and only if there is visibility, such as nodes 35 and 40 are connected as shown in Figure 8.1 (b). A time series can be characterized by network topologies, such as mean degree, clustering coefficient, average path etc (Newman, 2003). The average degree of a graph G with n nodes is defined as:

$$\bar{d} = \frac{1}{n}\sum_{j=1}^{n} d_j \tag{8.1}$$

The clustering coefficient (C) is another typical property of complex networks. The coefficient index c_i of node v_i is the number of existing edges between the nodes of neighbours divided by all their possible edges. The average C of a graph

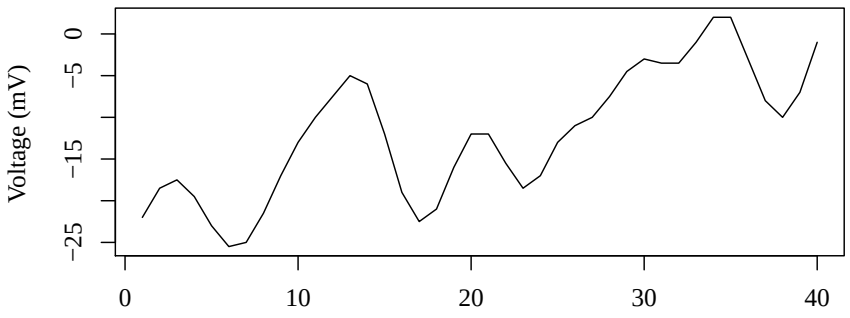

(a) Sleep EEG signals

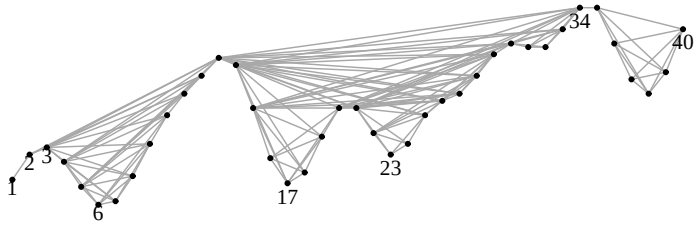

(b) Corresponding VG of (a)

Figure 8.1: (a) EEG signals; (b) Corresponding visibility graph

having n nodes is defined as:

$$\bar{c} = \frac{1}{n} \sum_{j=1}^{n} c_j \tag{8.2}$$

In addition, the average path length plays an important role in measuring the communication within a graph. The average path length (L) is defined by the average of geodesic lengths over all pairs of nodes:

$$\bar{l} = \frac{1}{n(n-1)} \sum_{i=1}^{n} \sum_{j=i+1}^{n} c_j \tag{8.3}$$

where l_{ij} is the length of the shortest path from node j to node i. The maximum value of l_{ij} is called the diameter of a graph.

8.2.3 Statistical analysis

To compare the differences of network topologies associated with the EEGs among four sleep stages in two sleep EEG databases, a non-parametric Wilcoxon test is used for measuring what occurs between the two sleep stages because the distribution of sleep EEG data does not satisfy a normal distribution. Analysis of variance (ANOVA) is applied to compare the statistical results from TCNs associated with the sleep stages AWA, LS and the sleep stage REM.

8.3 Results

To evaluate the performances of the proposed method discussed in Section 8.2, the algorithm is implemented with C programming language integrated into an R. The experiments consist of three parts: A. The analysis of the mean degrees of VGs associated with EEG signals; B. The analysis of the clustering coefficients on sleep stages; C. The analysis of the average shortest paths of sleep stages; D. The awake and deep sleep states are compared through the different topologies observed from the TCN and SCN.

8.3.1 Mean degrees of VGs associated with sleep EEGs

The mean degrees of VGs from the Sleep-EDF and Dream sleep datasets associated with four sleep stages are shown in Figures 8.2 (a) and (b), respectively. Figure 8.2 (a) shows statistical $\bar{d}$ of VGs associated with FpzCz and PzOz channels from Sleep-EDF database. Figure 8.2 (b) illustrates statistical $\bar{d}$ of VGs associated with Fp1A1, CzA1 and O1A1 channels from the Dream database. Compared with wakefulness, deep sleep was characterized by a diffuse increase in both Figures 8.2(a) and (b).

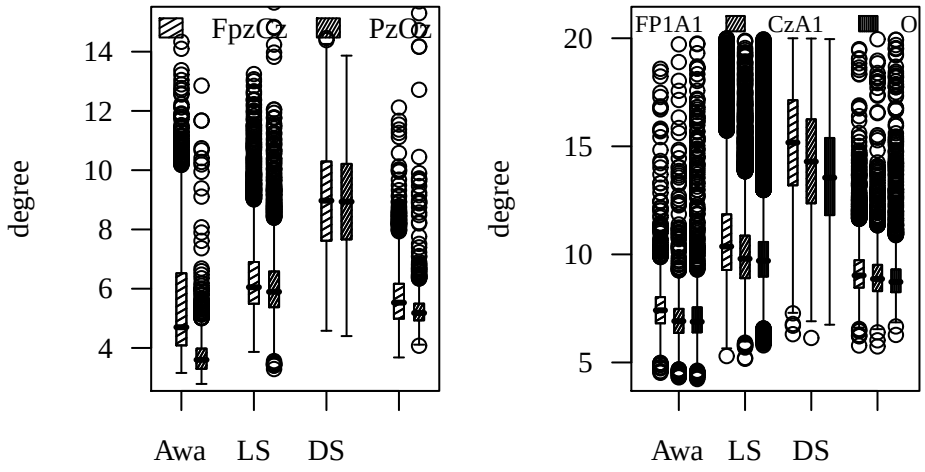

(a)Sleep−EDF database (b)Dream Sleep database

Figure 8.2: Statistical $\bar{d}$ of VGs associated with EEGs from two Sleep-EDF database

As shown in Figure 8.2(b), values between channels CzA1 and O1A2 are closer than those between channels Fp1A1 and CzA1, and between Fp1A1 and O1A2. It is important to understand whether VGs from the occipital and central regions are the same values as those from frontal area. Wilcoxon tests are applied to compare the differences of $\bar{d}$ of VGs between channel pairs: FpzCz vs PzOz and CzA1 vs O1A2. The results are listed in Table 8.2.

Table 8.2: Test results of $\bar{d}$ between channel pairs with two sleep databases

Stages	AWA		LS		DS		REM	
Pair Channels	FpzCz vs PzOz	CzA1 vs O1A2	FpzCz vs PzOz	CzA1 vs O1A2	FpzCz vs PzOz	CzA1 vs O1A2	FpzCz vs PzOz	CzA1 vs O1A2
p-value	$<$ 0.001	$<$ 0.001	$<$ 0.001	0.69	0.26	$<$ 0.001	$<$ 0.001	$<$ 0.001

8.3.2 Mean local cluster coefficients of VGs associated with EEGs

Figure 8.3 (a) shows statistical $\bar{c}$ on VGs associated with FpzCz and PzOz channels from Sleep-EDF database. $\bar{c}$ in stages Awa, LS and REM are larger than 0.70. Figure 8.3(b) shows statistical $\bar{c}$ on VGs associated with Fp1A1, CzA1 and O1A2 channels from Dream Sleep database. It shows that the ranges of $\bar{c}$ on all sleep stages are less than 0.70.

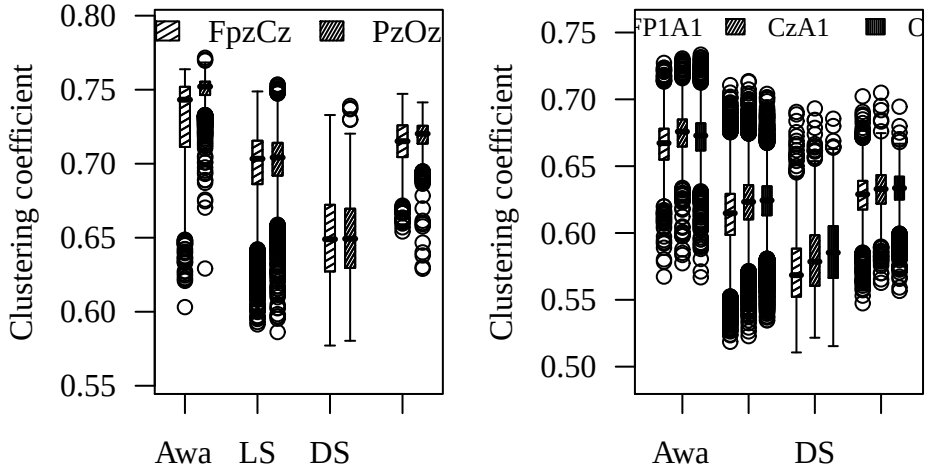

(a)Sleep−EDF database (b)Dream Sleep database

Figure 8.3: Statistical $\bar{c}$ of VGs associated with EEGs from the Sleep-EDF database

Unlike the findings of an increased trend of $\bar{c}$ for SCNs (Ferri et al. 2007), this study shows that $\bar{c}$ is significantly decreased from wakefulness to deep sleep. On the other hand, Figures 8.2 and 8.3 illustrate that $\bar{(d)}$ and $\bar{c}$ of VGs on REM stage are very close to the AWA and LS stages. ANOVA is applied to measure the differences between stage REM and the AWA and LS stages of all EEG channels. The results are shown in Table 8.3.

Table 8.3: ANOVA for testing the differences $bar(c)$ between REM stage and AWA and LS stage with different channels

Channels	FpzCz	PzOz	Fp1A1	CzA1	O1A2
p-Values	0.950	< 0.001	0.104	< 0.001	< 0.001

8.3.3 Average short path of VGs associated with EEG signals

Figure 8.4 illustrates the statistical average path length $\bar{l}$ of VGs associated with the two sleep EEG databases. The channels are FpzCz, PzOz, Fp1A1, CzA1 and O1A2 electrodes.

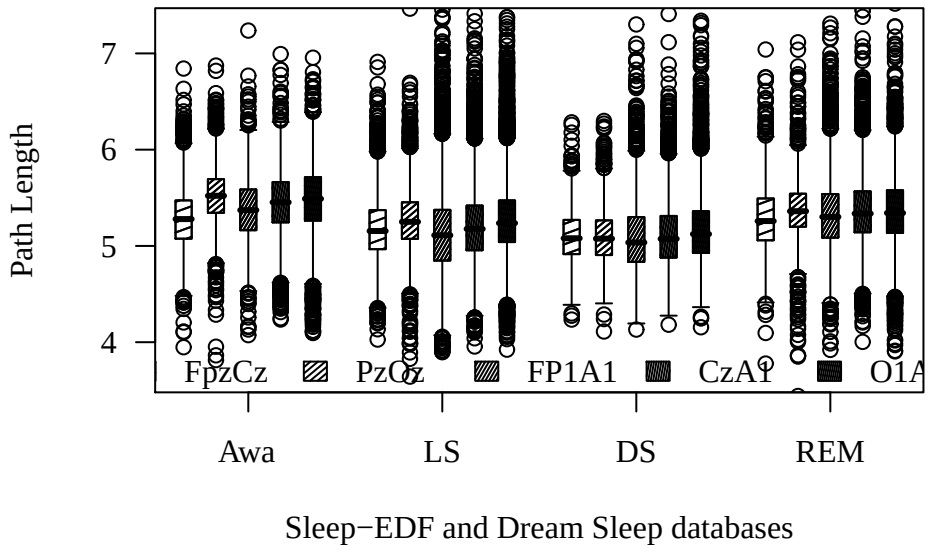

Figure 8.4: $\bar{l}$ of VGs associated with EEGs from Sleep-EDF database and Dream sleep database

Unlike Figures 8.2 and 8.3 are separated in two parts, $\bar{l}$ of VGs from all channels associated with all sleep stages (presented in Figure 8.4), because $\bar{l}$ are approximately equal in all sleep stages, even the channels come from two different databases with different sampling as shown in Table 8.3. By visual observation, $\bar{l}$ from deep sleep is less than those of other sleep stages, even when the signals come from two different databases with different sampling. Kolmogorov-Smirnov Tests show that the $\bar{l}$ on all stages do not satisfy normal distributions. Non-parameter Wilcoxon test is applied to check $\bar{l}$ of DS stage whether is less than other stages. The test results are listed in Table 8.4, where $\bar{l}$ of DS stages of all channels is 5.12, the statistical differences are considered significant ($p < 0.001$)

Table 8.4: $\bar{l}$ of deep sleep (DS) stage are lower than those from other stages

Channels Compared	AWA	SL	REM
p-Values	< 0.001	< 0.001	< 0.001

8.4 Discussions

8.4.1 Which electrode is suitable for single channel sleep stage scoring

Recently, researchers has focused on classifying sleep stages with a single channel EEG signal. It is interesting that many studies use the PzOz channel to score the sleep stages in Sleep-EDF (Berthomier & Brandewinder 2013, Liang et al. 2012, Zhu, Li & Wen 2014*a*). Selection of this electrode appears to depend research experience. In this study, the network topologies of TCNs could show how to select the optimal channel for sleep stage classification. Table 8.3 shows that $\bar{c}$ between stage REM and stages AWA, LS on PzOz channel is significantly different(p¡0.001). Conversely, those on FpzCz are the same (p=0.95). These differences indicate that EEG signals from the occipital or central regions are more suitable for sleep stages scoring than those from the frontal area. These results explain why researchers used the PzOz channel for single channel sleep stage scoring with the Sleep-EDF database (Berthomier & Brandewinder 2013, Liang et al. 2012, Zhu, Li & Wen 2014*a*). However, Table 8.3 shows that $\bar{d}$ of VGs from CzA1 is similar to that of O1A2 during light sleep ($p = 0.69$), $\bar{c}$ and $\bar{d}$ of VGs from FpzCz is no different from that of PzOz during deep sleep. All these facts indicate that the EEG signals in the occipital region are not significantly different from those in central areas. In fact, these results are consistent with the $R\&K$ rule (EA 1969) which recommended channel CzA1 to score the sleep stages, and also agrees with the American Association of Sleep Medicine manual (Iber 2007) which recommended that arousal scoring is better in detecting occipital EEG from central EEG derivations, and suggested that CzOz and FpzCz derivations be added to PSG.

8.4.2 Complexity of sleep EEG based on complex networks

Nonlinear and complexity measurements have been widely applied to the analysis of sleep EEG signals. Example save the fractal component (Pereda et al. 1998), approximate entropy (Burioka et al. 2005) and permutation entropy (Nicolaou & Georgiou 2011). Figure 8.3 shows that the changes in $\bar{c}$ of VGs for sleep stages are consistent with the existence of complexity measurement of sleep stages. The

changes of $\bar{c}$ in VGs are very similar to the changes of approximate entropies in Figure 1 of (Burioka et al. 2005, p. 22). Like the permutation entropies trends in Figure 1 of (Nicolaou & Georgiou 2011, p. 26), $\bar{c}$ of VGs is statistically lower during deep sleep and higher during AWA and REM stages.

From a physiological point of view, patterns from the human brain during awake are more active and exciting, the complexity indices are larger, and the clustering coefficients of complex brain graphs are also higher. During deep sleep, the cerebral cortex generates extremely slow waves, the complexity of brain signals is the lowest, and $\bar{c}$ of complex brain graphs is the lowest as well. When sleep state changes to REM stage, the breathing becomes more rapid and eyes jerk rapidly in various directions, and $\bar{c}$ of complex brain graphs increases. However, $\bar{c}$ in sleep of Figure 8.3 is lower than that in AWA, which more correctly reflects sleep complexity because the brain in this state is less active than in AWA.

8.4.3 Comparisons of network topologies between spatial and temporal

To highlight the outcomes in this study, the summary of the TCNs changes from wakefulness to deep sleep are listed in Table 8.5 compared with the SCNs. Because our results are based on single channels of EEG signals from different sleep EEG databases with different sampling, the statistical results are more robust than those of SCNs. According to Table 8.5, the network topology of TCNs associated with deep sleep EEGs not only have opposite changes in $\bar{c}$ and $\bar{d}$ but also decrease $\bar{l}$ compared with those of SCNs. Our study suggests that the network topologies based on TCNs during sleep can be more beneficial for clinical situations than those based on SCNs.

Table 8.5: Summary of the network analysis results for SCNs and TCNs

	Change from wakefulness to deep sleep	
Measures	(SCNs)	**TCNs**
$\bar{d}$	$\downarrow$ (Bashan et al. 2012, Spoormaker et al. 2012)	$\uparrow$
$\bar{c}$	$\uparrow$ (Boly et al. 2012, Ferri et al. 2007)	$\downarrow$
$\bar{l}$	$\updownarrow$ (Ferri et al. 2007)	$\downarrow$

8.5 Chapter Summary

In this chapter, temporal complex network topologies, such as mean degree, clustering coefficient and average path length are used to evaluate the brain function during different sleep stages from a single channel EEG time series. To our knowledge, there are no previous reports of complex brain networks associated with EEG signals deriving from PSGs. This is the first study of complex networks based on individual EEG signals (though SCNs have been used to measure the multi-channel EEG data sets). In contrast to the known SCN results, the clustering coefficient and average shortest path of TCNs associated with EEG time series during deep sleep are lower than those of wakefulness, while the mean degree of TCNs is the highest in deep sleep. In addition, this study illustrates that network topologies from occipital region EEGs, are more suited to measuring arousal than those in other areas. It also found that the TCN analysis results cannot identify the difference between light sleep and the REM stage. Because PSGs are the most commonly used for the diagnoses of sleep disorders in clinical settings (Berthomier & Brandewinder 2013), this study suggests that TCNs associated with EEG signals derived from PSGs can be an efficient and robust tool for sleep quality diagnosis in clinical settings.

Chapter 9

Classifying Sleep Stages Using Single-channel EEG Signal by Difference Visibility Graphs

There are many studies on sleep stage classification with multi-channel EEG signals. Chapter 7 evaluated six sleep stage scoring methods with two channel EEG signals and one channel EOG signal. This chapter classifies the sleep stages based on graph domain features from a single channel electroencephalogram (EEG) signal. First, each epoch (30s) EEG signal is mapped into a visibility graph (VG) and a horizontal visibility graph (HVG). Second, a difference visibility graph (DVG) is obtained by subtracting the edges set of the HVG from the edges set of the VG to extract essential degree sequences and to detect the gait-related movement artifact recordings. The mean degrees (MDs) and degree distributions P(k) on HVGs and DVGs are analysed epoch-by-epoch from 14,963 segments of EEG signals. Then the MDs of each DVG and HVG and seven distinguishable degree distribution values of P(k) from each DVG are extracted. Finally, nine extracted features are forwarded to a support vector machine to classify the sleep stages into 2-state, 3-state, 4-state, 5-state and 6-state. The accuracy and kappa coefficients of 6-state classification are 87.5% and 0.81, respectively. It was found that the MDs of the VGs on the deep sleep stage are higher than those on the awake and light sleep stages, and the MDs of the HVGs are just the reverse. These results are presented in (Zhu, Li & Wen 2014*a*).

The remaining sections of this chapter are organized as follows: the experimental data are described in the next section. The visibility graph, the horizontal visibility graph, and the difference visibility graph are introduced in Section 9.3. Section 9.4 presents the experimental results. The performances of the proposed method on 2-state, 3-state, 4-state, 5-state, and 6-state sleep stages classifications are also compared with the results reported from existing methods. Finally, conclusions are drawn in Section 9.5.

9.1 Sleep classification based on single channel EEG

Efficiently identifying sleep stages is beneficial for the treatment of sleep apnea, insomnia and narcolepsy. Polysomnogram (PSG) techniques are applied to the diagnosis and treatment of sleep disorders. The classification of sleep stages is traditionally performed by experts based on the visual interpretation of the PSG according to Rechtschaffens and Kales' ($R\&K$) recommendations (EA 1969) or a new guideline developed by the American Academy of Sleep Medicine (AASM) (Iber 2007). This study uses 6-state sleep stages in $R\&K$ standard: Awake (AWA), Stage 1 (S1), Stage 2 (S2), Stage 3 (S3), Stage 4 (S4) and rapid eye movement (REM). The 5-state stages combine S3 and S4 as a slow wave sleep (SWS) stage in 6-state, the 4-state stages join S1 and S2 in 5-state. Stages S1, S2, S3 and S4 are denoted as non-rapid eye movement (NREM). The 3-state stages include AWA, NREM and REM.

Manual scoring is subject to human errors and it is time consuming. An automatic identification of the sleep stages would reduce time dramatically and generate reliable results. The existing sleep stage analysis and classifying methods are mainly based on time or frequency domain features from EEG, EOG (electrooculogram), and EMG (electromyogram) signals (Krakovská & Mezeiová 2011, Anderer et al. 2005, Chapotot & Becq 2010, Charbonnier et al. 2011, Zhu et al. 2012*b*). Using discriminant analysis techniques based on different frequency bands of EEG, power of EMG, and variances of EOG, the accuracy of the sleep stages scoring can reach 74% for 5-state classification (Krakovská & Mezeiová 2011). Anderer et al. (2005) applied EEG, EOG and EMG features to obtain 80% accuracy for 6-state sleep classification. Chapotot and Becq (2010) applied EEG and EMG as features and obtained a 78% accuracy for 6-state sleep classification. Charbonnier et al. (2011) employed EEG, EMG and EOG as features and obtained a 85.5% accuracy for 5-state classification. Zhu et al.(2012*b*) presented a visibility graph similarity method to perform a 6-state classification with an 82.64% accuracy based on EEG and EOG features.

Multi-channel EEG equipment often place limitations on subjects' movement and are more difficult to use in ambulatory environment than single channel devices. Therefore, more researchers have focused on classifying sleep stages with a single channel EEG signal (Ronzhina et al. 2012, Flexer et al. 2005, Berthomier et al. 2007, Jo et al. 2010, Liang et al. 2012) or single lead ECG (electrocardiogram) signal (Mourad Adnane & Yan 2012). Flexer et al. (2005) used a hidden Markov model to obtain a 80% accuracy for 3-state sleep stages. Berthomier et al. (2007) presented a fuzzy logic iterative method to perform a 5-state sleep stages classification with a 82.9% accuracy. Jo et al. (2010) introduced a fuzzy classifier to identify 4-state sleep stages with a 84.6% accuracy. Ronzhina et al. (2012) used power spectral density (PSD) features and an artificial neural network (ANN) classifier to obtain an accuracy of 76.7% for 6-state sleep stage classification. Fraiwan et al. (2012) applied a random forest classifier and Wavelet features to identify the wakeful state with a 90% accuracy. However, unless applying an

extensive number of diverse extracted features, it is difficult to obtain a higher accuracy that is even close to the accuracy of levels achieved by experts using manual techniques (Sukhorukova et al. 2010, Berthomier & Brandewinder 2013) , which is $83 \pm 3\%$ (Chapotot & Becq 2010). Therefore, auto-sleep classifying remains a challenge (Berthomier & Brandewinder 2013), especially for sleep stages identification with a single channel EEG signal.

Recently, visibility graphs (VGs) which were first proposed by Lacasa et al. (2008) have been employed to analyse EEG signals (Zhu et al. 2012*b*, Tang et al. 2013, Ahmadlou et al. 2010). Previously, VGs have been used to study currency exchange rate time series (Yang et al. 2009), stock market indices (Meng-Cen Qian & Zhou 2010), and seismic sequences (Telesca & Lovallo 2012). They have also been employed by Shao (2010) to study heartbeat interval signals and applied by Xiang et al. (2012*b*) to analyse ECG signals. In addition, one of the modified VG, the horizontal visibility graphs (HVGs), have been used to distinguish chaotic series from random series (Bartolo Luque & Luque 2009). Since EEG signals demonstrate chaotic behaviors (Korn & Faure 2003), HVGs are able to represent the chaotic characteristics of EEGs according to the results from Luque et al. (2009).

This chapter presents a novel visibility graph model to classify sleep stages based on a single channel EEG signal. Firstly, each segment EEG signal (Pz-Oz channel) is mapped into a VG and a HVG. Then a difference visibility graph (DVG) is constructed epoch-by-epoch by subtracting the edges set of the HVG from the edges set of the VG. The mean degrees of the VGs and the HVGs are evaluated and the degree distributions of the DVGs are studied. In total, there are 14,963 EEG segments to be analysed. Then the features of the mean degrees of the HVGs and the DVGs and the seven optimal degree distributions of the DVGs are selected. Finally all the extracted features are forwarded to a support vector machine to perform 2-state, 3-state, 4-state, 5-state, and 6-state sleep stage EEG classification, respectively.

9.2 Experimental data

The experimental data used in this study were obtained from the Sleep-EDF database (Kemp 2013, Kemp et al. 2000), as shown in Section 3.4.1. Eight data recordings from subjects: sc4002e0, sc4012e0, sc4102e0, sc4112e0, st7022j0, st7052j0, st7121j0, and st7132j0, were used in this chapter. In this study, the Pz-Oz channel EEG signal was selected to analyse and identify the sleep stages because it can provide better automatic classification accuracy than the Fpz-Cz channel (Ronzhina et al. 2012, Berthomier et al. 2007, Liang et al. 2012). Since the hypnogram was generated by experts following the $R\&K$ recommendations (EA 1969) on every 30 seconds of EEG data, the interval of each segment (or epoch) in this study is defined as 30 seconds, and contains 3000 data points.

The original sleep stages of these segments are labeled with one of the eight

classes: AWA, S1, S2, S3, S4, REM and MVT (movement time) and UNS (unknown states). Note that only the recordings: sc4002e0, sc4102e0 and st7121j0 have the MVT data in the original EDF file. This study only deals with AWA, S1 to S4 and REM sleep stages. The whole EEG data was divided into a training set and a testing set except for analysing and 10-cross-validation classifying. The odd numbers of epochs were in the training set and the others were in the testing set. The six sleep stages of the training and testing data are listed in Table 9.1. It can be seen that the numbers of the training epochs and testing epochs were approximately balanced.

Table 9.1: Experimental data

	Training data (Epochs)	Testing data (Epochs)
AWA	3919	3911
S1	287	317
S2	1822	1799
S3	331	341
S4	316	311
REM	806	803
The total number of epochs	7481	7482

9.3 Methodology

The structural diagram of the automatic sleep stages classification method proposed in this study is shown in Fig 9.1 Each segment of the raw EEG signal was mapped into a VG and a HVG, without any frequency domain preprocessing. Then, a difference visibility graph (DVG) was constructed based on the VG and HVG for each of the EEG segments. The mean degrees of the DVG and the HVG were calculated and the degree distributions of the DVG were evaluated. Seven distinguishable degree distribution values for each DVG were selected as the representative features. Then the extracted features were forwarded to a support vector machine algorithm to perform 2-state, 3-state, 4-state, 5-state and 6-state sleep EEG classification, respectively. The details of the methodology are described in the following subsections.

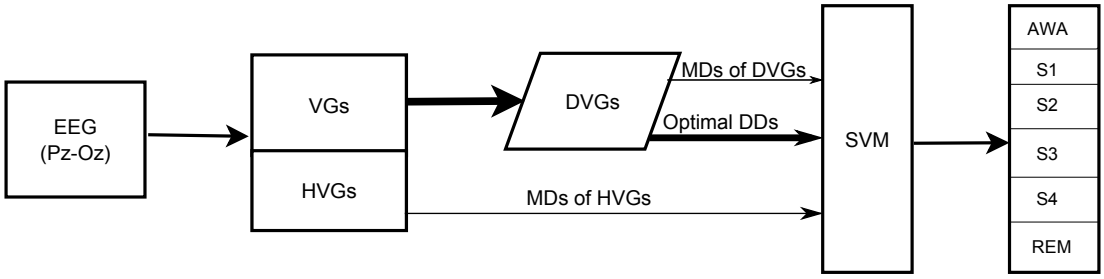

Figure 9.1: Automatic single channel sleep stages classification structural diagram

9.3.1 Difference visibility graphs (DVGs)

Let $G_{vg}(V, E_1)$ and $G_{hvg}(V, E_2)$ be a visibility graph and a horizontal visibility graph associated with a time series $\{x_t\}$, where, V is the node set, and E_1 and E_2 are the edge sets of the VG and HVG. The difference visibility graph $G_dvg(V, E_3)$ is a graph defined by $E_3 = E_2 - E_1$. For the same time series$\{x_t\}$, G_{hvg} is a subset of G_{vg}, the degree $k_{dvg}(i)$ of a DVG associated with a time point x_i satisfies

$$k_{dvg}(i) = k_{vg}(i) - k_{hvg}(i) \tag{9.1}$$

where $k_{dvg}(i)$, $k_{vg}(i)$ and $k_{hvg}(i)$ are the degrees of node v_i of the DVG, VG and HVG, respectively. Thus, the mean degree (MD) of a DVG is equal to the MD of a VG minus the MD of a HVG.

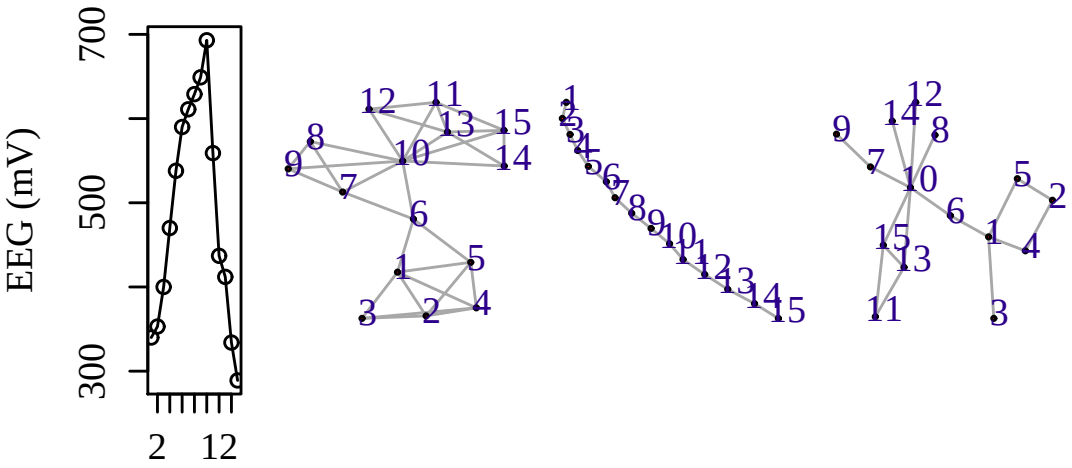

(a)A time seri (b) VG of (a) (c) HVG of (a) (d) DVG of (a)

Figure 9.2: Illustration of a time series (upper part) converted into its VG (bottom part)

DVGs could be more beneficial in obtaining the essential features of input signals than VGs and HVGs. They overcome the pitfall that there are often many nodes

with the degree value $k = 2$ on HVGs and VGs (Donner & Donges 2012), which are not distinguishable enough to analyze the different sleep stages using EEGs. Let us consider an example: the input time series in Figure 9.2(a) which is (340, 353, 400, 470, 538, 590, 611, 629, 649, 693, 559, 437, 412, 334, 289). Assume only those nodes with $d(v_i) > 2$ need be extracted.

The associated VG as shown in Figure 9.2(b) will extract all nodes, which is difficult for computing when the number of nodes exceeds thousands. There are no selected nodes in Figure 9.2(c) due to the maximum degree of HVG being two. In contrast, four essential nodes of the DVG in Figure 9.2(c) will be extracted, which is (1,10,13,15). Then the nodes v_1, v_{10}, v_{13} and v_{15} are obtained. Therefore, the degree sequence of DVG is more essential in representing EEGs. Moreover, if a time series is constant, $k_{dvg}(i)$ is always zero, which can detect the disconnected telemetry link event from EEG recordings.

9.3.2 Degree distribution of DVGs

The degree distribution (DD) is a probability that a node has a degree of k. It is obtained by counting the number of nodes having degree k divided by the total number of nodes. Let $p_{vg}(k)$ be denoted as the DD of a VG, $p_{hvg}(k)$ as the DD of a HVG and $p_{dvg}(k)$ as the DD of a DVG. Let us consider Fig. 9.2 again, $p_{vg}(k) = (0, 0, 0, \frac{5}{15}, \frac{7}{15}, \frac{2}{15}, 0, 0, 0, \frac{1}{15})$ and in Fig. 3, $p_{hvg}(k) = (0, \frac{2}{15}, \frac{13}{15})$. However, for the time series in Figure. 9.2, $p_{dvg}(k) = (0, \frac{5}{15}, \frac{6}{15}, \frac{2}{15}, \frac{1}{15}, 0, 0, \frac{1}{15})$. Therefore, unlike equation 9.1,

$$p_{dvg}(k) \neq p_{vg}(k) - p_{hvg}(k) \tag{9.2}$$

p_{hvg} has been used to distinguish the correlated stochastic, uncorrelated and chaotic processes by Lacasa and Toral (Lacasa & Toral 2010). It has been shown by Shao (2010) that the degree distribution of a VG associated with ECG approximately satisfies the power-law. Luque et al. (2009) proved that the HVGs on random signals satisfy exponential distribution rules. This study considers it as an efficient feature for sleep stage classification.

9.3.3 Extracted features for the multi sleep stages classification

Choosing appropriate features to represent the original EEG data is the most important and difficult task in pattern recognition and classification. For multi-sleep stage classification, it is difficult to obtain high accuracies with the same feature set that is used to identify different sleep stages, such as classifying 2-state sleep stages or classifying 5-state sleep stages. This study selected nine features: $\overline{k_{dvg}}$, $\overline{k_{hvg}}$ and seven other degree distribution values from $p_dvg(k)$, in association with degrees (k) ranging from 0 to 12, to classify 2-state to 6-state sleep stages. Let $p(k)$ be the value of the degree distribution p_{dvg} for a degree k. A specific

$p(k)$ is selected due to its distinguishable difference from other degree distribution values. The features used on each multi-sleep stages classification are listed in Table 9.2.

Table 9.2: The features selected in each multi-sleep stages classification

Sleep stages	Features selected
2-state	$\overline{k_{dvg}}$,$\overline{k_{hvg}}$,$p(0)$,$p(1)$,$p(2)$,$p(3)$,$p(5)$,$p(6)$,$p(7)$
3-state	$\overline{k_{dvg}}$,$\overline{k_{hvg}}$,$p(0)$,$p(1)$,$p(2)$,$p(3)$,$p(4)$,$p(5)$,$p(6)$
4-state	$\overline{k_{dvg}}$,$\overline{k_{hvg}}$,$p(0)$,$p(1)$,$p(2)$,$p(3)$,$p(4)$,$p(5)$,$p(6)$
5-state	$\overline{k_{dvg}}$,$\overline{k_{hvg}}$,$p(0)$,$p(1)$,$p(2)$,$p(3)$,$p(5)$,$p(6)$,$p(11)$
6-state	$\overline{k_{dvg}}$,$\overline{k_{hvg}}$,$p(0)$,$p(1)$,$p(2)$,$p(3)$,$p(5)$,$p(6)$,$p(11)$

9.3.4 Rejecting disconnected telemetry link EEGs with DVGs

As for the EEG data in PSG, it always contains some artifacts and the telemetry link was disconnected during recording in some cases. Some of artifacts or disconnected links were marked as UNS stage by experts in sleep-EDF database. However, not all disconnected links were defined as UNS stage. For example, in the third epoch of subject st7502j0, the state is AWA stage. Therefore, this study used the mean degree of DVGs to reject the artifact EEGs, when the mean degree of DVGs associated with an epoch of EEGs is less 5, the epoch is assigned as UNS even if it is marked as AWA stage in EDF files.

9.3.5 Statistical analysis

In order to evaluate the performance of the proposed method, the confusion matrix, accuracy, sensitivity and kappa coefficient (k_a) proposed by Cohen (1960) were computed to assess each multi-state sleep stages classification. The confusion matrix is a square matrix showing the relationship between experts scoring on sleep EEG classification and the outcomes obtained using the proposed algorithm. The values in the diagonal elements represent the number of correctly identified stages and the off-diagonal values are the number of misclassified ones. An element value in row i and column j indicates the number of times sleep stage i was misclassified as sleep stage j.

The accuracy is the sum of the diagonal values in the confusion matrix divided by the sum of all the values in the confusion matrix. The sensitivity is the number of sleep stages positively identified by the proposed method divided by

the total number obtained by experts scoring for the same sleep stage. The Kappa coefficient k_a was used as a means of assessing the performance agreement between the proposed method and the experts. If the value of k_a is greater than 0.80, it means a perfect agreement as suggested by Landis and Koch (1977). Otherwise a k_a value between 0.61 to 0.80, 0.41 to 0.60, 0.21 to 0.40, and 0 to 0.20 ranges, would represent substantial, moderate, fair, and slight agreement, respectively. To test the differences between the mean degrees of the VGs and HVGs of six stages of sleep data, a non-parametric Wilcoxon test was also used because the distribution of sleep EEG data does not satisfy a normal distribution.

9.4 Experiments and results

To evaluate the performances of the proposed approach discussed in Section III, a set of experiments was conducted. The features extraction program was implemented in C. The experiments consisted of four parts: 1) comparing the degree distribution of VGs, HVGs and DVGs; 2) analysing the mean degree of the DVGs and HVGs; 3) conducting the 2-state, 3-state, 4-state, 5-state and 6-state sleep stage classifications based on the extracted features; and 4) comparing the performances of the proposed method with the results reported by the existing methods.

9.4.1 Comparison of the degree distributions of VGs, HVGs and DVGs

First, an example is provided to show that the degree distribution could be used in sleep stage classification. Figure 9.3 illustrates a VG, HVG and DVG associated with two raw EEGs. The red solid line and green dash line in Figure 9.3(c), (d), and (e) are the trajectories of degree distribution values on the two VGs, two HVGs and two DVGs from epochs 312 and 346, respectively. Figures 9.3(c) and 9.3(e) illustrate how the differences among the degree distributions of a VG, a HVG and a DVG can be used to classify the sleep stages S2 and awake. Both X-axis and Y-axis in Figures 9.3(c) and 9.3(e) on both epochs are in log-log plot but Y-axis in Fig. 9.3(d) is in semi-log plot. In Figure 9.3(c), the trajectory of epoch 312 for subject $st7022j0$ from $k = 6$ to $k = 50$ is different from that in epoch 346. $p_{hvg}(k)$ of epoch 312 from $k = 4$ to $k = 15$ is also different from that in epoch 346. Note that the values of $p_{dvg}(k)$ from its trajectory are more distinguishable than those of $p_{vg}(k)$ and $p_{hvg}(k)$ to separate epochs 312 and 346. The phenomenon in Figure 9.3(e) indicates that the degree distribution of a DVG ($p_{dvg}(k)$) represents the original EEGs better than the degree distribution of a VG ($p_{dvg}(k)$) or a HVG ($p_{hvg}(k)$) for the sleep EEG classification. Therefore, this chapter selected seven extra distinguishable degree distribution values from each DVG as the optimal features to perform sleep stage classification.

Second, the statistical (mean $\pm$ SD) $p_{dvg}(k)$ of 6-state sleep stages from $Pz -$

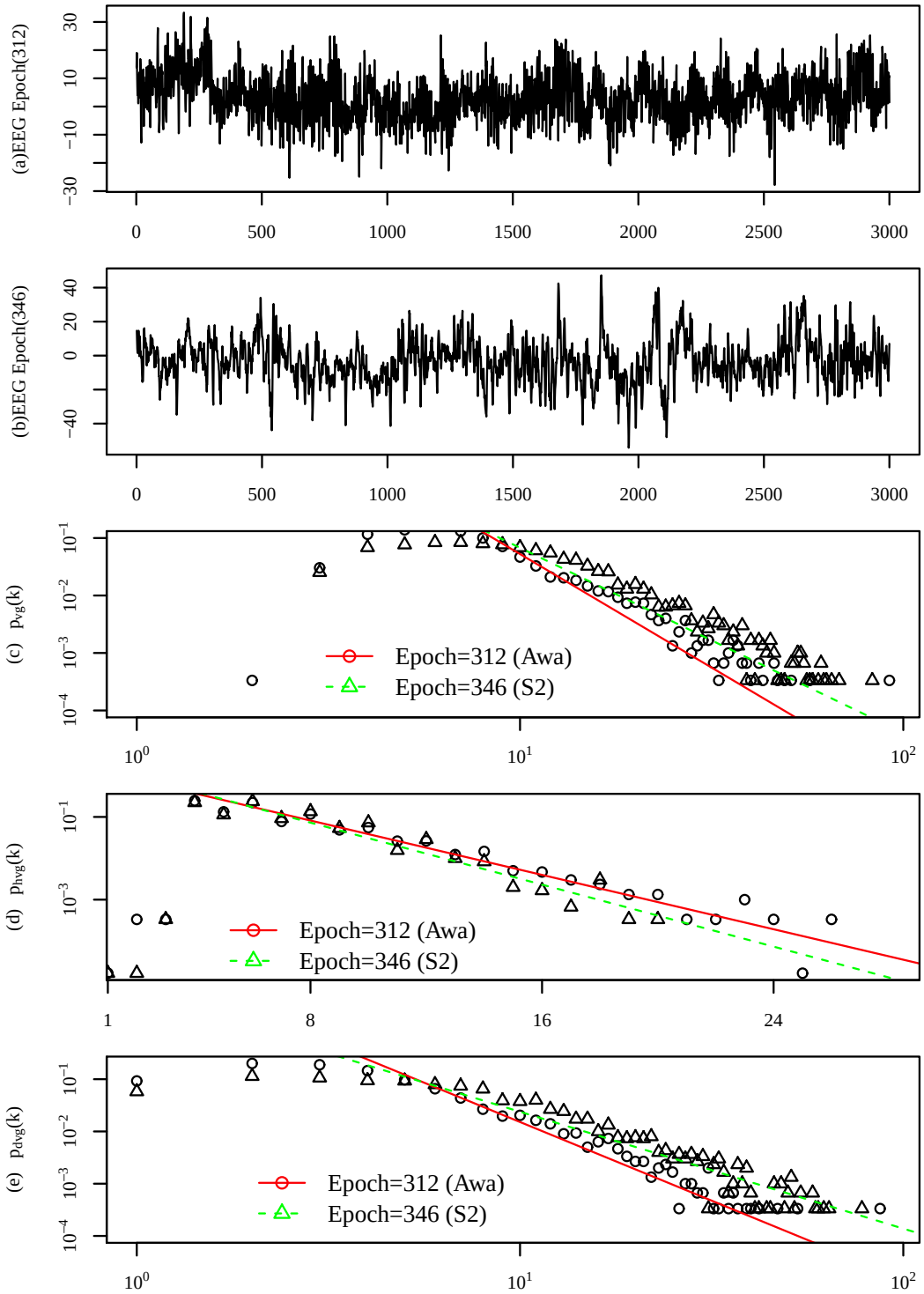

Figure 9.3: The illustration of $p_{vg}(k)$, $p_{hvg}(k)$ and $p_{dvg}(k)$ on epochs 312 and 346 (AWA and S2 stages, respectively) of subject St7022j0

Oz channel EEG is shown in Figure 9.4, where the X-axis and Y-axis use a logarithmic scale. It is noted that the trajectories of $p_{dvg}(k)$ of all sleep stages had strong potential to represent the original sleeping EEG data when the degree was from 0 to 3. As shown in Table 9.2, $\overline{k_{dvg}}$, $p(0)$, $p(1)$, $p(2)$ and $p(3)$ (for

degrees 0 to 3) were chosen as the key features for each 2-state classification, while $p(4)$ was ignored because $p(4)$ in the awake stage was overlapped by $p(4)$ of the other sleep stages. The degree distributions, $p(0)$ to $p(6)$, for degrees 0 to 6 were selected for 3-state and 4-state classifications because $p(4)$ of the awake stage was not overlapped by $p(4)$ of the REM stage. During 5-state and 6-state classifications, $p(11)$ was selected as the representative features as it was quite different in sleep stages S2, S3 and S4 with this degree (degree 11).

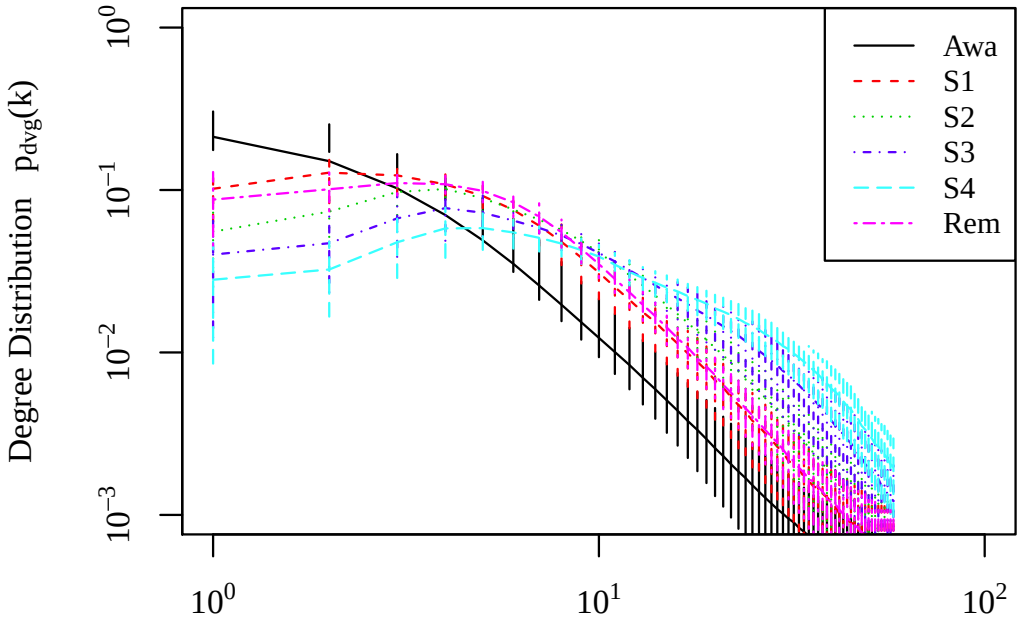

Figure 9.4: The log-log plot of $p_{dvg}(k)$ on 6-state sleep classification associated with the Pz-Oz channel EEG data

9.4.2 Significant characteristics of the mean degrees of DVGs and HVGs on 2-sleep stages

The mean degrees from the HVGs and DVGs are the key features representing the original EEG signal. The statistical mean degrees of the DVGs and HVGs associated with 6-state sleep stages are shown in Figure 9.5 and Figure 9.5, respectively.

Figure 9.5 shows the mean degree population on the DVGs associated with the Pz-Oz channel EEG data, obtained from 14,963 segments. It shows that the REM stage is similar to S1 stage.

Similar to the above, Figure 9.6 presents the statistical mean degree population on HVGs associated with the same EEG data, obtained from the 14,963 epochs. It shows that $3 < \overline{k_{dvg}} < 4$, which is consistent with the theoretical analysis by

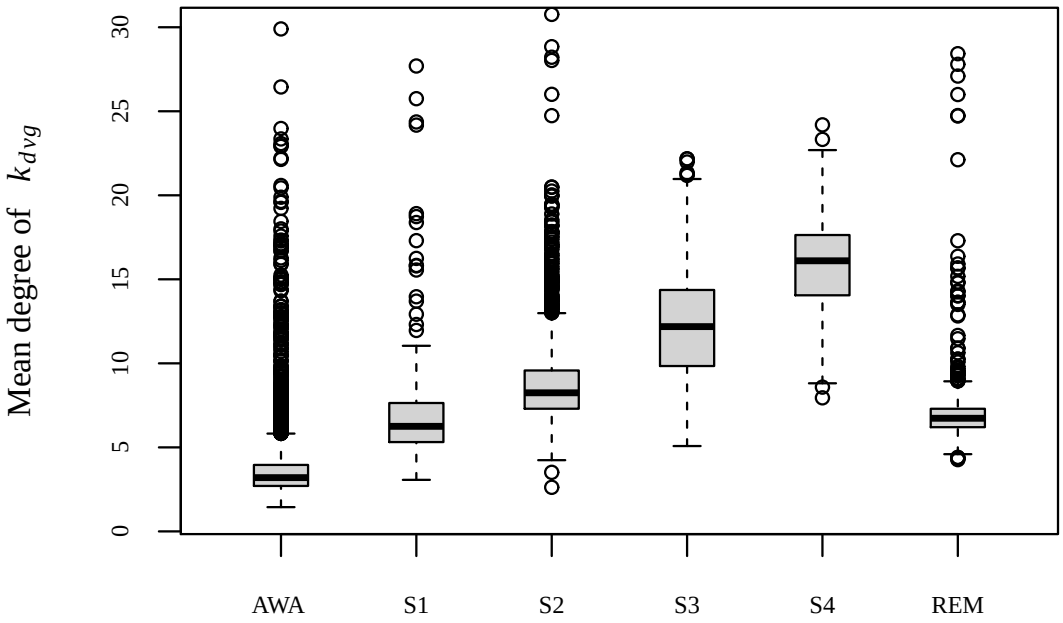

Figure 9.5: Box plot of the mean degrees of the VGs associated with six sleep stages of the Pz-Oz channel EEG.

Nez et al. (2012).

$$\overline{k_{hvg}} = 4(1 - \frac{1}{2T}) \tag{9.3}$$

where T is a period of a periodic time series. Equation 9.3 implies that the mean degree $\overline{k_{hvg}}$ is close to 4 if the period T of a time series is large enough. According to Equation 9.3, the raw EEGs in the sleep stages include more low frequency components than those in the wake stage. The outcome is consistent with the result reported by Achermann et al. (1997) that the EEG is dominated by slow wave activities in the low frequency range when sleeping. The non-parametric Wilcoxon rank sum test was conducted to test the difference of the mean degrees of DVGs and HVGs associated with three pairs of sleep stages: AWA and S1, S1 and REM, S2 and REM. The results are listed in Table 9.3. The results indicate that both mean degrees of the DVGs and HVGs on AWA and S1, S1 and REM, S2 and REM were also significantly different ($p < 0.05$).

Table 9.3: Results of the Wilcoxon test on the mean degree of the DVGs and HVGs for three pairs of sleep stages

	AWA and S1	S1 and REM	S2 and REM
p-Values of $\overline{k_{dvg}}$	$< 2.2e0 - 16$	$1.47e - 08$	$< 2.2e0 - 16$
p-Values of $\overline{k_{hvg}}$	$< 2.2e0 - 16$	< 0.012	$< 2.2e0 - 16$

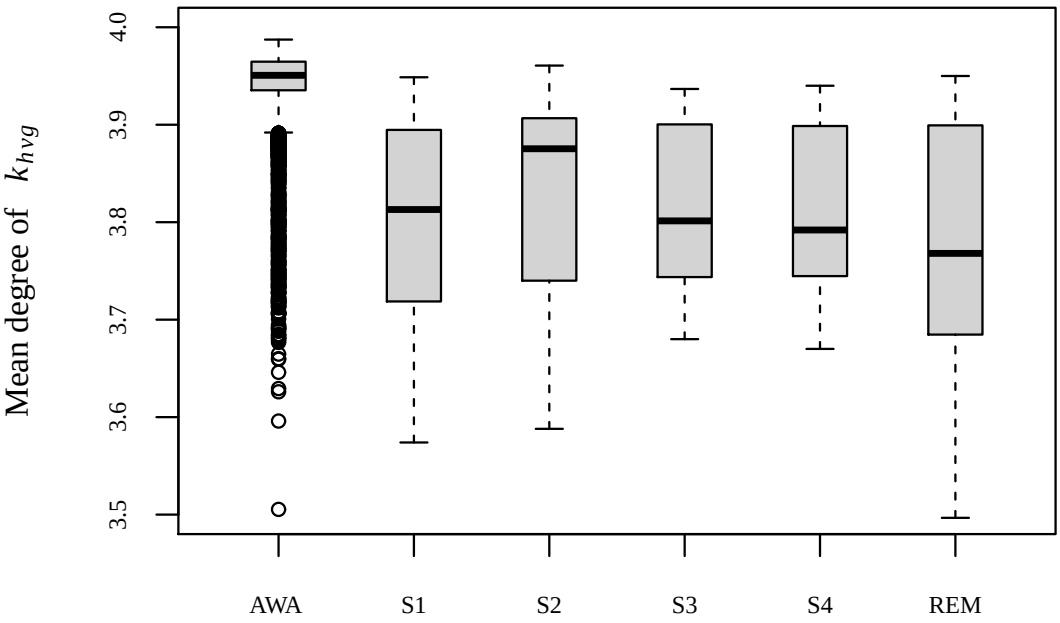

Figure 9.6: Box plot of the mean degrees of the HVGs associated with six sleep stages of the Pz-Oz channel EEG.

Given the outcomes reported in Tables 9.3, the two features, $\overline{k_{dvg}}$ and $\overline{k_{hvg}}$, were selected to perform the 2-state sleep stages classification between the pairs of: awake and sleep, AWA and REM, S1 and REM, $(S1, S2)$ and SWS, S1 and S2, S3 and S4. Their accuracies are listed in Table 9.4.

Table 9.4: The accuracy of 2-state sleep stages classification based on two features, $\overline{k_{dvg}}$ and $\overline{k_{hvg}}$

	Accuracy	Kappa coefficient
AWA-Sleep	96.1%	0.92
AWA-REM	96.7%	0.88
S1-REM	75.7%	0.19
(S1,S2)-SWS	90.6%	0.72
S1-S2	89.2%	0.42
S3-S4	77.0%	0.54

9.4.3 2-state, 3-state, 4-state, 5-state and 6-state sleep stages classification using mean degrees and degree distributions

To investigate the performance of the proposed method, the sleep-awake and other pairs of 2-state sleep classifications were evaluated. The accuracies of AWA-REM, NREM-REM, (S1, S2)-SWS, S1-S2, and S3-S4 are listed in Table 9.5. Compared with Table 9.5, the kappa coefficient of S1-REM sleep stage classification increased nearly two times in Table 9.5.

Table 9.5: Sleep stages classification for 2-state pairs with $\overline{k_{dvg}}$, $\overline{k_{hvg}}$ and nine degree distributions

	Accuracy	Kappa coefficient
AWA-Sleep	97.9%	0.96
AWA-REM	98.%	0.96
S1-REM	78.8%	0.34
(S1,S2)-SWS	91.2%	0.74
S1-S2	91.6%	0.61
S3-S4	83.0%	0.66

To demonstrate the performance of the proposed method, the 3-state to 6-state classifications were evaluated. The classification sensitivities of 3-state (AWA, NREM, and REM stages) were 97.1%, 91.1% and 74.1%, respectively, while the kappa K_a was 0.87 and accuracy was 92.6%. The recognition rates of 4-state sleep stages were 97.0%, 73.4%, 81.3% and 86.5%, respectively, while kappa K_a was 0.83 and accuracy was 89.3%. The confusion matrix and sensitivities of 5-state sleep scoring are listed in Table 9.6. The accuracy was 88.9% and kappa K_a was 0.83. The accuracy was 87.5% in 6-state classification and kappa K_a was 0.81.

A 10-fold cross-validation was applied to evaluate the average accuracy of 5-state sleep stage classification, where the dataset included the training data and testing data. The average 10 times of accuracy was 89.0%. The sensitivity of awake in Table 9.6 achieves 98.8%, which imply the proposed method with Pz-Oz channel is efficient in identifying the awake from sleep stages. This result confirms that the recommendation in AASM Manual (Iber 2007) that arousal scoring is better detected from occipital and central EEG derivations.

Now let us only consider the 5-state sleep stages: S1, S2, S3, S4 and REM stages sleep classification. The confusion matrix and sensitivities are listed in Table 9.7; the accuracy is 76.6% and kappa is 0.63. When 10-fold cross-validation was applied, 10 times average accuracy is 77.2%. Base on Tables 9.5, 9.6 and 9.7, the results show that distinguishing the S1 stage from REM, 5-state with awake,

Table 9.6: The confusion matrix and sensitivity on 5-state sleep stages

		Expert's scoring				
		AWA	S1	S2	SWS	REM
The proposed method	AWA	3863	66	23	4	20
	S1	11	50	5	3	12
	S2	5	80	1619	139	159
	SWS	1	1	74	504	0
	REM	31	120	75	2	612
Sensitivity		98.8%	15.8%	90.0%	77.3%	76.2%

and 5-state without awake by the proposed method is 78.8%, 15.8% and 27.4%, respectively. These results indicate that it is much harder to distinguish between $S1$ and REM stages using DVGs. However, our results agree with the conclusions reported by Corsi-Cabrera et al. (2006) that $S1$ stage was easily mistakenly categorized as any of AWA, S2 or REM stages.

Table 9.7: The confusion matrix and sensitivity on 5-state sleep stages (without awake)

		Expert's scoring				
		REM	S1	S2	S3	S4
The proposed method	REM	611	132	80	1	1
	S1	23	87	12	3	0
	S2	169	98	1648	147	23
	S3	0	0	51	151	50
	S4	0	0	8	39	237
Sensitivity		96.1%	27.4%	91.6%	44.3%	76.2%

9.4.4 Comparison of the proposed method with other single channel sleep classification methods

To verify the performance of the proposed approach, the comparisons of the classification results for 2-state to 6-state sleep stages were conducted with two existing methods proposed by Ronzhina et al. (2012) and Berthomier et al.

(2007). Both studies used the same EEG datasets as used in this chapter. The comparison performances are listed in Table 9.8.

Table 9.8: The comparison of accuracies for the three methods

Sleep stages	PSD with ANN (Ronzhina et al. 2012)	Fuzzy logic iterative system (Berthomier et al. 2007)	**The proposed method**
AWA, Sleep	96.9%	95.4%	97.9%
AWA,NREM,REM	88.97%	88.3%	92.6%
AWA,$S1/S2$,SWS,REM	81.42%	74.5%	89.3%
AWA,$S1$,$S2$,SWS,REM	-	71.2%	88.9%
AWA,$S1$,$S2$,$S3$,$S4$,REM	76.7%	-	87.5%

The performances of the proposed method from 2-state to 6-state sleep scoring were better than those in Ronzhina et al. (2012) and Berthornier et al. (2007). Berthornier et al. (2007) reported their sleep stage classification results using two sleep datasets: the Sleep-EDF dataset and their own sleeping recording data. Their reported accuracies with the first dataset are listed in Table 9.8. The accuracies of their own sleep data were 96%, 92.1%, 84.9% and 82.9%, respectively, for the 2-state, 3-state, 4-state and 5-state classifications. Both are lower than the results obtained in this study. In addition, our testing results were obtained from more EEG data segments and more numbers of epochs and subjects than those in Ronzhina et al. (2012) and Berthornier et al. (2007). The accuracy of AWA-REM state classification shown in Table 9.5 is better than that reported by Vatankhah et al. (2010) using the same Sleep-EDF database. Their accuracy is 98.15%. In fact, even only comparing the 5-states sleep scoring without awake, our proposed method is better than the method reported by Tagluk et al. (2010),which was 74.7% by cross validation and tested with 265 epochs.

Finally, the proposed method of classifying performance on 5-state sleep scoring was compared with other existing results on 5-state sleep stages. The results are shown in Table 9.9. The research reported by Liang et al. (2012) and Hsu et al. (2013) used the same EEG dataset. However, their classification accuracies were lower than the proposed method and the number of epochs on the data sets was also smaller than those used in this chapter. The average accuracies between deep sleep and paradoxical sleep stages in Tables 9.5 and 9.6 are higher than the accuracy obtained in inter-expert agreement, which is $83 \pm 3\%$ (Chapotot & Becq 2010) and 76.9% in (Anderer et al. 2005). The outcomes demonstrate that the features extracted from DVGs are more robust and accurate.

Table 9.9: The comparison of accuracies of known methods

Researchers	Features-Classifiers	Number of epochs	Accuracy
Charbonnier et al. (2011)	EEG, EMG and EOG features Artificial neural network	62,399	85.5%
Fraiwan et al. (2012)	Time frequency features Random forest	20,269	83%
Hsu et al. (2013)	Energy features Elman neural network	2,880	87.2%
Krakovsk and Mezeiov (2011)	EOG, EEG features Artificial neural network	18,058	74%
Liang et al. (2012)	Multiscale Entropy features Linear discriminate Analysis	3,708	83.6%
This proposed method	DVG and HVG features SVM	14,963	89.0%

9.5 Chapter Summary

This chapter applies difference visibility graphs to study the sleep EEG signals, and identifies the significant differences of mean degrees between DVGs and HVGs associated with the sleep EEG signals. Unlike existing sleep scoring methods which are based on time or frequency features, this method is based on graph domain features. It was found that the mean degrees of DVGs on the deep sleep stage are higher than those in awake and light sleep states, while the mean degrees of HVGs are just the opposite. Based on the analyses from this study, the mean degrees from each HVG and DVG and seven optimal values of the degree distribution of a DVG associated with sleep EEG signals were extracted to perform 2-state, 3-state, 4-state, 5-state and 6-state sleep stage classifications. The 10-fold cross-validation of 5-state sleep scoring showed that the average accuracy was 89.0% with $14,963$ epochs of EEGs. The accuracies are by far the best reported on the sleep stages classification using more than 10,000 epochs from the public sleep EEG dataset. More importantly, this chapter suggests that the graph domain features can be efficiently used to analyse and classify sleep EEG without any frequency domain preprocessing or time domain analysis. It can also detect disconnected telemetry link recordings. The 97.9% accuracy sleep-wake classification suggests that our proposed method is efficient for single channel sleep classification during human locomotion. However, this study detects the EEG recordings in disconnected telemetry link only by checking the mean degree of DVGs. Future work aims to denoise artifacts of EEGs effectively in graph

domain.

Chapter 10

Unsupervised Classification EEG Signals with Multi-scale K-means and Jump Visibility Graphs

Most EEG classification algorithms are supervised and require large training data sets, that hinder its use in real time applications. This chapter proposes an unsupervised Multi-Scale K-means (MSK-means) algorithm to detect seizures with epileptic EEG signals and localize the epileptic zone. The proposed MSK-means algorithm initializes the coarse-scale centroid of a cluster with a suitable scale factor. Due to random initialization, the K-means algorithm can lead to wrong clusters. In this chapter, the MSK-means algorithm is theoretically proved to be superior to the K-means algorithm on efficiency. In addition, three classifiers: the K-means, MSK-means and support vector machine (SVM), are used to identify seizures and localize epileptogenic zone using jump visibility graph features. The experimental results demonstrate that identifying seizures with the MSK-means algorithm and jump visibility graph can achieve 4.7% higher accuracy than that of K-means, and 0.7% higher accuracy than that of the SVM. The related work was presented in Zhu and Li et al. (2013), Zhu and Xi et al. (2013) and Zhu et al. (2014).

This chapter is organized as follows: the localization of epileptogenic zone was briefly introduced. The jump visibility graph, traditional K-means algorithm and the proposed MSK-means method are described in Section 10.3. In Section 10.4, the comparison results of the K-means, MSK-means and SVM with the JVG features to identify epileptic EEGs are presented. Classifying EEG signals from the epileptogenic zone with DPE from the non-epileptogenic area are shown in Section 10.5.

10.1 Known results

Epilepsy is a prevalent neurological disorder stemming from temporary abnormal discharges of the brain's electrical activities, leading to unprovoked seizures. About 1% of the world's population is diagnosed with epilepsy (Mormann et al. 2007). $20\% - 30\%$ patients developed drug resistant after they are treated with drugs. Patients with drug-resistant epilepsy require surgical removal of the epileptogenic zone (EZ) (Goffin et al. 2008). Identifying the EZ is regarded as a prerequisite for successful surgical treatment (Rosenow & Lüders 2001). Therefore, precisely localizing the EZ is an important breakthrough.

Many pre-surgical evaluations have been studied on the localization of the EZ. Epileptologists analyse features from video EEG, scalp EEG (sEEG), intracranial EEG (iEEG), magnetoencephalography (MEG) (Wu et al. 2006), positron emission tomography (PET) or single photon emission computed tomography (SPECT) (Krsek et al. 2013) to detect which areas of the cortex induce seizures during the ictal state. Among these, the iEEG signals recorded from the surface of the brain have been widely used by experienced epileptologists and are regarded as a gold standard for localiz the epileptogenic zone. A recent study showed that other methods, such as sEEG, MEG, PET and SPECT, cannot provided a substitute for iEEG (Zhang et al. 2014). Therefore, localization of the EZ with inter-ictal EEG recordings is worthy of research.

There are two problems in identifying the EZ from iEEG signals: hemisphere locations and methodical training data. Mistaking localization of the hemisphere for the EZ compromises patients; it not only wastes time needed treat the illness but also causes mental pressure to patients. Adamolekun et al. (2011) reported a false localization case. The other problem for the localization of EZ with iEEG is training sets selection. Different epilepsy patients have different localization of EZ. Even with the same patient, no two patterns are the same when EEG signals come from different regions.

To overcome these problems, many studies have been undertaken. These approaches include two steps: feature extraction and epileptic zone classification. Feature extractions are normally used to reduce the complexity of the raw EEG signals. The EZ has high interelectrode template similarity based on frequency entropy from 96 electrodes iEEG (Ben-Jacob et al. 2007). A time-variant connectivity analysis method has been used to localize the ictal-onset zone from iEEG recordings (Mierlo et al. 2013). A frequency domain source imaging approach was applied to identify epileptogenic zones in patients with secondary generalized epilepsy (Cho et al. 2013). Using a combined surrogate analysis method, Andrzejark et al. (2013) showed that iEEG signals from the epileptogenic zone are less random and more stationary than those from non-epileptogenic area. Zhu et al. (2013) showed that the delay permutation entropy (DPE) of the EZ is significantly lower than that of the NEZ when the delay factor is between 5 and 50. Because seizures often occur randomly and patients look and feel normal during seizure-free intervals, it is possible to have an extended normal period (5-10 days)

before suffering a seizure.

EZ locations from extracted features can be divided into two types according to their labeled methods: supervised and unsupervised. Supervised classifiers have been widely used in seizure detection and EZ localization. Most of traditional automatic epileptic classification systems use supervised learning classifiers, such as artificial neural networks (ANN), support vector machines (SVMs) and decision trees. Guo et al. (2011) applied wavelet discrete transform features and an ANN for discriminating ictal EEGs from normal EEGs. Nicolaou and Georgiou (2012) employed permutation entropies and a support vector machine to identify the seizure from EEG signals. Subasi (2006) fed wavelet features to a fuzzy classifier to identify seizure from EEG signals. Siuly et al. (2011) proposed a clustering technique to classify ictal and healthy EEGs. Song and Li (2010) classified ictal, inter-ictal and normal EEGs by features based on sample entropy (SE) and an extreme learning machine algorithm. Zhu et al. (2012*a*) implemented visibility graph (VG) based features and a discriminant classifier to identify ictal EEGs from healthy EEGs. However, an automatic epileptic classification system normally requires large sets of data to train a classifier, and to improve the accuracy.

Furthermore, all data are normally required in a specific format to meet certain conditions, eg. the number of data segments/epochs should be the same in the training data and testing data. Besides, the target categories for all the data segments in the training set rely on the labels obtained manually by experts. All these limitations preclude the current supervised epileptic EEG classification techniques from being used. However, the supervised methods require suitable training data sets and are difficult to be applied in large sets. To our knowledge, there are no unsupervised methods to be reported in the literature.

This chapter proposes a jump visibility graph (JVG) method and an unsupervised MSK-means classifier to localize the epileptogenic zone signals from non-epileptogenic zone signals based on only pair-channels of EEG signals. JVG are motivated by DPE and visibility graphs (VGs). The later was introduced by Lacasa et al. (2008) to map a time series into a graph. A periodic time series could be converted into a regular VG, a random signal into a random VG and a fractal series into a scale free VG. The purpose of this study is to classify the EZ and NEZ with JVGs. Our previous work (Zhu et al. 2012*a*) has shown that the VGs associated with epileptic EEGs have higher mean degrees than those of normal healthy subjects. However, the mean degrees of epileptogenic and non- epileptogenic signals are difficult to distinguish. This study employs a jump factor to enhance the time lag of the VGs.

To solve the classification issues, this study proposes a multi-scale K-means (MSK-means) algorithm to discri-minate epileptic EEGs from healthy EEGs. MSK-means is based on K-means clustering (MacQueen et al. 1967). Because Vattani (2011) showed that the running time of the K-means algorithm increases exponentially when the data size increases, MSK-means attempts to avoid this issue in EEG signal processing. Arthur and Vassilvitskii (2007) had proposed a

K-means++ algorithm and improved the classification accuracy by initializing centroids one by one. Bahmani et al. (2012) also reported that the K-means++ did not work well on large sets of data because it relies too much on the central point initialization. Our previous work (2013) presented an improved radius k-means algorithm to improve accuracy for clustering network data sets. However, no one has tested the K-means for the EEG features clustering. This study combines several continuous EEG segments as a scale central point to make the centroid choice more robust than that of the K-means algorithm. The calculation of the distance in the second phase can also be expanded to multi scales. Thus, the proposed methodology improves what efficiency by decreasing the times of iterations.

The jump visibility graph (JVG) is proposed to extract features from single channel EEG signals. The optimal delay factor is obtained from comparing the performances by zero to 50 delay lags. The extracted JVG features are then forwarded into a multi-scale K-means (MSK-means) classifier to discriminate epileptic EEGs from healthy EEGs, and to identity the epileptogenic zone signals from non-epileptogenic zone signals. The experimental results showed that the JVG features with MSK-means algorithms could distinguish epileptic EEGs and localize epileptic zone effectively.

10.2 Experimental data

Two databases were used in this chapter. The first was described by Andrzejak et al (2001), and was shown in Section 3.3.1. The second is obtained from a public Bern-Barcelona EEG database (Andrzejak et al. 2013) collected from ten patients. The database includes two distinct sets: one comes from epileptogenic zones (Set F) and the other is recorded from brain areas that were not involved in seizure onset (Set N). The sample rate is 512 Hz if the number of records is less than 64 channels. Otherwise, it is 1024 Hz. Each place of data contains two signals: signal x is the patient's focal EEG channel and signal y is the neighboring channel of the epileptogenic zone. Each signal in each recording has 10240 data points. The detailed description and usage of this database can be found in (Andrzejak et al. 2012).

This study divides the Bern-Barcelona EEG database into two sub-data sets. The number of recordings in the sets are 100 and 4500, respectively. The small set is named #50 which is the sample data used by Andrzejak et al. (2012), and the large set is denoted as #750.

10.3 Methodology

The proposed epileptic classification system includes two major steps as shown in Figure 10.1. The features, based on jump visibility graphs, are extracted from the raw EEG data. This chapter also introduces a MSK-means classifier for the classification. The K-means clustering algorithm and the SVM classifier in Figure 10.1 are utilised for comparison purpose.

10.3.1 K-means algorithm and K-means++ algorithm

Given a set of observations $X = (x_1, x_2, \ldots, x_n)$, the K-means clustering technique aims to partition n observations into k sets $(k \leq n)$ $C = (c_1, c_2, \ldots, c_k)$ based on the Euclidean distance. The Euclidean distance between the i^{th} data point and the j^{th} centroid is defined as follows:

$$d(x_i, c_j) = \sqrt{\sum_{j=1}^{k} (x_i - c_j)^2} \tag{10.1}$$

The central point of a cluster is recomputed as:

$$C_j = \frac{1}{|C_j|} \sum_{x \in c_j} x \tag{10.2}$$

The K-means algorithm minimizes the within-cluster sum of squares by Lloyd iteration to make the data of the same cluster more compact and dependent:

$$\omega = \sum_{j=1}^{k} \sum_{i=1}^{|C_j|} d(x_j, c_i) \tag{10.3}$$

The main idea of the K-means algorithm is to randomly choose k observations as the cluster central points (centroids) and assign all the remaining data to their nearest centroids based on Equation 10.1. Then the new centroid of each cluster is calculated using Equation 10.2. The algorithm converges when the new centroids

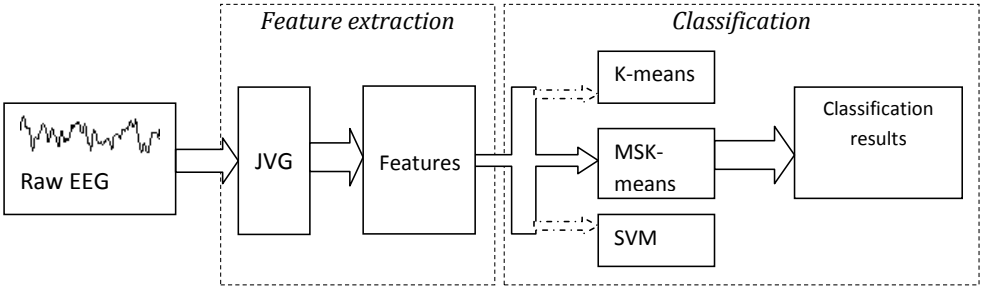

Figure 10.1: The structure of the proposed epileptic EEGs classification system

are the same as the old centroids. The randomness of initialization is error prone if some data points from the same class are assigned to different cluster centroids. The K-mean++ algorithm proposed by Arthur and Vassilvitskii (2007) improves the initialization by the Algorithm 3:

Algorithm 3: K-means++ algorithm init

```
Data: Input: X, k
  N= number of X
  C= randomly choose a point from X
  while |C| < k do
    Dist [1...n]=the distance between X and C
    U=sum(Dist[1...n])
    i=1
    repeat
      U=U-Dist[i], i=i+1
    until U > 0
    C=C union X[i]
  end while
```

The K-means++ algorithm has an additional computation time for initializing centroids. However, the time complexity of both K-means and K-means++ algorithms are NP-hard in (Arthur & Vassilvitskii 2007).

10.3.2 Multi scale K-means (MSK-means) algorithm

The scale of initialization of both K-means and K-means++ is small and limited to the data size, which is not suitable for large sizes of EEG signals. In this chapter, a MSK-means algorithm is proposed to improve the performance by optimizing the cluster initialization.

The concept of multi scale analysis of time series was first proposed by Costa et al. (2002). The multi scale technique transfers one dimensional time series $\{x_t\}_{t=1,\ldots,n}$ into another time series $\{y_t\}_{t=1,\ldots,\frac{n}{\tau}}$ with a different scale. Here τ is a scale factor. The transformation formula is as follows:

$$y = \frac{1}{\tau} \sum_{i=(j-1)\tau+1}^{j\tau} x_i,\ 1 \leq j \leq \frac{n}{\tau} \tag{10.4}$$

When the length of the epoch n can't divided by aτ, the last segment is ignored during the processing. For example, let us consider $x = \{3, 5, 7, 4, 6, 2, 12, 13, 5, 7, 8\}$ and $\tau = 3$, then $y = \{5, 4, 10\}$, the elements $\{7, 8\}$ are ignored.

Based on Equation 10.4, the original algorithm is adjusted as:

Algorithm 4: MSK-means init

Data: X, k, and scale factor

Y construct according to equation (4) and scale factor

Med=K median positions of (Y)

C=empty set

i=1

while $i < k$ **do**

C[i] = random a point in Med[i:i+1]

end while

Similar to the K-means++ algorithm, the MSK-means algorithm only improves the initialization part of the K-means algorithm. Lloyd repeat is conducted with the scaled time serious Y instead of the original times series X. The computational complexity of the MSK-means algorithm is as follows.

Theorem 1. *(Zhu, Li, Wen, Wang & Zhong 2013) Let us assume that n is the number of the data sets, d is the time of iterations, k is the number of clusters and τ is a parameter, the time complexity of the MSK-means algorithm is* $O(max\{\frac{ndk}{\tau}, n\})$.

Proof. In the MSK-means algorithm, the time complexity of Equation 10.4 is n. It indicates that the complexity of k median value is $\frac{n}{\tau}$. The time complexity of Lioyd repeat is $O(\frac{ndk}{\tau})$. The time complexity of the MSK-means algorithm is $O(max\{\frac{ndk}{\tau}, n\})$. ■

According to Theorem 1, the time complexity of the MSK-means algorithm can be $o(n)$ when τ is large enough, which means it can be of higher efficiency than both the K-means and K-means++ algorithms. The relation of τ and the time complexity of the multi-scale means algorithm is discussed in Section 10.4.

How to choice τ is very critical in some classifying cases. A small value of τ means that noise will have a higher influence on the result. A large value of τ defeats the non-stationary philosophy EEG time series. The brain signals will be changed each 30 seconds without outside sitimiling. In that case, a simple approach to select τ is that the length of combined continuous EEG segments is about 30 seconds.

10.3.3 Jump visibility graphs (JVG)

The JVG improves a delay lags $\lambda > 0$ for processing of a time series. Given a time series $\{x_i\}_{i=1,2,\ldots,n}$, the JVG algorithm is outlined as follows:

1. Convert the time series X into an λ dimensions sequence of a vectors X_λ by:

$$X_\lambda\{t\} = \{x_t, x_{t+\lambda}, \ldots, x_{t+(k-1)\lambda}\} \; ; \; 1 \leq t \leq (n - \lambda + 1) \tag{10.5}$$

   where $1 \leq \lambda < \sqrt{n}$.

2. Let each $X_\lambda\{t\}$ be mapped into a VG according to equation‘2.18. Then a JVG includes number of λ VG subgraphs.

Figure 10.2 shows a JVG associated with a time series *X=(16, 10, 8, 6, 18, 14, 9, 8, 17, 12, 7, 8, 10, 7, 4, 2)*. The cases, $\lambda = 1$ and $\lambda = 4$, are represented in Figure 10.2(b) and Figure 10.2(c). It is clear that the VG is a special case of JVG when $\lambda = 1$.

10.3.4 Detecting the nonlinear structure with the mean degree of JVGs

Let $\overline{d(X,\lambda)}$ represent the mean degree of a JVG with a fixed λ, $\overline{d(X,\lambda)}$ will become zero for a long time series when the input signal is a constant. For example, let us consider Figure 10.2 again, $\overline{d(X,1)}$ is 4, when $\lambda = 4$, $\overline{d(X,\lambda)}$ becomes 1.5 and $\overline{d(X,6)} = 1.624$. Therefore, the lag $\lambda = 4$ represents the fixed delay factor of a given signal.

Based on the example, the relation time delay and JVG can be obtained as following

Lemma 3. *Let* $\{x_i\}_{i=1,2,\ldots,n}$ *be a time series and* $\overline{d(X,\lambda)} \leq \overline{d(X,\lambda+1)}$ *is hold when* $\lambda < \frac{n}{2}$*, then the most relevant lag of the time series* $\{x_i\}_{i=1,2,\ldots,n}$ *is* $\lambda > 1$*.*

As an immediate consequence, Lemma 4 shows a regular time series under JVG with a fixed λ.

Lemma 4. *Let* $\{x_i\}_{i=1,2,\ldots,n}$ *be a time series and the slope of* $\overline{d(X,\lambda)}$ *decreases more sharply when* $\lambda < \frac{n}{2}$*, then the time series* $\{x_i\}$ *is more regular.*

It is noted that when $\lambda = \frac{n}{2}$, there are $\lfloor \frac{n}{2} \rfloor$ subgraphs of a VG. Each sub-graph has the degree as 1. In this study, λ is assigned from 1 to 30 to identify the seizure and to recognize EZ, while $n \geq 512$.

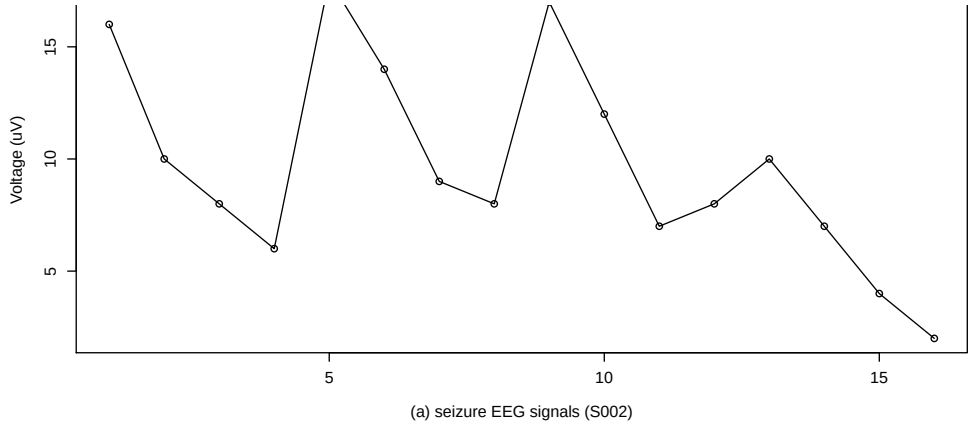

(a) seizure EEG signals (S002)

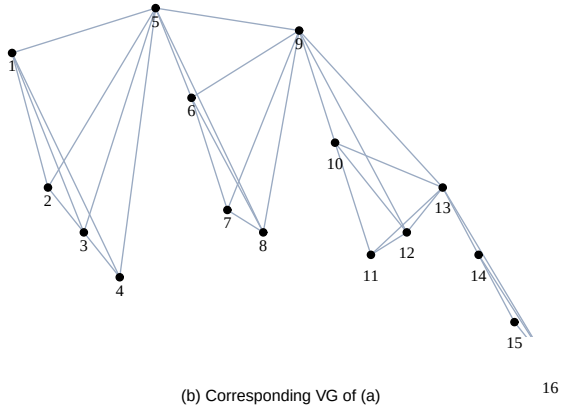

(b) Corresponding VG of (a)

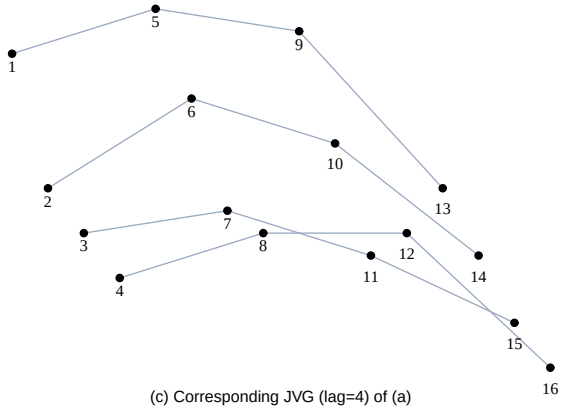

(c) Corresponding JVG (lag=4) of (a)

Figure 10.2: The relation between delay lag λ and the JVG indices for $m = 7$ for five groups EEG signals

10.4 Application for detecting seizures with JVGs

To evaluate the performance of the MSK-means algorithm presented in Section 10.3, C programming language is used to implement the JVG algorithm, while the SVM and K-means algorithms are implemented by R package e1071 (Karatzoglou et al. 2006). The experiments include three parts: (1) evaluating

the delay lag λ and JVG indices based on different groups of EEGs; (2) Evaluating the accuracies of classifying epileptic EEGs and healthy EEGs with different λ JVG; (3) comparing the accuracy level of the K-means, SVM and MSK-means for identifying seizures. For experiments (1) and (2), the JVG indices are changed from 1 to 30. During these experiments, each EEG recording is divided into four equal epochs, and a total of 4000 new EEG segments are used. During the SVM classification processing, the extracted features of the odd numbers of EEG segments are used in the training data set while those of the even numbers of epochs are used in the testing data set.

10.4.1 Evaluating five group EEGs with JVG features

This section evaluates the JVG with different delay lag λ associated with five EEG groups. Figure 10.3 shows the relation between delay lag λ and the JVG indices.

Based on Figure 10.3, the JVG indices associated with epileptic EEGs are close when delay lag λ are larger than 20. The healthy EEGs with eye closed (Set B) have a significant delay lag $\lambda = 11$ due to $\overline{d(SetB, 11)} > \overline{d(SetB, 10)}$. It is clear that the slope of invariants indices of JVG before 20 from healthy EEGs decrease more slowly than those from epileptic EEGs. This discovering agrees with the results from Popov et al.(2013): the epileptic EEG signals are more regular than healthy EEG signals.

10.4.2 Identifying seizures with JVGs

First, we use the K-means, MSK-means and SVM algorithms to discriminate seizure EEGs (Set E) from healthy EEGs (Set A). The results are demonstrated in Figure 10.4. To check the performances of the MSK-means, the values of scale factor τ of the MSK-Means are selected as 8. τ is changed from 1 to 30.

Figure 10.4 shows that the accuracy of the MSK-means algorithm with $\tau = 8$ achieves 89.0% when $\lambda = 1$. From $\lambda = 1$ to $\lambda = 2$ and from $\lambda = 11$ to $\lambda = 22$, the accuracies with MSK-means are better than those of K-Means and SVM. The highest accuracy of the MSK-means algorithm is 89.0% when $\lambda = 1$. Because accuracies use just one dimension features, they indicates that the healthy EEGs and epileptic EEGs can be effectively distinguished by JVGs.

Second, the performance comparison of the K-means, SVM and MSK-means algorithms for different pairs of data sets are presented. Four same sized data sets containing 2048 epochs and the three JVG indices extracted features from each epoch used. The results with average 10-times classification accuracy and execution time are shown in Table 10.1, where $\tau = 8$ and $n = 1024$.

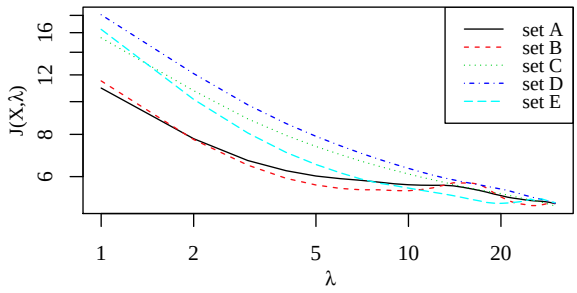

Figure 10.3: The relation between delay lag λ and the JVG indices for $m = 7$ for the five groups of EEG signals

According to Table 10.1, the classification accuracy of Set A versus Set E is 100% by the MSK-means classifier, while the performance of identifying Set E from Set C or Set D by MSK-means classifier is similar to that by SVM classifier. However, accuracy can be further improved by changing τ value (e.g. classifying Set E from Set C achieves 91.6% accuracy when $\tau = 32$).

The classification accuracies on the epileptic EEG database from different litera-

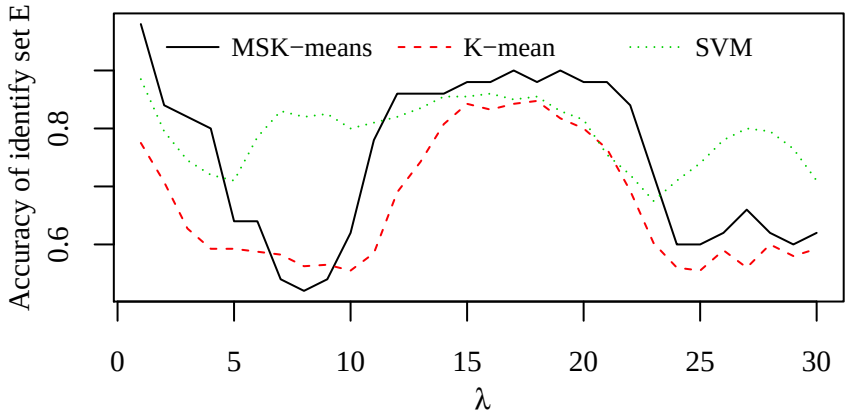

Figure 10.4: Identifying seizure EEG (Set E) and inter-ictal EEG (Sets C and D) with different λ JVG and three classifiers

Table 10.1: The performances for identify seizures with JVG features

Data groups	SVM		K-means		MSK-means	
(Set)	Accuracy	Time (ms)	Accuracy	Time (ms)	Accuracy	Time (ms)
A vs E	94.5%	80	87.3%	5	100.0%	10
B vs E	86.0%	80	85.8%	6	98.0%	20
C vs E	85.5%	80	63.8%	6	72.0%	10
D vs E	86.5%	80	50.8%	6	54.0%	10
(A, B,C, D) vs E	87.2%	170	54.9%	20	56.8%	50

ture are presented in Table 10.2.

Based on Tables 10.1 and 10.2, the proposed MSK-means method has better performance in distinguishing epileptic EEGs from normal EEGs. Without clinical history data records, it is impossible for a supervised algorithm to conduct classifications, while the MSK-means algorithm can work well because it is unsupervised.

10.5 Application for identifying epileptic zones with JVGs

To evaluate the performance of the methods in Section 10.3, the JVG features are statistically analysed in the epileptogenic zone and the nonepileptogenic zone.

Table 10.2: The classification accuracy by the MSK-means and other existing methods

Researchers	Features (Epochs length)	Classifier	Datasets	Accuracy
Polat and Gne (2007)	PSD,(n=256)	Decision Tree	A,E	98.72%
Guo et al. (2011)	DWT,(n=4097)	ANN	A, E	99.6%
Nicolaou and Georgiou (2012)	PE, (n=1024)	SVM	A, E	93.42%
			C, E	88.83%
Zhu et al. (2013)	Entropy,(n=1024)	MSK-means	A, E	100%
*Orhan et al. (2011)	DWT and K-means,(n=4097)	ANN	A, E	100%
			(A,B,C,D) , E	99.6%
The proposal method	JVG,(n=1024)	MSK-means	A, E	100%
			C, E	91.6%
			(A,B,C,D), E	61.3%

* The K-means algorithm was used by Orhan et al. (2011) as a feature extraction method instead of a classifier.

The experiments include two parts: (1) analysing JVG indices associated with epileptic iEEGs under different delay lags; (2) evaluating classification accuracy of the JVG features by different lags on two different sizes of datasets. Both experiments investigate data sets #50 and #750, and the value of λ ranging from 1 to 30.

10.5.1 Statistical analysis on the JVG indices with interictal EEGs

Figure 10.5 shows the relation between different λ and the JVG indices associated with channel x of epileptogenic zone iEEGs and non-epileptogenic area iEEGs in two datasets. In order to evaluate the relation between the JVG indices and λ , the value of λ changes from 1 to 30.

To make the relation between the JVG index and λ more clear, the comparison

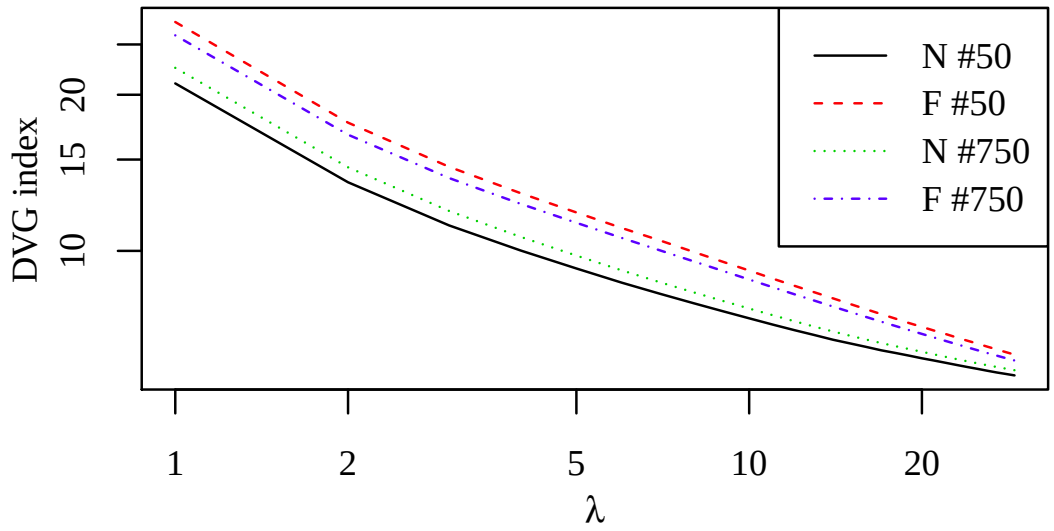

Figure 10.5: The relation between the JVG index and λ with iEEG channel x

between the JVG index of epileptogenic iEEG and those of non-epileptogenic signals are employed with the Students test. Two ranges of λ are measured based on data set #750. The first range of λ is from 1 to 30. The statistical JVG indices between Sets F and N are not significantly different ($p = 0.08$). The second range of λ is from 5 to 30, and the statistical difference are considered significant ($p = 0.01$).

10.5.2 The relationship between JVG indices and classification accuracy

This section investigates the relation between classification accuracy and λ when a one dimension JVG index is applied to identify epileptogenic iEEGs. First, each recorded signal x is extracted with JVG indices with λ from 1 to 30. For Set #50, a total of 100 by 30 dimensional JVG features are extracted, and for Set #750, 4500 by 30 dimensional JVG indices are also extracted. Each dimensional feature is forwarded into an K-mean, MSK-Means and SVM to conduct classification, where the odd indices of instances are used for training and the remaining features are used for testing. Finally, the relation of the accuracies and λ on two EEG data sets are obtained and illustrated in Figure 10.6.

Based on Figure 10.6, the maximum accuracy is 74.3% for the EEG Set #750 and λ is selected as 11 when the MSK-Means classifier ($\tau = 8$) is applied. It is clear that the accuracies of the MSK-Means is larger than those from SVM and K-Means when λ is between 1 and 30, while half the features are used as a training set and the others for testing with SVM. To be more clear, a confusion matrix between the experts scoring and SVM based on VGs ($\lambda = 12$ of JVG) is shown in Table 10.3. The accuracy is 59.2%.

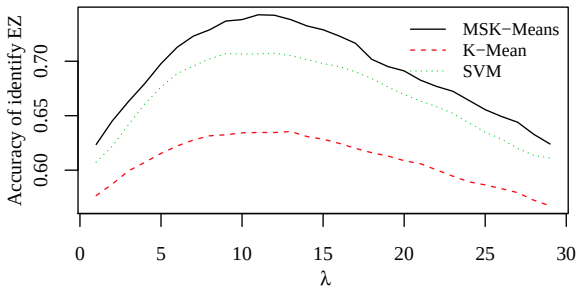

Figure 10.6: The relation between accuracy and λ of JVG with iEEG channel x for the identification of epileptogenic and nonepilptogenic

The confusion matrix based on the JVG index ($\lambda = 11$) with the MSK-Means ($\tau = 8$) classifier is shown in Table 10.4. The accuracy of Table 10.4 is 92.3%.

According to Tables 10.3 and 10.4, the classification accuracy based on the JVG index is 33.1% higher than that those based on JVG and SVM. Previous work (Zhu, Li, Wen, Wang & Xi 2013), found the 84% is the maximum accuracy based on SVM classifier with 50 tested recordi2ngs. This result of accuracy is

Table 10.3: Confusion matrix for identifying EZ with JVG $\lambda = 12$ features and SVM

	Set F	Set N
Set F	642	435
Set N	483	690

Table 10.4: Confusion matrix for identifying EZ with JVG index and MSK-Means

	Set F	Set N
Set F	269	13
Set N	26	254

higher. 4500 testing recordings shows that the JVG features is more robust. More importantly, the highest accuracy based on the JVG index in this study is higher than the existing recorded results, which are $50\% - 80\%$ (Spanaki et al. 1999, Henry & Van Heertum 2003, Knowlton et al. 2008). This proposed method demonstrates that the JVG indices and MSK-Means classifier can be applied to epileptogenic focus location based on iEEG signals.

10.6 Chapter Summary

Unsupervised classification algorithms play an important role in epilepsy detection. The proposed MSK-means algorithm in this study optimizes the initialization stage to improve the classification performance. Both theory and experimental results show that the complexity of the MSK-means algorithm is less than that of the K-means. This study also demonstrates that the MSK-means algorithm improves the classification accuracy by 0.7% over that of the K-means, and has 4.7% higher accuracy with 50% less execution time than the SVM classifier using the half the data as the training set. Hence, the MSK-means algorithm can be used efficiently for time series analysis and EEG classification.

In addition, the JVG index is applied to localize the epileptogenic zone from data in a public iEEG database. The optimal delay factor of JVGs is selected by analysing the different JVG indices between the epileptic zone and non-epileptic zone from delay lag zero to 50, then all JVG indices are forwarded to a K-Means, MSK-Means and SVM to identify the epileptogenic zone. The classification results show that the accuracy of epileptogenic zone detection with the JVG index and MSK-means is 92.3% when the delay lag is 11. Hence, the JVG index can

potentially be a suitable candidate for epileptic EEG processing, especially with MSK-Means classifiers. An implementation using R package of the JVG and MSK-Means algorithms can be found in the FHVA R package (http://braingraph.appspot.com/).

Chapter 11

Conclusion

In this work, temporal complex networks based on clinical EEG signals have been studied from three types of EEG signals: alcoholics, Epilepsy, and sleep. It is the first study identifying seizures from epileptic EEGs with complex network methods. The accuracy can achieve 100% with only two graph features based on a WHVG. Spatial brain networks are also investigated from two multi-model biomedical databases, the alcoholism EEG database and the Sleep-EDF database. It is shown that the topologies of a brain graph exhibit more small world network properties during deep sleep compared with those in wake states. Conversely, alcoholic brain networks show that the network topologies are more random in central area.

TCNs associated with the electrodes also have been studied from frontal, central, parietal and occipital regions. Our results suggest that the EEG channels from central, parietal and occipital regions are better than those from the frontal area. Thus, the sleep stages can be efficiently classified by graph features based on a single-channel EEG signals from parietal and occipital regions.

The fourth objective in Section 1.2 is solved by a jump visibility graph model based on epileptogenic zone EEG signals which are significantly different to the networks from non-epileptogenic zone EEG data. Finally, an efficient unsupervised classifier, MSK-means algorithm, is presented based on the K-means algorithm. The performances of this algorithm are verified with two epileptic EEG databases. This study proved that the accuracy of the epileptogenic zone localization with MSK-means is33.1% greater than that of SVM.

Complex brain networks were reviewed in Chapter 2. Scale free networks and small world networks were discussed. Two types of complex brain networks were illustrated. One is spatial complex networks, which are suitable for multi-channel EEG signals. The other is temporal complex networks, which are proved as an efficient tool for single-channel biomedical signals. The existing results of complex brain networks based on several clinical EEG signals have been discussed. In addition, the challenges of complex brain networks for the clinical applications

were addressed.

In the first application for seizure detection, VGs were applied to investigate ictal, healthy and inter-ictal EEG signals (Chapter 4). Three network topologies of VGs: mean degree, degree distributions, and graph entropy, are evaluated from 500 EEG recordings. A quadratic discriminant analysis was applied to identify seizures from healthy and inter-ictal EEG signals. The results showed that the accuracy for distinguishing seizures from healthy EEG signals achieves 100%. In addition, the mean degree of VGs associated with Epilepsy patients in seizure or inter-ictal are significant higher than those of healthy patients.

To overcome the slow speed of constructing VGs, a fast weighted horizontal visibility graph algorithm (FWHVA) was presented to improve the problem (Chapter 4). It is proved that the complexity is $O(n)$. Two chaotic signals were used to test the performance of FWHVA, sample entropy and FFT algorithms. Experiment results show that the speed of FWHVA is faster than the FFT algorithm and sample entropy. The mean strength features from HVG is more noise-robust than those of PSD and sample entropy. The accuracies of identifying seizures based on mean strength and mean degree features are higher than those based on two PSD and two sample entropies. In addition, the mean degree of HVGs associated with Epilepsy patients in seizure exhibit a higher mean degree than those of healthy subjects, while those of inter-ictal state are lower.

Although the FWHVA algorithm is fast, it is only useful for analysing single-channel EEG time series. Chapter 6 used an improved synchronization likelihood method to study the EEGs from alcoholic and controlled drinkers. Each channel signal was mapped into a node, and the edge between two nodes was defined by the synchronization likelihood from four frequency bands, θ (4-8 Hz), α (8-12.5 Hz),β (12.5-28.5Hz) and γ (28.5-45Hz). The maximal match algorithm was applied to investigate the function connectivity among brain regions.

However, the synchronization likelihood method is also slow and it is not suitable for analysis of long-term EEG signals. Chapter 7 introduced a linear complexity algorithm for measuring the couple between pair biomedical signals. A graph isomorphism algorithm, HVGI, first investigated the synchronization among coupled chaos signals and multi-channel sleep signals compared with two conventional methods, phase locked value (PLV) and visibility graph similarity (VGS). The results show that the sleep scoring accuracy from two EEG signals and one EOG signal by HVGI is better than those of PLV and VGS. In addition, both HVGI and PLV exhibit strong synchronized in deep sleep stages.

Although many researchers have studied the single-channel sleep scoring from Sleep EDF with the channel Pz-Oz. There is no one answer as to why they prefer to use this channel. Chapter 8 evaluates the complex brain networks associated with five individual channels from two public sleep EEG databases. It shows that all complex networks associated with EEG signals from frontal, central, parietal and occipital regions, satisfy a small world attribute during deep sleep. However, the sleep scoring based on EEG signals in central, occipital and parietal regions

better represent the sleep changes than those in the frontal area. In addition, network topologies from each individual EEG signal exhibits small networks in deeps sleep stages.

As single-channel EEGs becoming more popular for sleep scoring, a difference visibility graph (DVG) was presented to conduct a single-channel sleep stage classification (shown in chapter 9). A DVG is constructed from a VG and a HVG. The mean degree and degree distributions on DVGs are analysed. The features are forwarded into a SVM to conduct 2-state, 3-sate, 4-stat, 5-state and 6-state sleep stage classifications. The results show that the nine features from DVGs could obtain the 87.5% accuracy and 0.81 kappa coefficients by comparing them with the results reported from other existing methods. In addition, the mean degree of DVG in deep sleep is higher than those in the awake and light sleep, and the mean degree of HVGs are just the reverse.

Finally, this study proposed an efficient unsupervised classifier and a jump visibility graph in Chapter 10. A JVG can be efficient for detecting the delay lag in a time series even if it is non-stationary. Experiments proved that the MSK-Means algorithm is faster than K-Means and SVM classifier. In addition, this study is the first to discover that the epileptogenic zone has a different delay lag from that of the non-epileptogenic zone (based on the JVG method). The JVG analysing result shows that the epileptic EEG signals are more regular than those of healthy EEG signals.

11.1 Contributions to four research fields

This research has devoted time and hands-on research work to four fields: graph theories and networks, nonlinear time series, pattern recognition and novel diagnosing methods for clinical EEGs.

11.1.1 Graphs and network theories

Two novel temporal complex networks: a new algorithm for constructing graphs and a fast spatial graph modeling methods are discussed in this thesis.

Difference visibility graphs (DVGs) and jump visibility graphs (JVGs) are two novel temporal complex networks presented in this study. The first combines the advantages of VGs and HVGs, especially for the degree distribution performance. Gutin et al. (2011) showed that HVGs and VGs are Hamiltonian graphs, which implies that there are no nodes with degree zero in VGs and HVGs associated with an EEG time series. DVGs can overcome this pitfall by obtaining the isolate nodes in a graph when it is mapped from an input time series. It is also proved to be efficient for detecting the disconnected telemetry link in EEG recordings, as shown in Section 9.3.4. In Section 9.4.1, the variant of DD from a DVG illustrates

that the DVGs are more suitable for representing the sleep EEG signals than those of VGs and HVGs.

In addition, both VGs and HVGs lose the phase information when they are transferred from a time series. This drawback has been improved by a jump visibility graph (JVG) model presented in Section 10.3.3. The JVG absorbs the recurrence networks and adds a delay lag τ into the visibility graph. It enhances the complex networks for the non-stationary signal analysis.

The results were presented in Zhu et al. (2014*a*) and Zhu et al. (2013).

The second contributions to complex networks is to present a fast weighted horizontal visibility graph constructing algorithm (FWHVA) for HVGs. This algorithm has linear complexity. Compared with the sample entropy and FFT algorithms, the computational efficiency of the FWHVA is 76 times faster than that of the sample entropy and is 3.8 times faster than that of the FFT when the size of signals is more than 4000 data points.

The result was presented in Zhu et al. (2014*b*), and is also presented in Chapter 5.

The last contribution to complex networks is that the spatial complex networks can be derived from multi temporal complex networks. In general, the edges of spatial complex networks are generated based on the frequency domain or the time domain, such as correlation or coherence. This study introduces the graph isomorphism method to connect the edge between two graphs. The speed of constructing a spatial brain graph based on the multi horizontal visibility graph is linear.

The result was presented in Zhu et al. (2012*b*), and is also presented in Chapter 7.

11.1.2 Nonlinear time series analysis

This study investigates nonlinear time series analyses from three aspects. Firstly, the noise-robustness of the complex networks was evaluated with the FWHVA. It is shown that the mean strength of a WHVG is more noise-robust than those of the FFT and sample entropy.

The result was presented in Zhu et al. (2014*b*), and the related work is presented in Chapter 5.

Without considering the weighted properties, jump visibility graphs (JVGs) were developed for detecting the delay lag from the non-linear time series. Compared with the authors' previous work on delay permutation entropy, this method can be applied to a non-stationary signal application. It shows that JVGs can efficiently

distinguish the EEG signals with eyes closed and those with eyes open.

The result was presented in Zhu et al. (2013). The related work is presented in Chapter 10.

Unlike the conventional synchrony measuring methods, this study designed an efficient graph isomorphism method for measuring the synchronization from multi nonlinear time series. It is shown that the complexity is linear, and the performance for chaotic signals and EEG signals are more noise-robustness than phase value locking (PLV) and synchronization likelihood.

The result was presented in Zhu et al. (2012*b*). The related work is presented in Chapter 7.

11.1.3 Novel clinical EEG diagnosing methods

Three types of clinical EEGs from different subjects: alcoholic, epileptic and sleep EEGs, were discussed in this thesis. A HVGI algorithm was applied to identify the alcoholic from controlled drinkers based on 600 segments of EEG recordings. The main strength of this algorithm is that the classifying process only needs to analyse 256 points and a 95.8% accuracy can be achieved, which is better than existing results.

The result was presented in Zhu et al. (2011). The related work is presented in Chapter 6.

Seizure detection from EEG signals has been obtained with a high accuracy by many researchers. However, many high sensitivity methods are slow. A FHVA algorithm was presented in this study and shows that the accuracy for identifying seizures from healthy based EEG signals can be achieved 100% and faster than those of PSD methods and sample entropy approaches, even with just two features. At the same time, this study also shows two other methods, VG features with a QDA classifier and JVG features with MSK-means algorithm. Both can obtain the similar high performance.

These results were presented in Zhu et al. (2011), Zhu et al. (2013) and Zhu et al. (Zhu, Li & Wen 2014*b*). **The publication by co-authors and myself was also presented** in (Wang et al. 2014).

The localization of the epileptogenic zone (EZ) from inter-ictal EEGs is extremely challenging for presurgery assessment. This study shows that the EZ focus can be efficiently localized by JVG methods. Both EEGs from the EZ and NEZ satisfy the power-law distribution based on the distributions of the variant delay lag from JVGs. However, our study shows that the distribution of the variant delay lag of JVGs associated with EZ decreases slower than those from NEZ due to the EZ being more stationary than NEZ.

These results was presented in Zhu et al. (2013). The related work is presented in Chapter 10.

Sleep scoring based on a single-channel EEG signals is challenging for biomedical engineers and experts. First, this study applied temporal complex networks to extract features from sleep EEGs. The average shortest path of VGs associated with EEG channels shows that brain graphs exhibit a small world structure during deep sleep, whether or not the channel is located in the frontal, central or parietal region. In addition, our results explain that EEGs from a channel in potential area (such as Pz-Oz) for the wake-sleep stage classification is better than that channel from other regions. It is also shown that the performance for sleep stage identification without wake sleep stage is better using frontal electrode or central areas. Based on these analyses, a DVG is applied for a single-channel sleep classification with the accuracy achieves of 88.9% accuracy in 5-state.

These results were presented in Zhu et al. (Zhu, Li & Wen 2014*a*). The related work is presented in Chapters 8 and 9. This work also attracted a Scholarship Award from the Australasian Mathematical Sciences Institute (AMSI) Student Travel award for attending the Australian Mathematical Sciences Student Conference in Canberra, Australia in July 2013.

11.1.4 Pattern recognition

EEG patterns are complex and time-variant. For example, EEG signals from one subject are significantly different from those of another subject. Effectively performing supervised classifiers are difficult to obtain in these cases because the training set from one subject is significantly different from that of others. This study provided a novel unsupervised classifier, a MSK-means algorithm, for EEG signal classification. It does not require a priori knowledge of the input signal from epileptic location. This shows that the MSK-means classifier is capable of handling big data sets.

These results were presented in Zhu et al. (2013) and Zhu et al. (2014). The related work is also presented in Chapter 10.

11.2 Future Work

Complex brain network analysis faces significant challenges. Existing complex networks have successfully shown that the brain graphs are essentially different from random graphs. It is important to investigate the different complex brain networks from clinic biomedical signals in practice. The following three topics should be given a great deal of attention:

- **Denoising artifacts in EEG signals effectively using complex networks:** As suggested in Section 9.5, denoising artifacts is a challenge for complex networks analysis. Some researchers have applied VG algorithms to detect the white Gauss noise from Chaotic signals (Lacasa & Toral 2010). However, the white noise is not an artifact in EEG or ECG recordings. In addition, artifacts commonly exist in biomedical signals. For example, anaesthetic EEG signals are always mixed with EMG signals, which cannot be removed by filtering techniques because EEGs and EMGs share a frequency band, from 5 Hz to 45 Hz. Therefore, it is very challenging to identify the artifacts with complex networks;

- **Improvement visibility graph algorithms for biomedical image analysis:** The chapters 5, 9 and 10 proposed three improved visibility graph constructing approaches to analyse the EEG and EOG signals. These performances are better than those of existing methods. A report (Shao 2010) shows that the VG methods are efficient to analyse ECG signal. However, the popular biomedical signals in clinical include lots of biomedical image signals, such as PET, MRI and fMRI. These images include geometry information, such as anatomical structure and molecular imaging. The complex networks cannot deal with two-dimensional image data and time series together. It is an essential problem to improve the visibility graph constructing algorithms to solve the two-dimensional biomedical image signals with time information together.

- **Fusion spatial complex networks and temporal complex networks using multimodal data sets:** Scientific data have become more complex than before due to more big data set coming in. Multimodel data sets, for example EEG-fMRI, are widely used in clinical cases. The literature review in Chapter 2 illustrated that magnetic resonance imaging (fMRI) can be analysed with spatial complex networks. Chapter 7 also demonstrated that EEGs and EOGs can be synchronized analysis with HVGI methods. However, there are few graph model to support the spatial complex networks and temporal complex networks at the same time. More important, multimodal data sets (such as fMRI+EEG) have been more and more attracted the brain function researchers. Therefore, it will be beneficial to conduct the studies with multimodal data using complex networks.

  In addition, the improved future works show that the combined SCN and TCN can be applied in multi-model climate data, such as temperature, wind-speed and pressure. Currently, climate time series have been analysed by visibility graph methods (F.Donges et al. 2013). However, these studies have never consider the spatial information. Thus the idea of combined spatial and temporal complex networks for multimodel climate data is quite interesting and promising.

References

Abdullah, H., Maddage, N. C., Cosic, I. & Cvetkovic, D. (2010), 'Cross-correlation of eeg frequency bands and heart rate variability for sleep apnoea classification', *Medical & biological engineering & computing* **48**(12), 1261–1269.

Achermann, P. & Borbély, A. (1998), 'Coherence analysis of the human sleep electroencephalogram', *Neuroscience* **85**(4), 1195–1208.

Achermann, P. & Borbély, A. (1997), 'Low-frequency (¡1 hz) oscillations in the human sleep electroencephalogram', *Neuroscience* **81**(1), 213 – 222.

Adamolekun, B., Afra, P. & Boop, F. (2011), 'False lateralization of seizure onset by scalp eeg in neocortical temporal lobe epilepsy', *Seizure* **20**(6), 494–499.

Adeli, H., Ghosh-Dastidar, S. & Dadmehr, N. (2007), 'A wavelet-chaos methodology for analysis of eegs and eeg subbands to detect seizure and epilepsy', *IEEE Transactions on Biomedical Engineering* **54**(2), 205–211.

Adler, G., Brassen, S. & Jajcevic, A. (2003), 'Eeg coherence in alzheimers dementia', *Journal of neural transmission* **110**(9), 1051–1058.

Ahmadlou, M. & Adeli, H. (2012), 'Visibility graph similarity: A new measure of generalized synchronization in coupled dynamic systems', *Physica D: Nonlinear Phenomena* **241**(4), 326–332.

Ahmadlou, M., Adeli, H. & Adeli, A. (2010), 'New diagnostic eeg markers of the alzheimers disease using visibility graph', *Journal of Neural Transmission* **117**(9), 1099–1109.

Akahin, M., Aydın, S., Fırat, H. & Eroul, O. (2012), 'Artificial apnea classification with quantitative sleep eeg synchronization', *Journal of medical systems* **36**(1), 139–144.

Albert, R., Jeong, H. & Barabási, A.-L. (2000), 'Error and attack tolerance of complex networks', *nature* **406**(6794), 378–382.

Altschul, S. F., Gish, W., Miller, W., Myers, E. W. & Lipman, D. J. (1990), 'Basic local alignment search tool', *Journal of molecular biology* **215**(3), 403–410.

Anderer, P., Gruber, G., Parapatics, S., Woertz, M., Miazhynskaia, T., Klösch, G., Saletu, B., Zeitlhofer, J., Barbanoj, M. J., Danker-Hopfe, H. et al. (2005), 'An e-health solution for automatic sleep classification according to rechtschaffen and kales: validation study of the somnolyzer 24× 7 utilizing the siesta database', *Neuropsychobiology* **51**(3), 115–133.

Andrzejak, R. G., Lehnertz, K., Mormann, F., Rieke, C., David, P. & E Elger, C. (2001), 'Indications of nonlinear deterministic and finite-dimensional structures in time series of brain electrical activity: Dependence on recording region and brain state', *Physical Review E* **64**(6), 061907.

Andrzejak, R. G., Schindler, K. & Rummel, C. (2012), 'Nonrandomness, nonlinear dependence, and nonstationarity of electroencephalographic recordings from epilepsy patients', *Physical Review E* **86**(4), 046206.

Andrzejak, R. G., Schindler, K. & Rummel, C. (2013), 'The bern-barcelona eeg database', `http://ntsa.upf.edu/downloads`. Accessed August 10, 2013.

Ansari-Asl, K., Senhadji, L., Bellanger, J.-J. & Wendling, F. (2006), 'Quantitative evaluation of linear and nonlinear methods characterizing interdependencies between brain signals', *Physical Review E* **74**(3), 031916.

Anton Popov, O. A. & Kanaykin, O. (2013), Saturation of electroencephalogram permutation entropy for large time lags, *in* 'Electronics and Nanotechnology (ELNANO), 2013 IEEE XXXIII International Scientific Conference', pp. 251–254.

Apostol, G. & Creutzfeldt, O. D. (1974), 'Crosscorrelation between the activity of septal units and hippocampal eeg during arousal', *Brain Research* **67**(1), 65–75.

Arthur, D. & Vassilvitskii, S. (2007), k-means++: The advantages of careful seeding, *in* 'Proceedings of the eighteenth annual ACM-SIAM symposium on Discrete algorithms', Society for Industrial and Applied Mathematics, pp. 1027–1035.

Arzi, A., Shedlesky, L., Ben-Shaul, M., Nasser, K., Oksenberg, A., Hairston, I. S. & Sobel, N. (2012), 'Humans can learn new information during sleep', *Nature neuroscience* **15**(10), 1460–1465.

Bache, K. & Lichman, M. (2013), 'UCI machine learning repository'.

Bahmani, B., Moseley, B., Vattani, A., Kumar, R. & Vassilvitskii, S. (2012), 'Scalable k-means++', *Proceedings of the VLDB Endowment* **5**(7), 622–633.

Bai, D., Qiu, T. & Li, X. (2007), '[the sample entropy and its application in eeg based epilepsy detection].', *Sheng wu yi xue gong cheng xue za zhi= Journal of biomedical engineering= Shengwu yixue gongchengxue zazhi* **24**(1), 200–205.

Barabási, A.-L. & Albert, R. (1999), 'Emergence of scaling in random networks', *science* **286**(5439), 509–512.

Barlow, J. S. (1985), 'Methods of analysis of nonstationary eegs, with emphasis on segmentation techniques: a comparative review', *Journal of Clinical Neurophysiology* **2**(3), 267–304.

Barrat, A., Barthelemy, M., Pastor-Satorras, R. & Vespignani, A. (2004), 'The architecture of complex weighted networks', *Proceedings of the National Academy of Sciences of the United States of America* **101**(11), 3747–3752.

Bartolo Luque, Lucas Lacasa, F. B. & Luque, J. (2009), 'Horizontal visibility graphs: Exact results for random time series', *Phys. Rev. E* **80**, 046103.

Bashan, A., Bartsch, R. P., Kantelhardt, J. W., Havlin, S. & Ivanov, P. C. (2012), 'Network physiology reveals relations between network topology and physiological function', *Nature communications* **3**, 702.

Bassett, D. S. & Bullmore, E. (2006), 'Small-world brain networks', *The neuroscientist* **12**(6), 512–523.

Bassett, D. S., Meyer-Lindenberg, A., Achard, S., Duke, T. & Bullmore, E. (2006), 'Adaptive reconfiguration of fractal small-world human brain functional networks', *Proceedings of the National Academy of Sciences* **103**(51), 19518–19523.

Ben-Jacob, E., Doron, I., Gazit, T., Rephaeli, E., Rephaeli, O. & L Towle, V. (2007), 'Mapping and assessment of epileptogenic foci using frequency-entropy templates', *Physical Review E* **76**(5), 051903.

Benson, D. A., Karsch-Mizrachi, I., Lipman, D. J., Ostell, J. & Wheeler, D. L. (2008), 'Genbank', *Nucleic acids research* **36**(suppl 1), D25–D30.

Berger, H. (1929), 'On the electroencephalogram of man', *Journal fur Psychologie und Neurologie* **40**, 160–179.

Berthomier, C. & Brandewinder, M. (2013), 'Sleep scoring: man vs. machine?', *Sleep and Breathing* **17**(2), 461–462.

Berthomier, C., Drouot, X., Herman-Stoïca, M., Berthomier, P., J. Prado, D. B.-T., Benoit, O., Mattout, J. & dOrtho, M. (2007), 'Automatic analysis of single-channel sleep eeg: Validation in healthy individuals', *Sleep* **30**(11), 1587 – 1595.

Blinowska, K. J. & Kaminski, M. (2013), 'Functional brain networks: Random,small world or deterministic?', *PloS one* **8**(10), e78763.

Boccaletti, S., Latora, V., Moreno, Y., Chavez, M. & Hwang, D.-U. (2006), 'Complex networks: Structure and dynamics', *Physics reports* **424**(4), 175–308.

Boly, M., Perlbarg, V., Marrelec, G., Schabus, M., Laureys, S., Doyon, J., Pélégrini-Issac, M., Maquet, P. & Benali, H. (2012), 'Hierarchical clustering of brain activity during human nonrapid eye movement sleep', *Proceedings of the National Academy of Sciences* **109**(15), 5856–5861.

Bombois, S., Derambure, P., Pasquier, F. & Monaca, C. (2010), 'Sleep disorders in aging and dementia', *The journal of nutrition, health & aging* **14**(3), 212–217.

Brigo, F., Ausserer, H., Nardone, R., Tezzon, F., Manganotti, P. & Bongiovanni, L. G. (2013), 'Subclinical rhythmic electroencephalogram discharge of adults occurring during sleep a diagnostic challenge', *Clinical EEG and neuroscience* **44**(3), 227–231.

Buckner, R. L., Sepulcre, J., Talukdar, T., Krienen, F. M., Liu, H., Hedden, T., Andrews-Hanna, J. R., Sperling, R. A. & Johnson, K. A. (2009), 'Cortical hubs revealed by intrinsic functional connectivity: Mapping, assessment of stability, and relation to alzheimer's disease', *The Journal of Neuroscience* **29**(6), 1860–1873.

Bullmore, E. & Sporns, O. (2009), 'Complex brain networks: graph theoretical analysis of structural and functional systems', *Nat Rev Neurosci* **10**(3), 186–198.

Bullmore, E. & Sporns, O. (2012), 'The economy of brain network organization', *Nature Reviews Neuroscience* **13**(5), 336–349.

Bullmore, E. T. & Bassett, D. S. (2011), 'Brain graphs: graphical models of the human brain connectome', *Annual review of clinical psychology* **7**, 113–140.

Burioka, N., Miyata, M., Cornélissen, G., Halberg, F., Takeshima, T., Kaplan, D. T., Suyama, H., Endo, M., Maegaki, Y., Nomura, T. et al. (2005), 'Approximate entropy in the electroencephalogram during wake and sleep', *Clinical EEG and neuroscience* **36**(1), 21–24.

Chapotot, F. & Becq, G. (2010), 'Automated sleepwake staging combining robust feature extraction, artificial neural network classification, and flexible decision rules', *International Journal of Adaptive Control and Signal Processing* **24**(5), 409–423.

Charbonnier, S., Zoubek, L., Lesecq, S. & Chapotot, F. (2011), 'Self-evaluated automatic classifier as a decision-support tool for sleep/wake staging', *Computers in Biology and Medicine* **41**(6), 380 – 389.

Cho, J.-H., Kang, H.-C., Jung, Y.-J., Kim, J.-Y., Kim, H. D., Yoon, D. S., Lee, Y.-H. & Im, C.-H. (2013), 'Localization of epileptogenic zones in lennox–gastaut syndrome using frequency domain source imaging of intracranial electroencephalography: a preliminary investigation', *Physiological measurement* **34**(2), 247.

Cohen, J. et al. (1960), 'A coefficient of agreement for nominal scales', *Educational and psychological measurement* **20**(1), 37–46.

Commonwealth of Australia (2012), 'Living longer. living better', `http://www.health.gov.au/internet/publications/publishing.nsf/Content/ageing-aged-care-reform-measures-toc`. Accessed August 10, 2013.

Cook, S. A. (1971), The complexity of theorem-proving procedures, *in* 'Proceedings of the third annual ACM symposium on Theory of computing', STOC'71, ACM, New York, NY, USA, pp. 151–158.

Costa, M., Goldberger, A. L. & Peng, C.-K. (2002), 'Multiscale entropy analysis of complex physiologic time series', *Physical review letters* **89**(6), 068102.

Cover, T. & Hart, P. (1967), 'Nearest neighbor pattern classification', *Information Theory, IEEE Transactions on* **13**(1), 21–27.

Dapena, A. & Castedo, L. (2003), 'A novel frequency domain approach for separating convolutive mixtures of temporally-white signals', *Digital Signal Processing* **13**(2), 301–316.

de Bruin, E. A., Bijl, S., Stam, C. J., Böcker, K. B., Kenemans, J. L. & Verbaten, M. N. (2004), 'Abnormal eeg synchronisation in heavily drinking students', *Clinical Neurophysiology* **115**(9), 2048 – 2055.

Dehmer, M. & Mowshowitz, A. (2011), 'A history of graph entropy measures', *Information Sciences* **181**(1), 57 – 78.

Dong, Z. & Li, X. (2010), 'Comment on network analysis of human heartbeat dynamics[appl. phys. lett. 96, 073703 (2010)]', *Applied Physics Letters* **96**(26), 266101–266101.

Donges, J. F., Donner, R. V., Trauth, M. H., Marwan, N., Schellnhuber, H.-J. & Kurths, J. (2011), 'Nonlinear detection of paleoclimate-variability transitions possibly related to human evolution', *Proceedings of the National Academy of Sciences* **108**(51), 20422–20427.

Donner, R. & Donges, J. (2012), 'Visibility graph analysis of geophysical time series: Potentials and possible pitfalls', *Acta Geophysica* **60**(3), 589–623.

EA, W. (1969), 'A manual of standardized terminology, techniques and scoring system for sleep stages of human subjects.', *Archives of General Psychiatry* **20**(2), 246–247.

Fallani, F. D. V., Astolfi, L., Cincotti, F., Mattia, D., la Rocca, D., Maksuti, E., Salinari, S., Babiloni, F., Vegso, B., Kozmann, G. & Nagy, Z. (2009), 'Evaluation of the brain network organization from eeg signals: A preliminary evidence in stroke patient', *The Anatomical Record: Advances in Integrative Anatomy and Evolutionary Biology* **292**(12), 2023–2031.

F.Donges, J., Donner, R. V. & Kurths, J. (2013), 'Testing time series irreversibility using complex network methods', *EPL (Europhysics Letters)* **102**(1), 10004.

Fernandez-Blanco, E., Rivero, D., Rabuñal, J., Dorado, J., Pazos, A. & Munteanu, C. R. (2012), 'Automatic seizure detection based on star graph topological indices', *Journal of neuroscience methods* **209**(2), 410–419.

Ferri, R., Rundo, F., Bruni, O., Terzano, M. G. & Stam, C. J. (2007), 'Small-world network organization of functional connectivity of eeg slow-wave activity during sleep', *Clinical neurophysiology* **118**(2), 449–456.

Flexer, A., Gruber, G. & Dorffner, G. (2005), 'A reliable probabilistic sleep stager based on a single eeg signal', *Artificial Intelligence in Medicine* **33**(3), 199 – 207.

Fraiwan, L., Lweesy, K., Khasawneh, N., Wenz, H. & Dickhaus, H. (2012), 'Automated sleep stage identification system based on timefrequency analysis of a single eeg channel and random forest classifier', *Computer Methods and Programs in Biomedicine* **108**(1), 10 – 19.

Gabow, H. N. (1976), 'An efficient implementation of edmonds' algorithm for maximum matching on graphs', *Journal of the ACM (JACM)* **23**(2), 221–234.

Gallos, L. K., Sigman, M. & Makse, H. A. (2012), 'The conundrum of functional brain networks: small-world efficiency or fractal modularity', *Frontiers in physiology* **3**.

Gangwisch, J. E., Heymsfield, S. B., Boden-Albala, B., Buijs, R. M., Kreier, F., Pickering, T. G., Rundle, A. G., Zammit, G. K. & Malaspina, D. (2006), 'Short sleep duration as a risk factor for hypertension analyses of the first national health and nutrition examination survey', *Hypertension* **47**(5), 833–839.

Garrett, D., Peterson, D. A., Anderson, C. W. & Thaut, M. H. (2003), 'Comparison of linear, nonlinear, and feature selection methods for eeg signal classification', *Neural Systems and Rehabilitation Engineering, IEEE Transactions on* **11**(2), 141–144.

Goffin, K., Dedeurwaerdere, S., Van Laere, K. & Van Paesschen, W. (2008), Neuronuclear assessment of patients with epilepsy, *in* 'Seminars in nuclear medicine', Vol. 38, Elsevier, pp. 227–239.

Goldberg, A. V. & Radzik, T. (1993), 'A heuristic improvement of the bellman-ford algorithm', *Applied Mathematics Letters* **6**(3), 3–6.

Goldberger, A. L., Amaral, L. A. N., Glass, L., Hausdorff, J. M., Ivanov, P. C., Mark, R. G., Mietus, J. E., Moody, G. B., Peng, C.-K. & Stanley, H. E. (2000), 'Physiobank, physiotoolkit, and physionet: Components of a new research resource for complex physiologic signals', *Circulation* **101**(23), e215–e220.

Güler, N. F., Übeyli, E. D. & İnan Güler (2005), 'Recurrent neural networks employing lyapunov exponents for eeg signals classification', *Expert Systems with Applications* **29**(3), 506–514.

Guo, L., Rivero, D., Dorado, J., Munteanu, C. R. & Pazos, A. (2011), 'Automatic feature extraction using genetic programming: An application to epileptic eeg classification', *Expert Systems with Applications* **38**(8), 10425–10436.

Gutin, G., Mansour, T. & Severini, S. (2011), 'A characterization of horizontal visibility graphs and combinatorics on words', *Physica A: Statistical Mechanics and its Applications* **390**(12), 2421–2428.

Hayasaka, S. & Laurienti, P. J. (2010), 'Comparison of characteristics between region-and voxel-based network analyses in resting-state fmri data', *Neuroimage* **50**(2), 499–508.

Hayden, E. P., Wiegand, R. E., Meyer, E. T., Bauer, L. O., O'Connor, S. J., Nurnberger, J. I., Chorlian, D. B., Porjesz, B. & Begleiter, H. (2006), 'Patterns of regional brain activity in alcohol-dependent subjects', *Alcoholism: Clinical and Experimental Research* **30**(12), 1986–1991.

He, A., Yang, X., Yang, X. & Ning, X. (2007), Phase synchronization in sleep electroencephalogram, *in* 'Complex Medical Engineering, 2007. CME 2007. IEEE/ICME International Conference on', IEEE, pp. 1421–1424.

He, B., Coleman, T., Genin, G., Glover, G., Hu, X., Johnson, N., Liu, T., Makeig, S., Sajda, P. & Ye, K. (2013), 'Grand challenges in mapping the human brain: Nsf workshop report', *Biomedical Engineering, IEEE Transactions on* **60**(11), 2983–2992.

He, Y., Chen, Z. J. & Evans, A. C. (2007), 'Small-world anatomical networks in the human brain revealed by cortical thickness from mri', *Cerebral cortex* **17**(10), 2407–2419.

Henry, T. R. & Van Heertum, R. L. (2003), 'Positron emission tomography and single photon emission computed tomography in epilepsy care', *Seminars in nuclear medicine* **33**(2), 88–104.

Holme, P. & Saramäki, J. (2012), 'Temporal networks', *Physics reports* **519**(3), 97–125.

Hsu, Y.-L., Yang, Y.-T., Wang, J.-S. & Hsu, C.-Y. (2013), 'Automatic sleep stage recurrent neural classifier using energy features of eeg signals', *Neurocomputing* **104**(0), 105 – 114.

Hu, J., Gao, J. & White, K. (2004), 'Estimating measurement noise in a time series by exploiting nonstationarity', *Chaos, Solitons & Fractals* **22**(4), 807–819.

Humphries, M. D., Gurney, K. & Prescott, T. J. (2006), 'The brainstem reticular formation is a small-world, not scale-free, network', *Proceedings of the Royal Society B: Biological Sciences* **273**(1585), 503–511.

Hurd, M. D., Martorell, P., Delavande, A., Mullen, K. J. & Langa, K. M. (2013), 'Monetary costs of dementia in the united states', *New England Journal of Medicine* **368**(14), 1326–1334.

Iber (2007), *The AASM Manual for the Scoring of Sleep and Associated Events: Rules, Terminology and Technical Specification*.

Insel, T. R., Landis, S. C. & Collins, F. S. (2013), 'The nih brain initiative', *Science* **340**(6133), 687–688.

Iscan, Z., Dokur, Z. & Demiralp, T. (2011), 'Classification of electroencephalogram signals with combined time and frequency features', *Expert Systems with Applications* **38**(8), 10499–10505.

Jiaxin Liu, G. Z. & Xi, M. (2013), 'A k-means algorithm based on the radius', *Journal of Guilin University of Electronic Technology* **33**(2), 134–138.

Jo, H. G., Park, J. Y., Lee, C. K., An, S. K. & Yoo, S. K. (2010), 'Genetic fuzzy classifier for sleep stage identification', *Computers in Biology and Medicine* **40**(7), 629 – 634.

Joudaki, A., Salehi, N., Jalili, M. & Knyazeva, M. G. (2012), 'Eeg-based functional brain networks: does the network size matter?', *PloS one* **7**(4), e35673.

Kanz, C., Aldebert, P., Althorpe, N., Baker, W., Baldwin, A., Bates, K., Browne, P., van den Broek, A., Castro, M., Cochrane, G. et al. (2005), 'The embl nucleotide sequence database', *Nucleic Acids Research* **33**(suppl 1), D29–D33.

Karatzoglou, A., Meyer, D. & Hornik, K. (2006), 'Support vector machines in r', *Journal of Statistical Software* **15**(9), 1–28.

Keller, P. E., Knoblich, G. & Repp, B. H. (2007), 'Pianists duet better when they play with themselves: On the possible role of action simulation in synchronization', *Consciousness and Cognition* **16**(1), 102 – 111.

Kemp, B. (2013), 'The sleep-edf database'.

Kemp, B., Vrri, A., Rosa, A. C., Nielsen, K. D. & Gade, J. (1992), 'A simple format for exchange of digitized polygraphic recordings', *Electroencephalography and Clinical Neurophysiology* **82**(5), 391 – 393.

Kemp, B., Zwinderman, A., Tuk, B., Kamphuisen, H. & Oberye, J. (2000), 'Analysis of a sleep-dependent neuronal feedback loop: the slow-wave microcontinuity of the eeg', *Biomedical Engineering, IEEE Transactions on* **47**(9), 1185–1194.

Knapp, C. & Carter, G. C. (1976), 'The generalized correlation method for estimation of time delay', *Acoustics, Speech and Signal Processing, IEEE Transactions on* **24**(4), 320–327.

Knowlton, R. C., Elgavish, R. A., Bartolucci, A., Ojha, B., Limdi, N., Blount, J., Burneo, J. G., Ver Hoef, L., Paige, L., Faught, E. et al. (2008), 'Functional imaging: Ii. prediction of epilepsy surgery outcome', *Annals of neurology* **64**(1), 35–41.

Knyazeva, M. G., Jalili, M., Brioschi, A., Bourquin, I., Fornari, E., Hasler, M., Meuli, R., Maeder, P. & Ghika, J. (2010), 'Topography of eeg multivariate phase synchronization in early alzheimer's disease', *Neurobiology of Aging* **31**(7), 1132–1144.

Kogan, E., Korczyn, A., Virchovsky, R., Klimovizky, S. S., Treves, T. & Neufeld, M. (2001), 'Eeg changes during long-term treatment with donepezil in alzheimer's disease patients', *Journal of neural transmission* **108**(10), 1167–1173.

Korn, H. & Faure, P. (2003), 'Is there chaos in the brain? ii. experimental evidence and related models', *Comptes Rendus Biologies* **326**(9), 787 – 840.

Krakovská, A. & Mezeiová, K. (2011), 'Automatic sleep scoring: A search for an optimal combination of measures', *Artificial Intelligence in Medicine* **53**(1), 25 – 33.

Kramer, M. A., Kolaczyk, E. D. & Kirsch, H. E. (2008), 'Emergent network topology at seizure onset in humans', *Epilepsy research* **79**(2), 173–186.

Krsek, P., Kudr, M., Jahodova, A., Komarek, V., Maton, B., Maton, S., Miller, I., Jayakar, P., Resnick, T. & Duchowny, M. (2013), 'Localizing value of ictal spect is comparable to mri and eeg in children with focal cortical dysplasia', *Epilepsia* **54**(2), 351–358.

Lacasa, L., Luque, B., Ballesteros, F., Luque, J. & no, J. C. N. (2008), 'From time series to complex networks: The visibility graph', *Proceedings of the National Academy of Sciences* **105**(13), 4972–4975.

Lacasa, L. & Toral, R. (2010), 'Description of stochastic and chaotic series using visibility graphs', *Phys. Rev. E* **82**, 036120.

Landis, J. R. & Koch, G. G. (1977), 'The measurement of observer agreement for categorical data', *biometrics* pp. 159–174.

Lang, P., Liu, D.-B., Cai, S.-M., Hong, L. & Zhou, P.-L. (2013), 'Recurrence network analysis of the synchronous eeg time series in normal and epileptic brains', *Cell Biochemistry and Biophysics* **66**(2), 331–336.

Lee, U., Müller, M., Noh, G.-J., Choi, B. & Mashour, G. A. (2011), 'Dissociable network properties of anesthetic state transitions', *Anesthesiology* **114**(4), 872–881.

Li, X., Yang, D., Liu, X. & Wu, X.-M. (2012*a*), 'Bridging time series dynamics and complex network theory with application to electrocardiogram analysis', *Circuits and Systems Magazine, IEEE* **12**(4), 33–46.

Li, X., Yang, D., Liu, X. & Wu, X.-M. (2012*b*), 'Bridging time series dynamics and complex network theory with application to electrocardiogram analysis', *IEEE Circuits and Systems Magazine* **12**(4), 33–46.

Liang, S.-F., Kuo, C.-E., Hu, Y.-H., Pan, Y.-H. & Wang, Y.-H. (2012), 'Automatic stage scoring of single-channel sleep eeg by using multiscale entropy and autoregressive models', *IEEE Transactions on Instrumentation and Measurement* **61**(6), 1649–1657.

Luque, B., Lacasa, L., Ballesteros, F. J. & Robledo, A. (2012), 'Analytical properties of horizontal visibility graphs in the feigenbaum scenario', *Chaos: An Interdisciplinary Journal of Nonlinear Science* **22**(1), 013109–013109.

M. Corsi-Cabrera, Z. Muñoz-Torres, Y. d. R.-P. & Guevara, M. (2006), 'Power and coherent oscillations distinguish rem sleep, stage 1 and wakefulness', *International Journal of Psychophysiology* **60**(1), 59 – 66.

M. Emin Tagluk, N. S. & Akin, M. (2010), 'Estimation of sleep stages by an artificial neural network employing eeg, emg and eog', *Journal of Medical Systems* **34**(4), 717–725.

MacQueen, J. et al. (1967), Some methods for classification and analysis of multivariate observations, *in* 'Proceedings of the fifth Berkeley symposium on mathematical statistics and probability', Vol. 1, California, USA, p. 14.

Marwan, N., Donges, J. F., Zou, Y., Donner, R. V. & Kurths, J. (2009), 'Complex network approach for recurrence analysis of time series', *Physics Letters A* **373**(46), 4246 – 4254.

Marzano, C., Moroni, F., Gorgoni, M., Nobili, L., Ferrara, M. & De Gennaro, L. (2013), 'How we fall asleep: regional and temporal differences in electroencephalographic synchronization at sleep onset', *Sleep medicine* **14**(11), 1112–1122.

McCall, W. V. & Black, C. G. (2013), 'The link between suicide and insomnia: Theoretical mechanisms', *Current psychiatry reports* **15**(9), 1–9.

Meng-Cen Qian, Z.-Q. J. & Zhou, W.-X. (2010), 'Universal and nonuniversal allometric scaling behaviors in the visibility graphs of world stock market indices', *Journal of Physics A: Mathematical and Theoretical* **43**(33), 335002.

Michael, A., Mirza, K. A. H., Mukundan, C. R. & Channabasavanna, S. M. (1993), 'Interhemispheric electroencephalographic coherence as a biological marker in alcoholism', *Acta Psychiatrica Scandinavica* **87**(3), 213–217.

Micheloyannis, S., Pachou, E., Stam, C. J., Vourkas, M., Erimaki, S. & Tsirka, V. (2006), 'Using graph theoretical analysis of multi channel eeg to evaluate the neural efficiency hypothesis', *Neuroscience letters* **402**(3), 273–277.

Mierlo, P., Carrette, E., Hallez, H., Raedt, R., Meurs, A., Vandenberghe, S., Roost, D., Boon, P., Staelens, S. & Vonck, K. (2013), 'Ictal-onset localization through connectivity analysis of intracranial eeg signals in patients with refractory epilepsy', *Epilepsia* **54**(8), 1409–1418.

Mölle, M., Marshall, L., Gais, S. & Born, J. (2004), 'Learning increases human electroencephalographic coherence during subsequent slow sleep oscillations', *Proceedings of the National Academy of Sciences of the United States of America* **101**(38), 13963–13968.

Mormann, F., Andrzejak, R. G., Elger, C. E. & Lehnertz, K. (2007), 'Seizure prediction: the long and winding road', *Brain* **130**(2), 314–333.

Mormann, F., Lehnertz, K., David, P. & Elger, C. E. (2000), 'Mean phase coherence as a measure for phase synchronization and its application to the eeg of epilepsy patients', *Physica D: Nonlinear Phenomena* **144**(3), 358–369.

Morse, T. M. (2007), 'Neuroinformatics: from bioinformatics to databasing the brain.', *Bioinformatics and biology insights* **2**, 253–264.

Mourad Adnane, Z. J. & Yan, Z. (2012), 'Sleepwake stages classification and sleep efficiency estimation using single-lead electrocardiogram', *Expert Systems with Applications* **39**(1), 1401 – 1413.

Newman, M. E. (2003), 'The structure and function of complex networks', *SIAM review* **45**(2), 167–256.

nez, A. N., Lacasa, L., Valero, E., Gómez, J. P. & Luque, B. (2012), 'Detecting series periodicity with horizontal visibility graphs', *International Journal of Bifurcation and Chaos* **22**(07), 1250160.

Ni, X.-H., Jiang, Z.-Q. & Zhou, W.-X. (2009), 'Degree distributions of the visibility graphs mapped from fractional brownian motions and multifractal random walks', *Physics Letters A* **373**(42), 3822–3826.

Nicolaou, N. & Georgiou, J. (2011), 'The use of permutation entropy to characterize sleep electroencephalograms', *Clinical EEG and Neuroscience* **42**(1), 24–28.

Nicolaou, N. & Georgiou, J. (2012), 'Detection of epileptic electroencephalogram based on permutation entropy and support vector machines', *Expert Systems with Applications* **39**(1), 202–209.

Nicolaou, N. & Georgiou, J. (2014), 'Spatial analytic phase difference of eeg activity during anesthetic-induced unconsciousness', *Clinical Neurophysiology* .

Niedermeyer, E. & da Silva, F. L. (2005), *Electroencephalography: basic principles, clinical applications, and related fields*, Lippincott Williams & Wilkins.

Orhan, U., Hekim, M. & Ozer, M. (2011), 'Eeg signals classification using the¡ i¿ k¡/i¿-means clustering and a multilayer perceptron neural network model', *Expert Systems with Applications* **38**(10), 13475–13481.

Osorio, I., Frei, M. G. & Wilkinson, S. B. (1998), 'Real-time automated detection and quantitative analysis of seizures and short-term prediction of clinical onset', *Epilepsia* **39**(6), 615–627.

Ouyang, G., Li, J., Liu, X. & Li, X. (2012), 'Dynamic characteristics of absence eeg recordings with multiscale permutation entropy analysis', *Epilepsy research* .

Ouyang, G., Li, X., Dang, C. & Richards, D. A. (2008), 'Using recurrence plot for determinism analysis of {EEG} recordings in genetic absence epilepsy rats', *Clinical Neurophysiology* **119**(8), 1747 – 1755.

Percha, B., Dzakpasu, R., Żochowski, M. & Parent, J. (2005), 'Transition from local to global phase synchrony in small world neural network and its possible implications for epilepsy', *Phys. Rev. E* **72**, 031909.

Pereda, E., Gamundi, A., Rial, R. & Gonzalez, J. (1998), 'Non-linear behaviour of human eeg: fractal exponent versus correlation dimension in awake and sleep stages', *Neuroscience letters* **250**(2), 91–94.

Peters, J. M., Taquet, M., Vega, C., Jeste, S. S., Fernández, I. S., Tan, J., Nelson, C. A., Sahin, M. & Warfield, S. K. (2013), 'Brain functional networks in syndromic and non-syndromic autism: a graph theoretical study of eeg connectivity', *BMC medicine* **11**(1), 54.

Polat, K. & Güneş, S. (2007), 'Classification of epileptiform eeg using a hybrid system based on decision tree classifier and fast fourier transform', *Applied Mathematics and Computation* **187**(2), 1017–1026.

Ponten, S., Bartolomei, F. & Stam, C. (2007), 'Small-world networks and epilepsy: graph theoretical analysis of intracerebrally recorded mesial temporal lobe seizures', *Clinical neurophysiology* **118**(4), 918–927.

Pritchard, W. S., Duke, D. W. & Krieble, K. K. (1995), 'Dimensional analysis of resting human eeg ii: Surrogate-data testing indicates nonlinearity but not low-dimensional chaos', *Psychophysiology* **32**(5), 486–491.

Quiroga, R. Q., Kraskov, A., Kreuz, T. & Grassberger, P. (2002), 'Performance of different synchronization measures in real data: A case study on electroencephalographic signals', *Phys. Rev. E* **65**, 041903.

Ramaswamy Palaniappan, P. R. & Omatu, S. (2002), 'Vep optimal channel selection using genetic algorithm for neural network classification of alcoholics', *Neural Networks, IEEE Transactions on* **13**(2), 486–491.

Rangaswamy, M., Porjesz, B., Chorlian, D. B., Wang, K., Jones, K. A., Kuperman, S., Rohrbaugh, J., O'Connor, S. J., Bauer, L. O., Reich, T. et al. (2004), 'Resting eeg in offspring of male alcoholics: beta frequencies', *International Journal of Psychophysiology* **51**(3), 239–251.

Ravi, K. & Palaniappan, R. (2006), 'Neural network classification of late gamma band electroencephalogram features', *Soft Computing* **10**(2), 163–169.

Reijneveld, J. C., Ponten, S. C., Berendse, H. W. & Stam, C. J. (2007), 'The application of graph theoretical analysis to complex networks in the brain', *Clinical Neurophysiology* **118**(11), 2317–2331.

Richman, J. S. & Moorman, J. R. (2000), 'Physiological time-series analysis using approximate entropy and sample entropy', *American Journal of Physiology-Heart and Circulatory Physiology* **278**(6), H2039–H2049.

Ripley, B., Venables, B., Bates, D. M., Hornik, K. & Ripley, M. B. (2012), 'Mass: Support functions and datasets for venables and ripley's mass', `http://cran.r-project.org/package=MASS`. Accessed March 3, 2014.

Ronzhina, M., Janoušek, O., Kolářová, J., Nováková, M., Honzk, P. & Provaznk, I. (2012), 'Sleep scoring using artificial neural networks', *Sleep Medicine Reviews* **16**(3), 251 – 263.

Rosenblum, M. G., Pikovsky, A. S. & Kurths, J. (1996), 'Phase synchronization of chaotic oscillators', *Physical Review Letters* **76**(11), 1804.

Rosenow, F. & Lüders, H. (2001), 'Presurgical evaluation of epilepsy', *Brain* **124**(9), 1683–1700.

Sakkalis, V., Tsiaras, V., Zervakis, M. & Tollis, I. (2007), Optimal brain network synchrony visualization: Application in an alcoholism paradigm, *in* '29th Annual International Conference of the IEEE Engineering in Medicine and Biology Society, 2007. EMBS 2007.', pp. 4285–4288.

Sanz-Arigita, E. J., Schoonheim, M. M., Damoiseaux, J. S., Rombouts, S. A., Maris, E., Barkhof, F., Scheltens, P. & Stam, C. J. (2010), 'Loss of small-worldnetworks in alzheimer's disease: graph analysis of fmri resting-state functional connectivity', *PloS one* **5**(11), e13788.

Schank, T. & Wagner, D. (2005), Finding, counting and listing all triangles in large graphs, an experimental study, *in* 'Experimental and Efficient Algorithms', Springer, pp. 606–609.

Schindler, K. A., Bialonski, S., Horstmann, M.-T., Elger, C. E. & Lehnertz, K. (2008), 'Evolving functional network properties and synchronizability during human epileptic seizures', *Chaos: An Interdisciplinary Journal of Nonlinear Science* **18**(3), 033119.

Shannon, C. E. (2001), 'A mathematical theory of communication', *SIGMOBILE Mob. Comput. Commun. Rev.* **5**(1), 3–55.

Shao, Z.-G. (2010), 'Network analysis of human heartbeat dynamics', *Applied Physics Letters* **96**(7), –.

Siuly, Li, Y. & Wen, P. P. (2011), 'Clustering technique-based least square support vector machine for eeg signal classification', *Computer methods and programs in biomedicine* **104**(3), 358–372.

Song, Y. & Liò, P. (2010), 'A new approach for epileptic seizure detection: sample entropy based feature extraction and extreme learning machine.', *Journal of Biomedical Science & Engineering* **3**(6).

Spanaki, M. V., Spencer, S. S., Corsi, M., MacMullan, J., Seibyl, J., Zubal, I. G. et al. (1999), 'Sensitivity and specificity of quantitative difference spect analysis in seizure localization.', *Journal of nuclear medicine: official publication, Society of Nuclear Medicine* **40**(5), 730–736.

Spoormaker, V. I., Gleiser, P. M. & Czisch, M. (2012), 'Frontoparietal connectivity and hierarchical structure of the brain's functional network during sleep.', *Frontiers in neurology* **3**.

Srinivasan, V., Eswaran, C. & Sriraam, N. (2005), 'Artificial neural network based epileptic detection using time-domain and frequency-domain features', *Journal of Medical Systems* **29**(6), 647–660.

Stam, C., Jones, B., Nolte, G., Breakspear, M. & Scheltens, P. (2007), 'Small-world networks and functional connectivity in alzheimer's disease', *Cerebral Cortex* **17**(1), 92–99.

Stam, C. & Van Dijk, B. (2002), 'Synchronization likelihood: an unbiased measure of generalized synchronization in multivariate data sets', *Physica D: Nonlinear Phenomena* **163**(3), 236–251.

Subasi, A. (2005), 'Epileptic seizure detection using dynamic wavelet network', *Expert Systems with Applications* **29**(2), 343–355.

Subasi, A. (2006), 'Automatic detection of epileptic seizure using dynamic fuzzy neural networks', *Expert Systems with Applications* **31**(2), 320–328.

Subasi, A. & Gursoy, M. I. (2010), 'Eeg signal classification using pca, ica, lda and support vector machines', *Expert Systems with Applications* **37**(12), 8659–8666.

Sueur, J., Aubin, T. & Simonis, C. (2008), 'Equipment review: seewave, a free modular tool for sound analysis and synthesis', *Bioacoustics* **18**(2), 213–226.

Sukhorukova, N., Stranieri, A., Ofoghi, B., Vamplew, P., Saleem, M., Ma, L., Ugon, A., Ugon, J., Muecke, N., Amiel, H., Philippe, C., Bani-Mustafa, A., Huda, S., Bertoli, M., Lévy, P. & Ganascia, J.-G. (2010), Automatic sleep stage identification: Difficulties and possible solutions, *in* 'Proceedings of the Fourth Australasian Workshop on Health Informatics and Knowledge Management - Volume 108', HIKM '10, Australian Computer Society, Inc., Darlinghurst, Australia, Australia, pp. 39–44.

Supekar, K., Menon, V., Rubin, D., Musen, M. & Greicius, M. D. (2008), 'Network analysis of intrinsic functional brain connectivity in alzheimer's disease', *PLoS Comput Biol* **4**(6), e1000100.

Tagliazucchi, E., Von Wegner, F., Morzelewski, A., Brodbeck, V., Borisov, S., Jahnke, K. & Laufs, H. (2013), 'Large-scale brain functional modularity is reflected in slow electroencephalographic rhythms across the human non-rapid eye movement sleep cycle', *Neuroimage* **70**, 327–339.

Takens, F. (1981), Detecting strange attractors in turbulence, *in* 'Dynamical systems and turbulence, Warwick 1980', Springer, pp. 366–381.

Takigawa, M., Wang, G., Kawasaki, H. & Fukuzako, H. (1996), 'Eeg analysis of epilepsy by directed coherence method a data processing approach', *International Journal of Psychophysiology* **21**(23), 65 – 73.

Tang, X., Xia, L., Liao, Y., Liu, W., Peng, Y., Gao, T. & Zeng, Y. (2013), 'New approach to epileptic diagnosis using visibility graph of high-frequency signal', *Clinical EEG and Neuroscience* .

Telesca, L. & Lovallo, M. (2012), 'Analysis of seismic sequences by using the method of visibility graph', *EPL (Europhysics Letters)* **97**(5), 50002.

Theiler, J. (1986), 'Spurious dimension from correlation algorithms applied to limited time-series data', *Physical Review A* **34**(3), 2427.

Thomasson, N., Hoeppner, T. J., Webber, C. L. & Zbilut, J. P. (2001), 'Recurrence quantification in epileptic eegs', *Physics Letters A* **279**(1), 94–101.

Tichavsky, P. & Koldovsky, Z. (2004), 'Optimal pairing of signal components separated by blind techniques', *Signal Processing Letters, IEEE* **11**(2), 119–122.

Tijms, B. M., Wink, A. M., de Haan, W., van der Flier, W. M., Stam, C. J., Scheltens, P. & Barkhof, F. (2013), 'Alzheimer's disease: connecting findings from graph theoretical studies of brain networks', *Neurobiology of aging* **34**(8), 2023–2036.

van Dellen, E., Douw, L., Baayen, J. C., Heimans, J. J., Ponten, S. C., Vandertop, W. P., Velis, D. N., Stam, C. J. & Reijneveld, J. C. (2009), 'Long-term effects of temporal lobe epilepsy on local neural networks: a graph theoretical analysis of corticography recordings', *PLoS One* **4**(11), e8081.

van Diessen, E., Otte, W. M., Braun, K. P., Stam, C. J. & Jansen, F. E. (2014), 'Does sleep deprivation alter functional eeg networks in children with focal epilepsy?', *Frontiers in systems neuroscience* **8**.

Vatankhah, M., Totonchi, M. R. A., Moghimi, A. & Asadpour, V. (2010), Ga/svm for diagnosis sleep stages using non-linear and spectral features, *in* 'Soft Computing in Industrial Applications', Springer, pp. 175–184.

Vattani, A. (2011), 'K-means requires exponentially many iterations even in the plane', *Discrete & Computational Geometry* **45**(4), 596–616.

Venter, J. C., Adams, M. D., Myers, E. W., Li, P. W., Mural, R. J., Sutton, G. G., Smith, H. O., Yandell, M., Evans, C. A., Holt, R. A. et al. (2001), 'The sequence of the human genome', *science* **291**(5507), 1304–1351.

Walters, A. S. & Rye, D. B. (2009), 'Review of the relationship of restless legs syndrome and periodic limb movements in sleep to hypertension, heart disease, and stroke', *Sleep* **32**(5), 589.

Wang, B., Wong, C. M., Wan, F., Mak, P. U., Mak, P. I. & Vai, M. I. (2009), Comparison of different classification methods for eeg-based brain computer interfaces: a case study, *in* 'Information and Automation, 2009. ICIA'09. International Conference on', IEEE, pp. 1416–1421.

Wang, J., Zuo, X., Dai, Z., Xia, M., Zhao, Z., Zhao, X., Jia, J., Han, Y. & He, Y. (2013), 'Disrupted functional brain connectome in individuals at risk for alzheimer's disease', *Biological Psychiatry* **73**(5), 472 – 481. Disturbances in the Connectome and Risk for Alzheimers Disease.

Wang, S., Zhu, G., Li, Y., Wen, P. & Song, B. (2014), 'Analysis of epileptic eeg signals with simple random sampling j48 algorithm', *International Journal of Bioscience, Biochemistry and Bioinformatics* **4**(2).

Watts, D. J. & Strogatz, S. H. (1998), 'Collective dynamics of small-worldnetworks', *nature* **393**(6684), 440–442.

Winterer, G., Enoch, M.-A., White, K., Saylan, M., Coppola, R. & Goldman, D. (2003), 'Eeg phenotype in alcoholism: increased coherence in the depressivesubtype', *Acta Psychiatrica Scandinavica* **108**(1), 51–60.

Wu, J., Sutherling, W., Koh, S., Salamon, N., Jonas, R., Yudovin, S., Sankar, R., Shields, W. & Mathern, G. (2006), 'Magnetic source imaging localizes epileptogenic zone in children with tuberous sclerosis complex', *Neurology* **66**(8), 1270–1272.

Xia, W., Wang, B. & Zhang, L. (2013), 'Band selection for hyperspectral imagery: A new approach based on complex networks', *IEEE GEOSCIENCE AND REMOTE SENSING LETTERS* **10**(5), 1229.

Xu, X., Zhang, J. & Small, M. (2008), 'Superfamily phenomena and motifs of networks induced from time series', *Proceedings of the National Academy of Sciences* **105**(50), 19601–19605.

Yang, Y., Wang, J., Yang, H. & Mang, J. (2009), 'Visibility graph approach to exchange rate series', *Physica A: Statistical Mechanics and its Applications* **388**(20), 4431 – 4437.

Zhang, J., Liu, W., Chen, H., Xia, H., Zhou, Z., Mei, S., Liu, Q. & Li, Y. (2014), 'Multimodal neuroimaging in presurgical evaluation of drug-resistant epilepsy', *NeuroImage: Clinical* **4**, 35–44.

Zhang, J. & Small, M. (2006), 'Complex network from pseudoperiodic time series: Topology versus dynamics', *Physical Review Letters* **96**(23), 238701.

Zhang, X. L., Begleiter, H., Porjesz, B. & Litke, A. (1997), 'Electrophysiological evidence of memory impairment in alcoholic patients', *Biological Psychiatry* **42**(12), 1157 – 1171.

Zhu, G., Li, Y. & Wen, P. P. (2011), 'Evaluating functional connectivity in alcoholics based on maximal weight matching', *Journal of Advanced Computational Intelligence and Intelligent Informatics* **15**(9), 1221–1227.

Zhu, G., Li, Y. & Wen, P. P. (2012*a*), Analysing epileptic eegs with a visibility graph algorithm, *in* 'Biomedical Engineering and Informatics (BMEI), 2012 5th International Conference on', IEEE, pp. 432–436.

Zhu, G., Li, Y. & Wen, P. P. (2012*b*), An efficient visibility graph similarity algorithm and its applicationon sleep stages classification, *in* 'Proceedings of the 2012 international conference on Brain Informatics', BI'12, Springer-Verlag, Berlin, Heidelberg, pp. 185–195.

Zhu, G., Li, Y. & Wen, P. P. (2014*a*), 'Analysis and classification of sleep stages based on difference visibility graphs from a single channel eeg signal', *Biomedical and Health Informatics, IEEE Journal of* **PP**(99), 1–1.

Zhu, G., Li, Y. & Wen, P. P. (2014*b*), 'Epileptic seizure detection in eegs signals using a fast weighted horizontal visibility algorithm', *Computer methods and programs in biomedicine* **PP**(99), 1–1.

Zhu, G., Li, Y., Wen, P. P. & Wang, S. (2014), *Classifying epileptic EEG signals with delay permutation Entropy and multi-scale K-means*, Springer.

Zhu, G., Li, Y., Wen, P. P., Wang, S. & Xi, M. (2013), Epileptogenic focus detection in intracranial eeg based on delay permutation entropy, *in* 'AIP Conference Proceedings', Vol. 1559, American Institute of Physics, pp. 31–36.

Zhu, G., Li, Y., Wen, P. P., Wang, S. & Zhong, N. (2013), Unsupervised classification of epileptic eeg signals with multi scale k-means algorithm, *in* 'Brain and Health Informatics', Springer, pp. 158–167.

Zutshi, Y. (2013), 'Alzheimer's disease therapeutics and diagnostics: Global markets', `http://www.bccresearch.com/market-research/pharmaceuticals/alzheimers-disease-phm062b.html`. Accessed August 10, 2013.